



Dynamics and architecture of *Bacillus subtilis* cell division

Citation

Holmes, Matthew. 2021. Dynamics and architecture of *Bacillus subtilis* cell division. Doctoral dissertation, Harvard University Graduate School of Arts and Sciences.

Permanent link

<https://nrs.harvard.edu/URN-3:HUL.INSTREPOS:37371135>

Terms of Use

This article was downloaded from Harvard University's DASH repository, and is made available under the terms and conditions applicable to Other Posted Material, as set forth at <http://nrs.harvard.edu/urn-3:HUL.InstRepos:dash.current.terms-of-use#LAA>

Share Your Story

The Harvard community has made this article openly available.
Please share how this access benefits you. [Submit a story](#).

[Accessibility](#)

HARVARD UNIVERSITY
Graduate School of Arts and Sciences




DISSERTATION ACCEPTANCE CERTIFICATE

The undersigned, appointed by the
Department of Molecular and Cellular Biology
have examined a dissertation entitled
Dynamics and architecture of *Bacillus subtilis* cell division

presented by **Matthew Holmes**

candidate for the degree of Doctor of Philosophy and hereby
certify that it is worthy of acceptance.

Signature 
Richard Losick (Dec 16, 2021 08:51 EST)

Typed name: Prof. Richard Losick

Signature *Zhuang Xiaowei*

Typed name: Prof. Xiaowei Zhuang

Signature *Karine Gibbs*

Typed name: Prof. Karine Gibbs

Signature _____

Typed name: Prof.

Signature _____

Typed name: Prof.

Date: December 15, 2021

Dynamics and architecture of *Bacillus subtilis* cell division

A dissertation presented

by

Matthew Holmes

to

The Department of Molecular and Cellular Biology

In partial fulfillment of the requirements for the degree of

Doctor of Philosophy

in the subject of

Biology

Harvard University

Cambridge, Massachusetts

December 2021

© 2022 Matthew Holmes

All rights reserved

Dynamics and architecture of *Bacillus subtilis* cell division

Abstract

Cells generate more cells. This proliferation requires multiple cellular-scale morphological changes from one generation to the next. One cell must physically separate into two daughters in cytokinesis. In bacteria, this change represents the generation not only of separate cells, but also of separate organisms. However, the mechanisms by which nanometer scale proteins coordinate this micron scale reorganization is not understood. The filament-forming protein FtsZ organizes the division site, forming a Z-ring that recruits cell wall synthesis enzymes to build a septum between daughters. Understanding how FtsZ organizes division's cellular-scale change requires studying 1) what spatiotemporal patterns are established by FtsZ, 2) how these patterns are regulated by other factors, and 3) how these patterns effect physiology downstream of the Z-ring.

In addition to forming a ring at midcell, FtsZ filaments treadmill around the division site; this treading is required for the coincident motion of the cell wall synthesis enzyme Pbp2B, as well as efficient cell division. To understand how the division machinery collectively functions, here I present single-molecule imaging of the dynamics of the entire *Bacillus subtilis* division machinery using TIRF microscopy. The proteins previously shown to bind FtsZ (ZapA, SepF, and EzrA) remain stationary, associated with their bound FtsZ subunits. Meanwhile, Pbp2B moves in complex with the cell wall synthesis protein FtsW and the DivIB-DivIC-FtsL

complex. The division complex is therefore actually made of two distinct subcomplexes: one stationary and the other moving around the cell.

Further, I present a characterization of Z-ring architecture: FtsZ condensation into narrow rings by the FtsZ binding proteins ZapA, SepF, and EzrA. Removing synthetically lethal combinations of these proteins results in FtsZ being unable to bundle into narrow rings as cells die. This lethality cannot be explained solely by decreased recruitment of Pbp2B, and cell wall synthesis dynamics are unperturbed in uncondensed Z-rings.

Taken together, these results show that a subset of stationary divisome proteins coordinate essential changes in FtsZ architecture, while another subset of divisome proteins—cell wall synthesis proteins and their putative regulators—move collectively dependent on FtsZ treadmilling.

Table of contents

Abstract	iii
Table of contents	v
List of Figures	viii
List of Tables	ix
Acknowledgements	x
Chapter I—Introduction	1
Prokaryotic cytokinesis	1
FtsZ	2
FtsZ's molecular properties.....	2
The Z-ring	3
Physiology of cell division	3
Constructing the septum.....	3
Force.....	4
Division dynamics	6
FtsZ treadmilling.....	6
Physiological effect of treadmilling	7
The divisome	8
FtsZ binding proteins.....	8
Cell wall synthesis proteins	12
Structural proteins	13
Divisome Assembly.....	14
FtsZ organization and the divisome	15
Chapter II—Divisome dynamics and FtsZ condensation	17
Abstract	18
Introduction	18
The divisome displays two distinct sets of dynamics	19
FtsZ binding proteins are necessary for correct Z-ring architecture	24
FtsZ bundling is responsible for Z-ring condensation	29
Z-ring condensation increases cell wall synthesis, but this is not essential	30
FtsA knockouts are severely perturbed, unlike for other FtsZ binding proteins	33
Discussion	35
Chapter III—Discussion	37
The stationary divisome	37
The dynamic divisome	38

FtsW-Pbp2B.....	38
DivIB-DivIC-FtsL	40
Coordination of stationary and dynamic divisome subcomplexes	43
Direct interaction	43
Indirect Interaction.....	44
Separability of modes of FtsZ organization	46
The essential nature of Z-ring condensation	47
Cytokinesis and bacterial cell biology	49
<i>Appendix A—Methods for Chapter II</i>	<i>51</i>
Culture growth	51
Microscopy.....	51
Sample preparation.....	51
Phase contrast, epifluorescence, and TIRFM	52
Confocal.....	52
Induction, depletion, and HaloTag labelling.....	52
Antibiotic treatment.....	54
Cell length measurements	54
Velocity measurements	55
Cell segmentation.....	56
Single-molecule lifetime measurements	56
Automated	56
Manual	58
Z-ring identification, spacing, width, and average projections.....	58
Z-ring features across the cell cycle.....	59
Pbp2B localization	60
Cell wall synthesis labelling	61
ΔftsA analysis	62
Pbp2B dynamics	63
Suppressor screen	64
Strain construction	66
Statistical analysis	67
Code.....	67
<i>Appendix B—Supplemental figures for Chapter II</i>	<i>68</i>
<i>Appendix C—Supplemental tables for Chapter II.....</i>	<i>71</i>
<i>Appendix D—Strains used in Chapter II.....</i>	<i>73</i>
Strains and conditions listed by figure	73

Strain descriptions.....	81
Construct descriptions.....	86
<i>References.....</i>	93

List of Figures

Figure 1—The divisome	8
Figure 2—Sole copy SepF-HaloTag is non-functional when expressed at the native site but localizes to the division site when expressed as a second copy	19
Figure 3—Cell lengths of HaloTag (HT) fusions	20
Figure 4—Cell lengths of non-essential divisome protein knockouts	21
Figure 5—EzrA, ZapA, and SepF HT fusion are functional.....	21
Figure 6—EzrA, SepF, and ZapA are stationary.....	22
Figure 7—Lifetime distributions of stationary division proteins.....	22
Figure 8—Structural and cell wall synthesis proteins move directionally	23
Figure 9—Directionally-moving proteins have similar velocities.....	23
Figure 10—DivIB motion is halted in the presence of Penicillin G.....	23
Figure 11—Velocity and Lifetime are unaffected by synthetically lethal ZBP perturbations	25
Figure 12—Synthetically lethal ZBP perturbations result in altered Z ring architecture	26
Figure 13—Z rings are wider in synthetically lethal ZBP perturbations	27
Figure 14—Perturbation of Z ring width does not perturb Z ring spacing along filaments	27
Figure 15—Z rings condense in healthy cells	28
Figure 16—Z ring condensation correlates with Pbp2B recruitment in healthy cells.....	28
Figure 17—FtsZ(K86E) rescues Z ring morphology in synthetically lethal $\Delta ezrA \Delta zapA$	29
Figure 18—Quantification of FtsZ(K86E) rescue of Z ring width in $\Delta ezrA \Delta zapA$	30
Figure 19—Cell wall synthesis protein localization and activity are reduced at non-condensed Z rings.....	31
Figure 20—Pbp2B dynamics are observed at non-condensed Z rings.....	32
Figure 21—Pbp2B directional motion is seen at Z rings of all widths.....	32
Figure 22—Pbp2B recruitment is not rescued by FtsZ(K86E)	33
Figure 23—FtsZ motion is perturbed in $\Delta ftsA$ cells.....	34
Figure 24—FtsZ localization is severely perturbed in $\Delta ftsA$ cells	34
Figure 25—Condensation is necessary for cell division	35
Supplemental Figure 1—Z ring architecture in individual ZBP knockouts	68
Supplemental Figure 2—Z-ring architecture with ZBP overexpression	69
Supplemental Figure 3—Z-ring architecture in $\Delta sepF \Delta zapA$ cells	70

List of Tables

Supplemental Table 1—Lifetimes of stationary proteins.....	71
Supplemental Table 2—Velocities of directionally-moving proteins.....	71
Supplemental Table 3—Z-ring widths	72
Supplemental Table 4—Strains and conditions listed by figure.....	73
Supplemental Table 5—Strain descriptions	81
Supplemental Table 6—Construct descriptions.....	86

Acknowledgements

This section is by far the longest in the making—really my entire life. It has also been the most fun to write as it reminds me how lucky I am to have so many reservoirs of advice, support, and love.

The scientific foundation of this work comes from my advisor and committee. In some ways, Ethan's mentorship style reflects the self-organizing principles he taught my class about (via Lego) during my first graduate school lecture. Ethan wants nothing more than to put a bunch of fascinating people in a room, make sure there is passion and energy, give them total freedom, and see what happens. The resulting environment required and allowed me to grow into a more flexible, curious, open-minded, exploratory scientist. I also want to thank my committee who have readily helped me whenever I sought advice: Rich Losick, Karine Gibbs, and Xiaowei Zhuang.

The Garner lab consistently attracts wonderful people and I've been lucky enough to meet almost everyone who has ever been in the lab. Throughout my time here, there has been a culture where people are genuinely interested in each other and their science. This means that between bench-side chats, ever amusing lunches, and Cambridge Common beers, this work has been touched by every single one of my colleagues. Thank you, Jenna, Alex, Zach, Saman, Mrinal, Mike, Carl, Yingjie, Peter, Sean, Georgia, Patrick, Laura, Devon, Jeff, Jenny, Sylvia, Will, Andres, Charlie, Diego, Navish, Adi, Luis, Dan, and Anastasia. Peter is dearly missed. Special thanks are due to Alex, Patrick, Sean, and Georgia. Alex's infectious enthusiasm, deep passion about division, and instinctive drive to mentor makes him my scientific role model par excellence. Patrick knows how to balance his passion for science with passion for life beyond

the lab and his humor and perspective have been invaluable. Georgia and Sean have been with me through every high and low of graduate school; their support was instrumental in me making it through. I continue to be inspired by Georgia's dedication to science and commitment to those around her. Sean is profoundly creative and insists on the creativity of everyone around him—and by insisting that I can in fact create he has made me a braver person.

I am also grateful to the support in our building, department, and graduate program that made this work possible, especially Polina Kehayova.

Beyond Harvard, I was very lucky to be part of a vibrant scientific community at the 2017 Physiology Course in Woods Hole. Since then, Dan Fletcher and Rob Phillips have continued to offer valuable advice for which I am grateful. I would like to thank my entire course, and in particular Miranda, Victoria, and Navish.

Finally (from an academic perspective), I want to thank my undergraduate professors who introduced me to research and helped me navigate applying to and starting at graduate school. Thank you Iruka, Phil, Andre, and Rachel.

This doctoral thesis is probably not where I will best express my love and care for the following people, who are my life beyond academic biology, so I will keep these comments brief. However, I could not have done this work without their support and they have all had an indelible impact on me.

My family—my parents, my brother, and I—moved to the States almost twenty years ago. I am so grateful to share this, along with our many other American adventures, with them.

I have relatively few blood relatives, but am blessed with an extended family throughout the US, particularly in Rhode Island and Virginia. Thank you for welcoming me into your families.

Thank you to my friends from every stage in life who have continued to support me in graduate school: those from Rhode Island, my college flatmates, teammates, Dan and Jess, my roommates Sarah and James, and my Oxford family.

Finally, my partner, Darcy, who made this time of my life a worthwhile adventure.

Chapter I—Introduction

Prokaryotic cytokinesis

Cells are the fundamental units by which life is organized. Yet this level of organization is orders of magnitude larger than the monomers and chemical reactions that underpin life.

Proteins that interact with themselves recursively to form filaments (and reach larger spatial scales) are critical to bridge the gap between the nanometer and micron scales. To grasp the molecular organization of cells, we must understand how such polymerizing proteins organize, how accessory proteins influence this organization, and how this organization impacts physiological processes.

Cytokinesis is one such fundamental cellular re-organization in which a cell is physically separated into two daughter cells. Throughout prokaryotes, cytokinesis is organized by the filament-forming FtsZ. Its widespread presence in bacteria and archaea suggest early origin in life¹⁻³. FtsZ persists in chloroplast division and, rarely, some mitochondrial divisions³⁻⁶. FtsZ is essential in most prokaryotes, with FtsZ-less prokaryotes the exception.

Indeed, bacteria that tolerate FtsZ deletion often divide by extreme and inefficient mechanisms such as *Mycoplasma genitalium*, which tear themselves apart with gliding motility, or *Bacillus subtilis* L-forms (lacking cell wall) that divide by membrane extrusion^{7,8}. In either case these division mechanisms are slower than those of wildtype cells^{7,8}. Bacteria lacking FtsZ often have unusual cellular contexts, being parasitic or obligate endosymbionts such as *Chlamydia*^{2,9}. However, there are some clades of prokaryotes without host cells that do not use FtsZ. *Crenarchaeota* utilize ESCRT-III homologs, and the diversity of bacteria that do not divide by

binary fission (like the budding *Planctomyces*)^{2,8}. In any case, FtsZ represents a widespread, evolutionary conserved filament for division in most free-living prokaryotes.

FtsZ

FtsZ's molecular properties

FtsZ's best known homolog is tubulin¹⁰. Like tubulin, FtsZ is a GTPase, but unlike tubulin FtsZ does not form organized tubules through lateral associations^{6,11,12}. However, FtsZ protofilaments do interact laterally *in vitro* to form aggregated bundles, particularly in conditions that mimic the crowding of cells¹³. Both the molecular basis and the physiological relevance of these lateral interactions are still unclear^{6,13}.

FtsZ consists of a variable N-terminal region followed by two core domains that make up most of the protein and form the polymer interfaces¹. This core region is separated from the C terminus by a disordered variable length linker region¹. The sequence of this linker can be altered, but its length and disordered nature are functionally important; while its charge is important for FtsZ lateral interactions *in vitro*, it does not show an effect *in vivo*¹⁴. After this linker is a short C-terminal peptide, which contains a conserved motif followed by a terminal variable region¹. *Escherichia coli* are viable when the entire FtsZ gene is replaced by the *B. subtilis* sequence except this short C-terminal peptide, albeit with suppressor mutations and minor division defects¹⁵. The negatively charged C-terminal variable region in *B. subtilis* promotes bundling *in vitro* and can even induce bundling when introduced to *E. coli* FtsZ¹⁶. To the extent that these results suggest that the C terminus (structurally and spatially separated from the core polymerizing domains) encodes variability across bacteria, it is interesting to note that this C terminus is where many FtsZ binding proteins interact.

The Z-ring

FtsZ forms a ring at midcell: the future division site¹². Ring placement involves the Min system (which defines the location of cell poles) and the Noc system (which defines the location of chromosomes). This placement system is not fully understood as *B. subtilis* forms Z-rings at midcell in the absence of both systems¹⁷. Once formed, this Z-ring is likely not a single, homogenous structure. Rather, super resolution microscopy shows clusters of protofilaments around the cell form a loose, discontinuous ring in *E. coli*, *B. subtilis*, and *Caulobacter crescentus*^{18–23}. It should be mentioned that, in contrast, electron cryotomography has suggested a continuous Z-ring around the circumference of *E. coli* and *C. crescentus*²⁴. However, more recent evidence that FtsZ protofilaments are dynamic in Z-rings strongly argues against a single, continuous, stable ring^{25,26}. Some symbiotic bacteria that divide lengthwise utilize discontinuous Z-rings or have FtsZ that does not form a ring at all^{27,28}.

The Z-ring constricts as the cell divides separating the mother cell into two daughters¹². Z-ring disassembly during and after constriction is not well understood¹³. Throughout all these processes, FtsZ levels remain consistent in *E. coli* and *B. subtilis*, and therefore expression levels cannot explain Z-ring development and constriction^{29,30}.

Physiology of cell division

Constructing the septum

The Z-ring constricts concurrent with the construction of a cell wall septum between daughter cells, separating the bacterium in two. The peptidoglycan cell wall provides structural integrity to bacteria, so constructing and modifying peptidoglycan is instrumental to maintaining and changing bacterial cell shape³¹. Peptidoglycan consists of the disaccharide

MurNAc. MurNAc is synthesized into extended glycan strands by transglycosylation; these strands are crosslinked to one another through transpeptidation of MurNAc's peptide sidechains. The architecture of this mesh-like peptidoglycan (and by extension, the precise molecular details of division) vary among bacteria. Gram-positive bacteria, including *B. subtilis*, have a thicker peptidoglycan cell wall than Gram-negatives. Purified and hydrated *B. subtilis* cell walls are 34+/-10nm thick³². Unlike Gram-negatives, material is not routinely recaptured by Gram-positives, rather peptidoglycan gradually moves to the exterior of the wall as new material is synthesized underneath³³. There are differences at the molecular level, too: while *E. coli* glycan strands are relatively short (~21 disaccharides long), *B. subtilis* has extremely elongated strands of >500 disaccharides³⁴.

Force

While not the direct subject of this study, all discussions on how FtsZ and cell wall synthesis are organized exist in the context of force. Cell division not only involves the constriction of a Z-ring and the construction of a cell wall septum, but also the generation of force sufficient to overcome the turgor pressure of the cell. The *B. subtilis* cell wall is subject to approximately 2MPa of turgor³⁵. The constriction of the membrane and new cell wall construction are in opposition to this, requiring 50-300nN of force³⁵.

One model posits that FtsZ is responsible for generating this force. Many FtsZ-based models have been proposed—invoking conformation change, lateral interactions, sliding, and so on—but these models have been plagued with problems; lack of theoretical clarity persists despite an abundance of models³⁶. Yet strong empirical evidence demonstrates FtsZ can generate force on membranes. *E. coli* FtsZ fused to a membrane targeting sequence can

constrict vesicles into tubules in the presence of GTP, though full constriction is not observed³⁷. Switching the side of FtsZ with the membrane targeting sequence switches the direction of constriction, allowing FtsZ to constrict vesicles from the outside instead³⁸. Finally, when *E. coli* FtsA is added instead of the membrane targeting sequence along with GTP and ATP, Z-rings form (albeit rarely) that constrict half of the time and fully septate membrane a quarter of the time³⁹. However, *in vivo* CLEM (correlative light-electron microscopy) of *E. coli* show that FtsZ is only ever associated with even minor membrane invaginations when cell wall synthesis proteins and the division protein FtsN are also present⁴⁰.

The other predominant model of force generation invokes the chemical energy inherent to cell wall synthesis. Perhaps the most direct evidence of this model comes from mutants of the *E. coli* transpeptidase FtsI, which have slower septum closure rates²⁰. An equivalent effect is not found for *E. coli* FtsZ GTPase mutants, which might perturb any mechanism by which FtsZ generates force²⁰. This result is not consistent across bacteria, with *B. subtilis* FtsZ GTPase mutants having a reduced septum closure rate²⁶. However, at some late point *B. subtilis* division can proceed independent of FtsZ treadmilling^{41,42}. This FtsZ-independence seems to correlate with the Pbp2B levels at the division site, but specifics about this relationship are still unclear^{41,42}. A similar transition from FtsZ-dependence to independence has been observed in *Staphylococcus aureus*⁴³. While numerous models have implicated either FtsZ or cell wall synthesis in generating force to divide cells, the mechanism remain unclear³⁵.

One additional model has emerged in recent years: that the entire force question is misguided. It has recently been argued that cell division need not overcome turgor in Gram-negative or Gram-positive bacteria⁴⁴. In the Gram-positive case, the model supposes that

teichoic acids are so prevalent in the cell wall that each side of the plasma membrane is isosmotic⁴⁴.

Division dynamics

FtsZ treadmilling

Both polymers—FtsZ and peptidoglycan—undergo spatial reorganization as daughter cells separate. Z-rings constrict as a peptidoglycan septum is constructed between daughters. It has long been known that FtsZ scaffolds septum construction through localizing peptidoglycan synthesis proteins, essential for division, to midcell⁴⁵. However, new physiologically relevant modalities of FtsZ organization are still being discovered, driven by recent improvements in imaging techniques⁴⁶.

Rapid turnover of FtsZ subunits within polymers became clear in early FRAP experiments^{47,48}. More recently, FtsZ was shown to treadmill *in vitro* on membrane in the presence of membrane anchor FtsZ⁴⁹. Treadmilling, as the name perhaps evokes, describes a mechanism in which the motions of the filament as a whole and its constituent subunits are distinct. In the case of FtsZ, individual subunits remain stationary, as had been demonstrated earlier in *E. coli*⁵⁰. Meanwhile, filaments move, with subunits preferentially associating to one end and dissociating from the other end.

These dynamic FtsZ protofilaments were first observed *in vivo* in *E. coli* and *B. subtilis*^{25,26}. FtsZ treadmills in the range of 30-40 nm/sec and this motion derives from the intrinsic GTPase activity of FtsZ and is not dependent on cell wall synthesis^{25,26,51}. The mechanism by which individual protofilaments can robustly treadmill is not intuitive, but may be explained by the ability of FtsZ self-interaction interfaces to form two distinct

confirmations⁵². The combination of these states (relaxed and tense), GTP hydrolysis, and distinct kinetics at each end of the filament allows modelling of treadmilling protofilaments, with GTP bound FtsZ enriched at the growing end and GDP bound FtsZ enriched at the shrinking end⁵³.

Physiological effect of treadmilling

Downstream of the treadmilling filament, details vary between species. The *B. subtilis* cell wall synthesis enzyme Pbp2B and its *E. coli* homolog FtsI both move circumferentially around the division site at a similar velocity to FtsZ^{25,26}. When FtsZ is slowed down by chemical or genetic perturbations, these cell wall synthesis enzymes are slowed down accordingly^{25,26}. In contrast to these rod-shaped bacteria, a Pbp2B homolog from *Streptococcus pneumoniae* (an ovoid Gram-positive whose elongation occurs exclusively at midcell) does not slow down to the same extent as FtsZ⁵⁴. Indeed, the *S. pneumoniae* Pbp2B homolog can move up to four times faster than FtsZ⁵⁴.

In *E. coli* changing FtsZ velocity perturbs the distribution of cell wall synthesis, but not the amount of cell wall synthesis or septum closure rate^{20,25}. In contrast, reducing the velocity of *B. subtilis* FtsZ leads to less efficient division, with reduced distribution and amount of cell wall synthesis and slowed septum closure rate²⁶. However, *B. subtilis* Z-rings that have begun dividing can complete division in the absence of FtsZ treadmilling^{41,42}. Similarly, *S. aureus* FtsZ treadmilling is necessary early in cell division, but not late in constriction⁴³. FtsZ treadmilling is physiologically relevant, with details of downstream effects varying between species.

The divisome

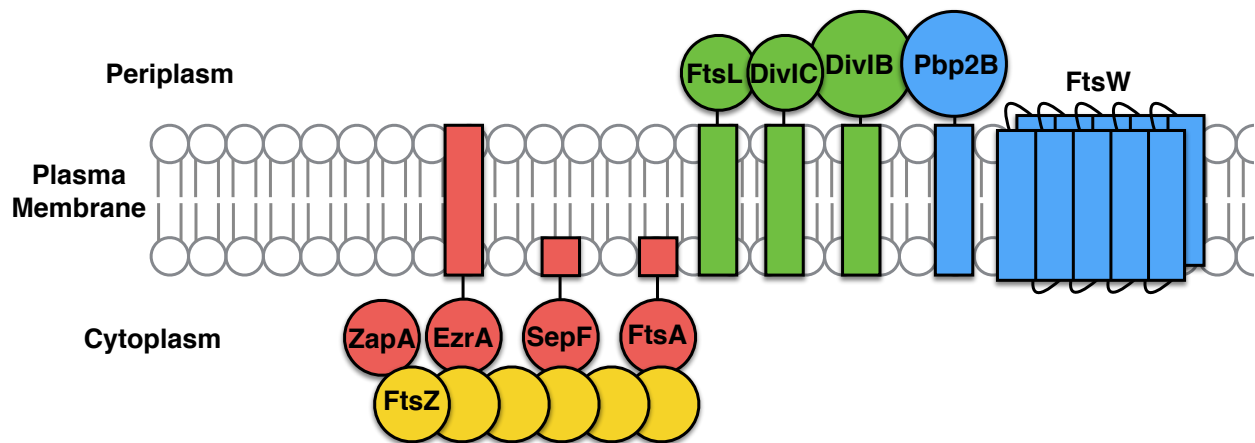


Figure 1—The divisome

The divisome: 1) FtsZ (yellow) 2) FtsZ binding proteins (red) 3) the non-enzymatic structural proteins with a periplasmic domain (green) and 4) cell wall synthesis enzymes (blue).

The preceding introduction has focused exclusively on FtsZ and one cell wall synthesis protein, Pbp2B. However, there is no evidence that FtsZ directly interacts with Pbp2B or any other cell wall synthesis protein. Rather, division is orchestrated by a larger complex of proteins: the divisome⁵⁵. Understanding how FtsZ organizes cell wall synthesis and cell division overall requires an understanding of how this entire complex coordinates division, which is poorly understood. This introduction focuses on the divisome of *B. subtilis*, the subject of this work (Figure 1). While many proteins interact with FtsZ and the divisome in certain conditions to regulate division, this study focuses on proteins that are constitutively found at the division site, arriving with the Z-ring or cell wall synthesis enzymes^{55,56}. In this study these nine proteins that join FtsZ at the division site are separated into three groups based on various properties discussed below: FtsZ binding proteins, cell wall synthesis proteins, and structural proteins.

FtsZ binding proteins

As the name suggests, these are all the divisome proteins known to bind directly to FtsZ: FtsA, ZapA, EzrA, and SepF. These proteins all have soluble cytoplasmic domains and all except ZapA associate with the membrane through an amphipathic helix or a transmembrane region.

FtsA

FtsA is an actin homolog^{3,57}. Crystal structures from *Thermotoga maritima* show FtsA binds to the C-terminal peptide of FtsZ. FtsA anchors FtsZ to the membrane through a C-terminal amphipathic helix⁵⁸. The function of this helix does not seem sequence specific, as it can be replaced in *E. coli* by MinD's amphipathic helix⁵⁸. The specific ratio of FtsA to FtsZ is necessary for healthy division, with 1 FtsA for every 5 FtsZ in *B. subtilis*^{59,60}.

FtsA polymers have been observed in *B. subtilis*, but not *E. coli* or *C. crescentus*⁵¹. Polymer formation *in vivo* does not correlate with ATP hydrolysis *in vitro*, which has been observed for both *B. subtilis* and *E. coli* FtsA^{60,61}. In any case, the function of *in vivo* FtsA polymerization is not understood⁵¹.

While FtsA is not essential, Δ *ftsA* *B. subtilis* are extremely filamented and less viable⁶². Populations of Δ *ftsA* cells have twice the doubling time of wildtype cells due to frequent lysis⁶³.

ZapA

ZapA is a cytoplasmic protein that does not associate with the membrane and is found throughout bacteria. ZapA was identified in a screen for proteins that promote FtsZ polymerization⁶⁴. Accordingly, ZapA stabilizes FtsZ polymers and decreases FtsZ GTPase activity *in vitro*⁵⁵. ZapA also promotes large FtsZ bundles *in vitro*⁶⁴.

In vivo, $\Delta zapA$ displays no obvious division defects⁶⁴. $\Delta zapA$ division defects only occur when FtsZ levels are artificially reduced, or in the absence of another FtsZ binding protein, EzrA⁶⁴. Specifically, EzrA and ZapA are synthetically lethal⁶⁴.

Structures from *Pseudomonas aeruginosa* demonstrate that ZapA can form dimers and tetramers, with dimerization at physiologically relevant concentration⁶⁵. The dimerization region is conserved in *B. subtilis*⁶⁵.

EzrA

EzrA has a cytoplasmic domain and an N-terminal transmembrane helix and is found in Gram-positive bacteria^{55,66}. This transmembrane helix is important for EzrA function, but can be replaced by another, non-division transmembrane helix⁶⁷. In contrast to ZapA, EzrA was initially identified as a *negative* regulator of FtsZ polymer formation⁶⁶. $\Delta ezrA$ cells are more tolerant of FtsZ depletion while still forming Z-rings⁶⁶. Additionally, an *ezrA* null mutation restores Z-rings in a condition (MinCD overexpression) where they are otherwise destabilized⁶⁸. *In vitro*, EzrA inhibits FtsZ polymerization but does not impact disassembly of previously formed FtsZ polymers and bundles⁶⁹. Specifically, EzrA increases FtsZ critical concentration about five-fold and reduces GTP binding to FtsZ by one-third^{70,71}. EzrA also increases FtsZ turnover *in vitro*⁴⁸. Intriguingly, the C-terminal half of EzrA decreases FtsZ polymerization *in vitro* to a greater extent than the full-length protein⁷². Like FtsA, EzrA binds to the C-terminal tail of FtsZ⁷⁰.

EzrA is essential in some Gram-positives, such as *S. aureus* (where it is required for localization of cell wall synthesis enzymes to midcell), but not in *B. subtilis*^{66,73}. ZapA and SepF are each synthetically lethal with EzrA^{64,74}. $\Delta ezrA$ cells have extra Z-rings at the poles and depleting EzrA increases cell length, a common result of division defects^{66,75}. The extra Z-ring

phenotype is genetically separable from EzrA's role in Z-ring stabilization: a 7-residue patch at the EzrA C terminus—the QNR patch—is required for midcell localization and destabilization of the Z-ring *in vivo* but is not necessary to inhibit extra Z-rings at the poles⁷⁶. The QNR patch is dispensable for destabilizing FtsZ *in vitro*⁷⁶.

EzrA has an unusual and intriguing structure, whose specific function is still not understood. An EzrA crystal structure forms a semicircle with a 12nm diameter, formed of triple helix bundles like those found in eukaryotic spectrin proteins—which can form scaffolds on plasma membranes⁷².

SepF

SepF is a cytoplasmic protein with an N-terminal amphipathic membrane which can recruit FtsZ to the membrane⁷⁷. Absent from *E. coli* and other proteobacteria, SepF was the most recently discovered division component. Despite this late discovery, SepF may be among the more ancient division proteins. In addition to cyanobacteria, Gram-positive bacteria, and some other bacterial clades, SepF is found in all FtsZ-containing archaea⁷⁸. Bacterial and archaeal SepF clearly separate in phylogenetic trees, suggesting conservation in their common ancestor⁷⁸. Studies of archaeal SepF are novel and ongoing^{78,79}.

Like ZapA, SepF is an FtsZ stabilizer, promoting FtsZ filaments and bundle formation *in vitro*⁸⁰. However, SepF is synthetic lethal not with fellow FtsZ stabilizer ZapA, but with the FtsZ destabilizing EzrA⁷⁴.

Δ *sepF* cells have slightly thicker septa and are slightly longer than wildtype cells^{74,81}. In bacteria without the membrane anchor FtsA, SepF is essential. *Mycobacterium* and the Actinobacteria *Corynebacterium glutamicum* need SepF for Z-ring formation^{82,83}. Perhaps this

membrane anchoring role explains how increasing SepF levels suppresses lysis and recovers the growth rate in $\Delta ftsA$ cells⁸¹. Like FtsA and EzrA, SepF binds to the C-terminus of FtsZ^{80,84}.

SepF self-interacts and forms rings *in vitro*^{74,77,85}. Mutants that are unable to form these *in vitro* tubules are dominant negative for Z-ring formation *in vivo*, strongly suggesting the physiological relevance of SepF interaction (if not these structures specifically)⁸⁵. Curiously, the size of these *in vitro* SepF rings varies between species and this correlates somewhat to septum thickness⁸⁶.

Cell wall synthesis proteins

Pbp2B and FtsW are the division-specific cell wall synthesis enzymes in *B. subtilis*.

Pbp2B

Pbp2B is an essential protein with an N-terminal transmembrane domain and a C-terminal catalytic domain in the periplasm⁸⁷. Pbp2B was discovered, named, and implicated in cell wall synthesis based on its binding to penicillin⁸⁸. It is required for division and constriction of the Z-ring, with its depletion leading to lethal filamentation (where cells grow without dividing, become extremely long, and lyse)⁴⁵. Pbp2B's catalytic domain is responsible for transpeptidation of the peptidoglycan (crosslinking glycan strands). Additionally, *B. subtilis* Pbp2B has two PASTA (penicillin-binding protein and serine threonine kinase associated) domains absent in Gram-negative homologs⁸⁹. These domains are often involved in binding peptidoglycan, but these binding residues are absent in the Pbp2B PASTA domains⁸⁹. As mentioned above, Pbp2B and its homologs move circumferentially around the cell with treadmilling FtsZ filaments^{25,26,54}.

FtsW

FtsW has 10 transmembrane regions, with no large soluble domains. As a member of the SEDS (shape, elongation, division, sporulation) family, FtsW was recently identified as the division glycosyltransferase, synthesizing elongated glycan strands out of disaccharide precursors *in vitro*^{90,91}. Recently, this activity has been confirmed *in vivo* in *E. coli*⁹².

Structural proteins

Three non-enzymatic proteins with a single transmembrane region and a soluble periplasmic region are critical for division: FtsL, DivIC, and DivIB. They are referred to as structural proteins due to this lack of enzymatic activity.

FtsL

Immediately adjacent to Pbp2B on the chromosome, *B. subtilis* FtsL was identified by homology to *E. coli* FtsL, despite a poorly conserved sequence^{87,93}. It is essential; depletion of FtsL leads to lethal filamentation. FtsL is unstable, with its cytoplasmic N terminus required not for division, but for degradation by the metalloprotease RasP⁹⁴. FtsL interacts with another structural protein, DivIC, by a periplasmic coiled coil; this dimerization protects FtsL from RasP degradation^{95,96}.

DivIC

DivIC is similar in size and structure to FtsL and is also essential⁹⁷. Its cytoplasmic region and transmembrane region are not necessary for division⁹⁸. FtsB is the *E. coli* DivIC homolog, with DivIC having an extended cytoplasmic tail relative to FtsB⁹⁹.

DivIB

DivIB is non-essential at lower temperatures, but viability decreases—and cell length increases—from 30°C to 37°C; it is essential at higher temperatures^{100,101}. DivIB is abundant in

B. subtilis (about 5000 molecules per cell) whereas there are only a few molecules of the *E. coli* homolog FtsQ per cell¹⁰¹. Depleting this large amount of DivIB has little effect on cell length at 30°C and below¹⁰¹. While dispensable for cell division at lower temperatures, $\Delta divIB$ cells are almost entirely unable to sporulate and have abnormally thick sporulation septa, resembling vegetative division septa¹⁰².

The cytoplasmic and transmembrane regions of DivIB are unnecessary even at high temperatures⁹⁸. In the periplasm, DivIB is larger than FtsL and DivIC, with three periplasmic domains: alpha, beta, and gamma¹⁰³. The alpha domain has been suggested as a chaperone for the other structural proteins based on its POTRA domain (also found in beta barrel outer membrane proteins involved in protein assembly)¹⁰³. If this speculation is true, though, chaperoning is not an essential function of DivIB as the alpha domain is dispensable at high temperatures¹⁰⁴. Less is known about the beta domain. The gamma domain is required at high temperatures and is believed to be unstructured in the absence of other proteins due to its rapid degradation *in vitro*¹⁰³. DivIB may interact with many facets of the divisome as its localization is highly redundant: the cytoplasmic and transmembrane region, the alpha domain alone, and the beta and gamma domains are each sufficient for localization to the division site¹⁰⁴. DivIB not only interacts with other divisome proteins, as it binds purified peptidoglycan *in vitro*¹⁰⁵.

Divisome Assembly

Recruitment to the divisome occurs in discrete stages across bacteria, as observed in *E. coli*, *B. subtilis*, and *S. aureus*^{43,106–108}. In *B. subtilis* FtsZ and FtsZ binding proteins arrive early in

the division cycle, with the structural and cell wall synthesis proteins arriving after a further 25% of the division cycle^{107,108}.

FtsZ is required for the localization of other divisome components, but the reciprocal is not true^{45,66,74,81,87,93,108,109}. Beyond this, a clear protein-by-protein recruitment hierarchy has been established in *E. coli*^{87,110}. In contrast, in *B. subtilis* no direct interaction is known between the early arriving proteins (FtsZ and the FtsZ binding proteins) and the later arriving proteins (the structural and cell wall synthesis proteins). Additionally, these late proteins do not have a recruitment hierarchy, but are all mutually co-dependent on each other for localization in *B. subtilis*^{45,93,108,109}. Each of these late proteins is needed for the recruitment of the others (with DivIB required only at the high temperatures at which it is essential).

FtsZ organization and the divisome

Clearly, a varied and extensive literature has emerged from investigating how bacteria employ nanometer scale proteins to effect micron scale rearrangement of the cell in division. This study is informed by two themes from the literature in particular:

1) Advances in imaging techniques are identifying new modalities of FtsZ organization. This work begins by extending the recent understanding of *in vivo* FtsZ dynamics to the entire divisome. While each of these proteins are known to be important for division, their specific role into translating FtsZ dynamics into the consequently efficient cell wall synthesis is unclear. This work is followed by investigation of a novel form of FtsZ organization: architecture.

2) Systematic study of the divisome. Study of division in the 1990's and 2000's identified many members of the divisome and focused study on classification of each. While often focused through the lens of investigating one protein, these studies make observations—from

synthetic lethality to co-dependent localization—that motivate questions about the divisome as a complex. By performing a systematic study of divisome dynamics, this study identifies two distinct sub-complexes of the divisome that demonstrate distinct dynamics at midcell.

FtsZ is a sophisticated, self-interacting protein that is capable of multiple distinct modes of spatiotemporal organization. But FtsZ is not alone in coordinating bacterial cell division. This work seeks to advance systematic understanding of how the divisome impacts FtsZ organization and how FtsZ organization in turn impacts the divisome as a whole.

Chapter II—Divisome dynamics and FtsZ condensation

This chapter, with the accompanying methods and appendices, was published previously as “Single-molecule imaging reveals that Z-ring condensation is essential for cell division in *Bacillus subtilis*” by Georgia R. Squyres*, Matthew J. Holmes*, Sarah R. Barger, Betheny R. Pennycook, Joel Ryan, Victoria T. Yan, and Ethan C. Garner.

* These authors contributed equally.

This paper was a collaboration encompassing work that Georgia and I had done independently, with us then working together on a series of experiments that incorporated ideas from both of our doctoral work. Parts of the manuscript and some figures that only bear on Georgia’s work and not my own are omitted. In particular, the design of a single molecule lifetime assay which Sarah, Betheny, and Joel helped develop. This assay was implemented here in my work on stationary protein dynamics (Figure 7). I performed the imaging and characterization of the divisome’s single molecule dynamics presented here. Georgia, with help at the early stages from Victoria, characterized the ZBP synthetic lethal mutants; Georgia also conducted the suppressor screen and FtsA perturbation experiments. Georgia and I collaborated on experiments characterizing the downstream effects of ZBP perturbation. Ethan, Georgia, and I co-wrote the manuscript, which I have adapted in parts. Figure 2 and Figure 10 have not been previously published.

Supplementary videos are available with the original publication at <https://www.nature.com/articles/s41564-021-00878-z>.

Abstract

Although many components of the cell division machinery in bacteria have been identified, the mechanisms by which they work together to divide the cell remain poorly understood. Key among these components is the tubulin FtsZ, which forms a Z-ring at midcell. FtsZ recruits the other cell division proteins, collectively called the divisome, and the Z-ring constricts as the cell divides. We applied live-cell single molecule imaging to describe the dynamics of the divisome in detail, and to evaluate the individual roles of FtsZ binding proteins, specifically FtsA and the ZBPs (EzrA, SepF, and ZapA), in cytokinesis. We show that the divisome comprises two subcomplexes that move differently: stationary ZBPs that transiently bind to treadmilling FtsZ filaments, and a moving complex that includes cell wall synthases. Our imaging analyses reveal that ZBPs bundle FtsZ filaments together and condense them into Z-rings, and that this condensation is necessary for cytokinesis.

Introduction

The mechanism by which bacteria divide remains poorly understood. In *B. subtilis*, as in most other bacteria, division begins when filaments of FtsZ, a tubulin homolog, form a “Z-ring” at midcell¹³. The Z-ring recruits other cell division proteins, collectively called the divisome (Figure 1). The first group of these proteins (early proteins) arrives concurrently with FtsZ and includes the actin homolog FtsA and several other FtsZ binding proteins (ZBPs): the cytoplasmic protein ZapA, the integral membrane protein EzrA, and the peripheral membrane protein SepF. The second group of integral membrane proteins (late proteins) is then recruited, including DivIB, DivIC, and FtsL, and the cell wall synthesis enzymes Pbp2B and FtsW^{55,107}. During cytokinesis, the Z-ring constricts while the associated cell wall synthesis enzymes build a

septum that divides the cell in half¹¹¹. Recent work has shown that FtsZ filaments treadmill around the division plane, moving at the same rate as the transpeptidase Pbp2B (Supplementary Video 1)^{25,26}. FtsZ treadmilling dynamics are critical for cell division: In *B. subtilis*, the rate of treadmilling limits Pbp2B motion, the rate of septal cell wall synthesis, and the overall rate of septation²⁶.

To understand how these proteins work to divide cells, we sought to build a dynamic characterization of how this multi-component machine functions in *B. subtilis*. We first worked to identify groups of divisome proteins that move together, then investigated how the FtsZ-associated proteins modulate FtsZ filaments, cell wall synthesis, and the overall process of cell division.

The divisome displays two distinct sets of dynamics

First, to understand which of the divisome proteins in *B. subtilis* associate with each other and work together, we characterized their dynamics using single-molecule imaging, as

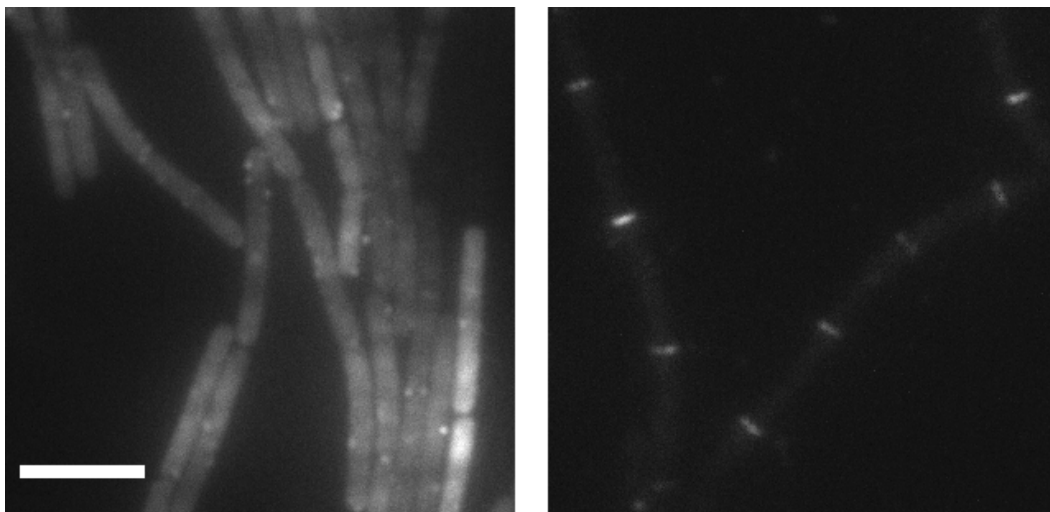


Figure 2—Sole copy SepF-HaloTag is non-functional when expressed at the native site but localizes to the division site when expressed as a second copy

When SepF-HaloTag is promoted under the native protein's promoter as a sole copy, it does not localize correctly to the division site and forms aggregates (left). SepF expressed as a second copy using the background leakiness of the pHyperspank promoter shows correct localization to the division site (right).

associated proteins should have similar motions. We expressed HaloTag fusions of each protein either as a sole copy, except for SepF. A sole copy fusion of SepF was not functional and appeared to aggregate (Figure 2). Overexpressing unlabeled SepF causes inclusion bodies and membrane aggregation^{80,112}. The sole copy SepF may be more stable, leading to overexpression; alternatively, the HaloTag may cause the protein to aggregate at lower levels. However, a SepF fusion expressed at low levels from an ectopic site localized to the division site (Figure 2). Cell length measurements confirm that these fusions are functional (or non-perturbative in the case of SepF) (Figure 3). Cells lethally filament in the absence of DivIC, FtsL, FtsW, or Pbp2B^{45,93,97,108}. Additionally, cells lacking EzrA, SepF, or DivIB all show clear cell

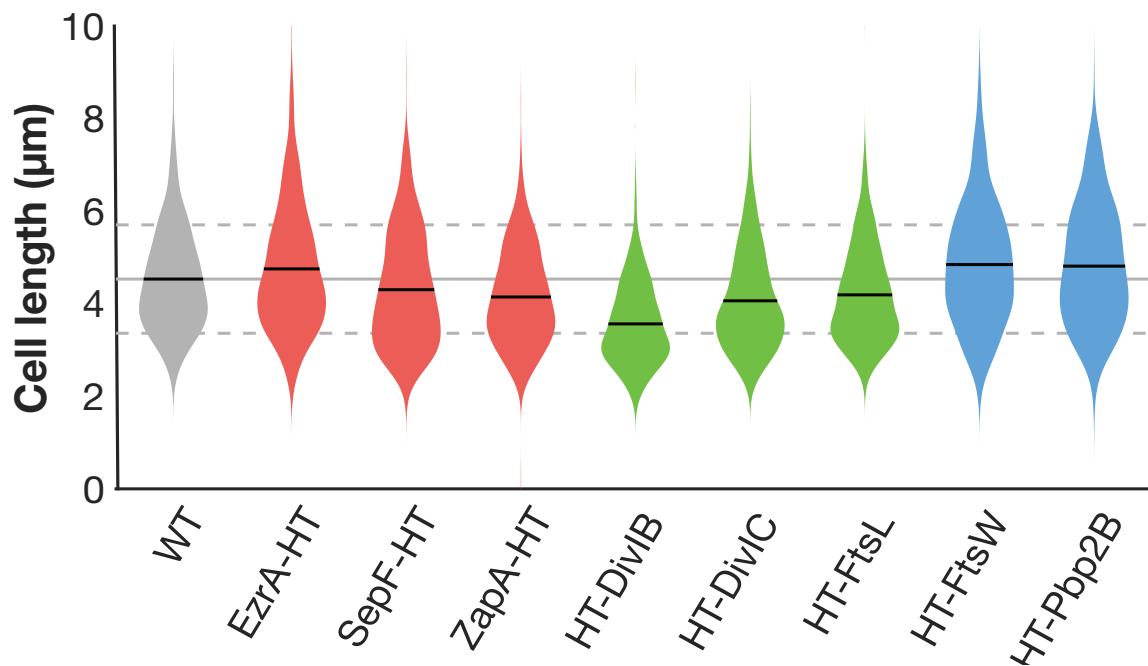


Figure 3—Cell lengths of HaloTag (HT) fusions

Cell lengths were measured from confocal microscopy of FM5-95 membrane-stained cells. When cell division is inhibited, cell length increases; that cell lengths in each strain are equal to or less than that of wild type (WT) cells indicates that these fluorescent fusions do not strongly inhibit cell division. In some cases where the fluorescent fusion is merodiploid or expressed under inducible control, cells are shorter than WT, as might be expected when components of the cell division machinery are overexpressed. Gray lines: mean (solid line) \pm standard deviation (dashed lines) for WT cell lengths.

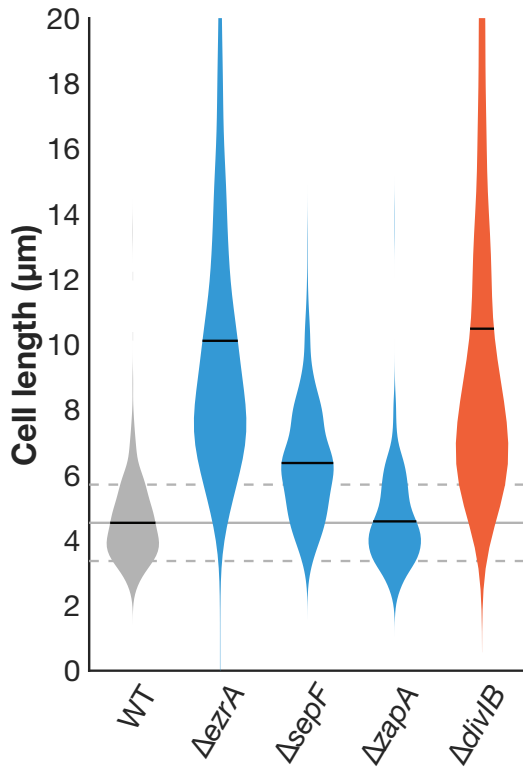


Figure 4—Cell lengths of non-essential divisome protein knockouts

Lengths of cells with non-essential division proteins knocked out. FtsA is also non-essential, but cells are so elongated that length measurements are impractical (**Figure 24**).

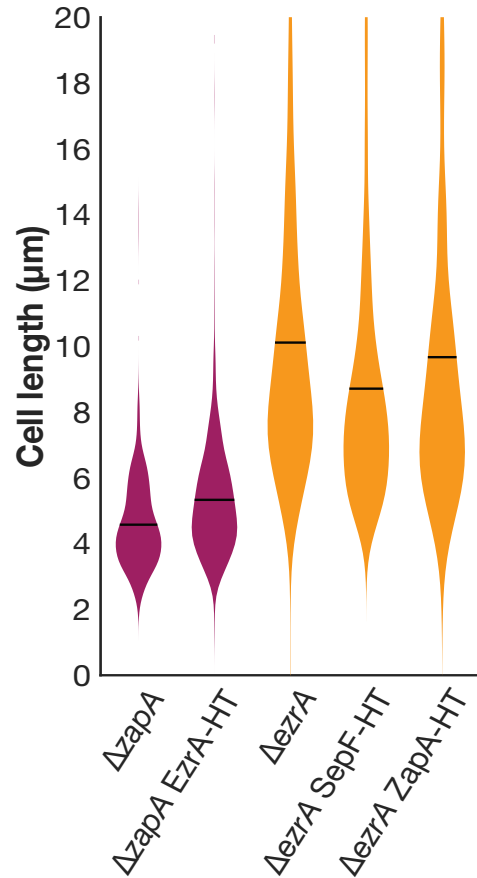


Figure 5—EzrA, ZapA, and SepF HT fusion are functional

EzrA and ZapA HT fusions are functional and SepF HT fusion expressed at an ectopic site does not disrupt SepF function.

length phenotypes, unlike the fusion proteins (Figure 4). All these strains allow cells to grow at a wildtype length indicating functionality (Figure 3).

Finally, EzrA is synthetically lethal with SepF and ZapA^{64,74}. We therefore knocked out one of these proteins and then expressed our HT fusion to the other protein; if HT fusion induced a critical defect in protein function, this combination will be lethal. Instead, in each case cells remained viable, with comparable lengths to the knockout alone (Figure 5).

Cells were sparsely labelled with JF549-HaloTag Ligand and imaged with Total Internal Reflection Fluorescence Microscopy (TIRFM)¹¹³. Just as single molecules of FtsZ and FtsA are

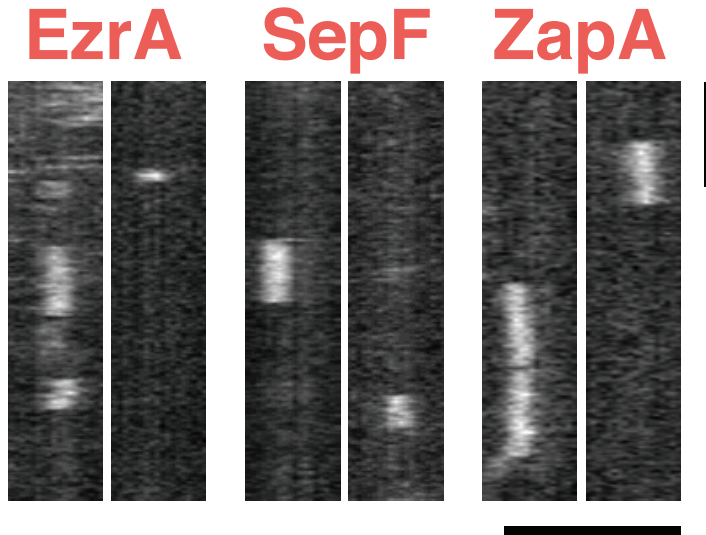


Figure 6—EzrA, SepF, and ZapA are stationary
 Kymographs of single molecules of stationary ZBPs at division sites, from two replicates for each condition. Scale bars: horizontal: 2 μ m, vertical: 1 min.

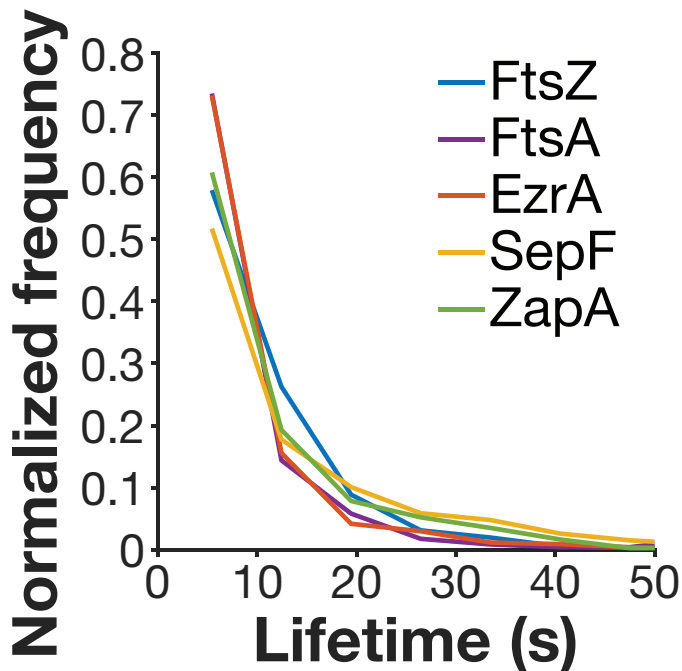


Figure 7—Lifetime distributions of stationary division proteins
 Subunit lifetime distributions of all divisible proteins found to be stationary at the division site: FtsZ, FtsA, EzrA, SepF, and ZapA.

immobile, single molecules of the ZBPs were stationary (Figure 6, Supplementary Video 2), consistent with their binding to stationary FtsZ subunits within treadmilling filaments²⁶. We measured the lifetimes—the amount of time the protein remains stationary at the division site—of these stationary proteins and found that the lifetimes were similar to or slightly shorter than that of FtsZ (Figure 7, Supplemental Table 1). In contrast, the late proteins all moved directionally, with velocity distributions similar to Pbp2B (Figure 8, Figure 9, Supplemental Table 2). Next, we tested if the DivIB, DivIC, FtsL complex’s motion depends on cell wall synthesis, as has

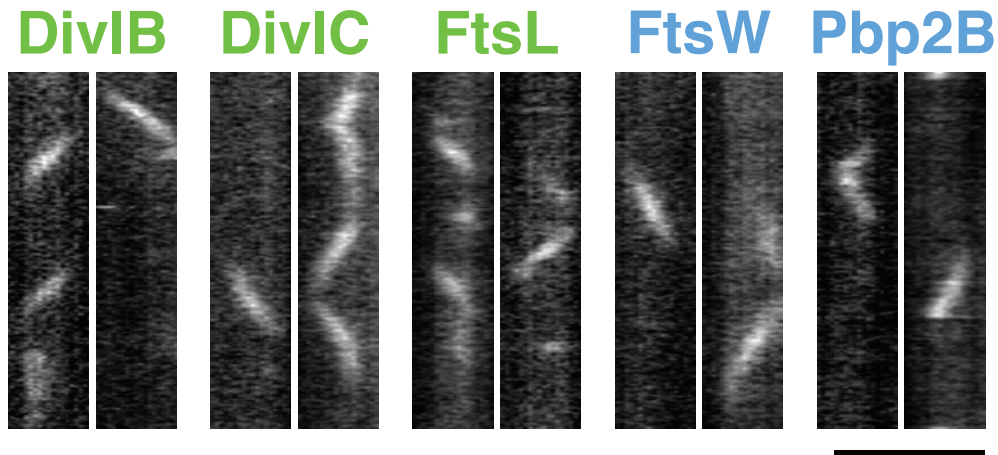


Figure 8—Structural and cell wall synthesis proteins move directionally
Kymographs of single molecules of directionally-moving proteins at division sites, from at least two replicates for each condition. Scale bars: horizontal: 2 μm , vertical: 1 min.

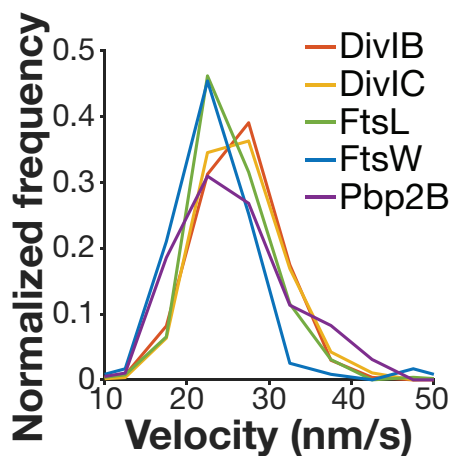


Figure 9—Directionally-moving proteins have similar velocities
Velocity distributions of all directionally-moving proteins, measured from kymographs.

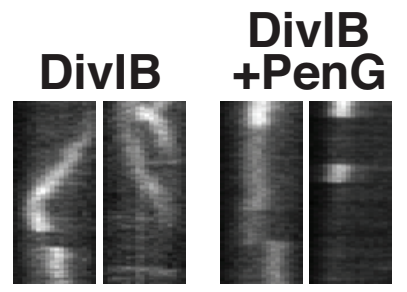


Figure 10—DivIB motion is halted in the presence of Penicillin G
DivIB single-molecule imaging displays directional motion (left) that is halted in the same sample upon addition of Penicillin G (right). Scale bars: horizontal: 2 μm , vertical: 1 min.

previously been shown for Pbp2B²⁶. We imaged DivIB in the presence of Penicillin G, which prevents transpeptidation and stops Pbp2B motion²⁶. DivIB no longer moved directionally in the absence of cell wall synthesis (Figure 10). The divisome-associated cell wall synthesis enzymes are known to function together, and these data also show that the DivIB-DivIC-FtsL trimeric complex remains persistently associated with these enzymes as they move around the division

site^{54,90,114}. Thus, the divisome is composed of two distinct dynamic subcomplexes: 1) a directionally-moving group of periplasmic-facing membrane proteins that includes the cell wall synthesis enzymes, and 2) a group of cytoplasmic-facing proteins that bind to the stationary subunits within treadmilling FtsZ filaments.

FtsZ binding proteins are necessary for correct Z-ring architecture

Next, we investigated the function of the stationary subcomplex, in particular the ZBPs SepF, ZapA, and EzrA. While none of the ZBPs are individually essential, $\Delta sepF$ and $\Delta zapA$ are each synthetically lethal with $\Delta ezrA$ ⁵⁵. We created a $\Delta ZBPs$ strain that lacked all ZBPs by knocking out *sepF* and *zapA* and depleting *ezrA* using a xylose-inducible promoter. We depleted EzrA for 7 hours, at which point cells were filamented, indicating that division was blocked. We additionally repeated this for all other synthetically lethal combinations of ZBPs.

Past work has suggested that FtsZ filament dynamics are modulated by other proteins *in vivo*, including the ZBPs ZapA, SepF, and EzrA⁵⁵. Both ZapA and SepF have been shown *in vitro* to promote FtsZ filament formation, stability and bundling, and to decrease FtsZ's GTPase activity^{64,65,80,85,115–118}. *In vivo*, ZapA has been shown to promote the formation of a coherent Z-ring, while SepF is involved in both tethering FtsZ to the membrane and modulating septum morphology^{19,74,77,116,119}. EzrA, meanwhile, both increases FtsZ's critical concentration and decreases filament bundling *in vitro* and inhibits Z-ring formation and modulates the rate of Z-ring recovery after photobleaching *in vivo*^{48,66,69,70,72,76}. Thus, ZapA and SepF have both been described broadly as FtsZ stabilizing proteins, and EzrA as a FtsZ destabilizer. However, FtsZ treadmilling velocity and subunit lifetime were unchanged in all synthetic lethal backgrounds (Figure 11, Supplementary Video 6). We note that, although $\Delta ezrA$ cells have longer FtsZ

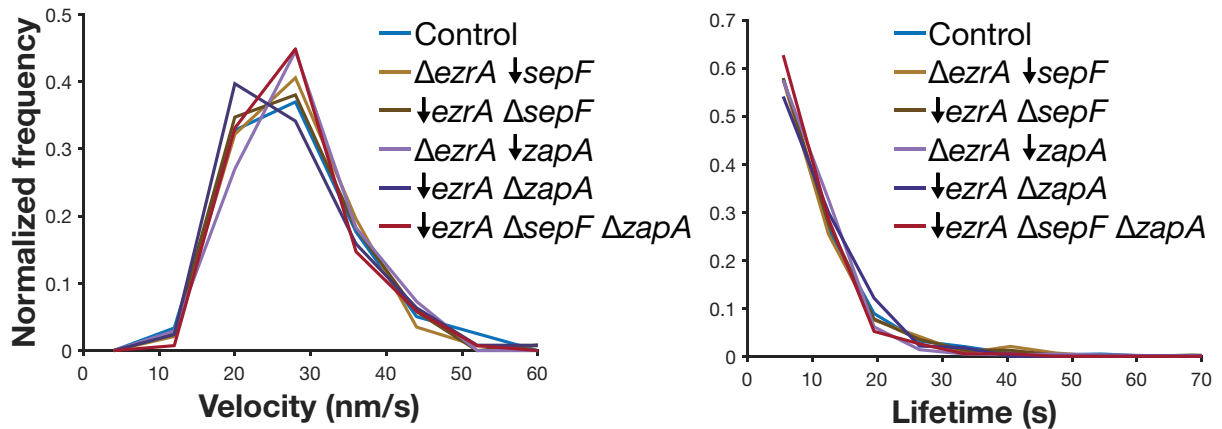


Figure 11—Velocity and Lifetime are unaffected by synthetically lethal ZBP perturbations

Velocity (*left*) and lifetime (*right*) of cells missing synthetically lethal combinations of ZBPs are unchanged from control. All synthetic lethal combinations were investigated by a combination of knockouts (indicated by Δ) and depletions (indicated by \downarrow); depletions were performed by expressing the gene under an inducible promoter until the start of the experiment, then withdrawing the inducer for 7 hours. Velocity measurements were analysed from kymographs.

subunit lifetimes, the lifetimes under these synthetic lethal conditions are statistically indistinguishable from the control¹²⁰. This suggests that EzrA's roles in bundling and in filament length modulation are separate from one another. Regardless, together these data indicate that ZBPs do not affect FtsZ treadmilling *in vivo*.

Next, we investigated whether the ZBPs instead mediated filament bundling. ZBPs have been shown to mediate FtsZ filament bundling *in vitro*, and lateral interactions between FtsZ filaments have been proposed to play a functional role in cytokinesis^{64,70,72,80,85,117–119,121}. We therefore investigated how each ZBP knockout, individually and in combination, affected Z-ring morphology. Z-ring morphology is normal in single ZBP knockouts, in the only viable double knockout ($\Delta sepF \Delta zapA$), and in all overexpression conditions except EzrA (Supplemental Figure 1, Supplemental Figure 2, Supplemental Figure 3, Supplemental Table 3).

However, in the absence of synthetically lethal combinations of ZBPs, cells showed severely altered Z-rings. Filaments no longer condensed, instead forming bands: regions of loosely-organized FtsZ filaments $\sim 1.6\times$ as wide as control Z-rings (Figure 12, Figure 13, Supplemental Table 3).

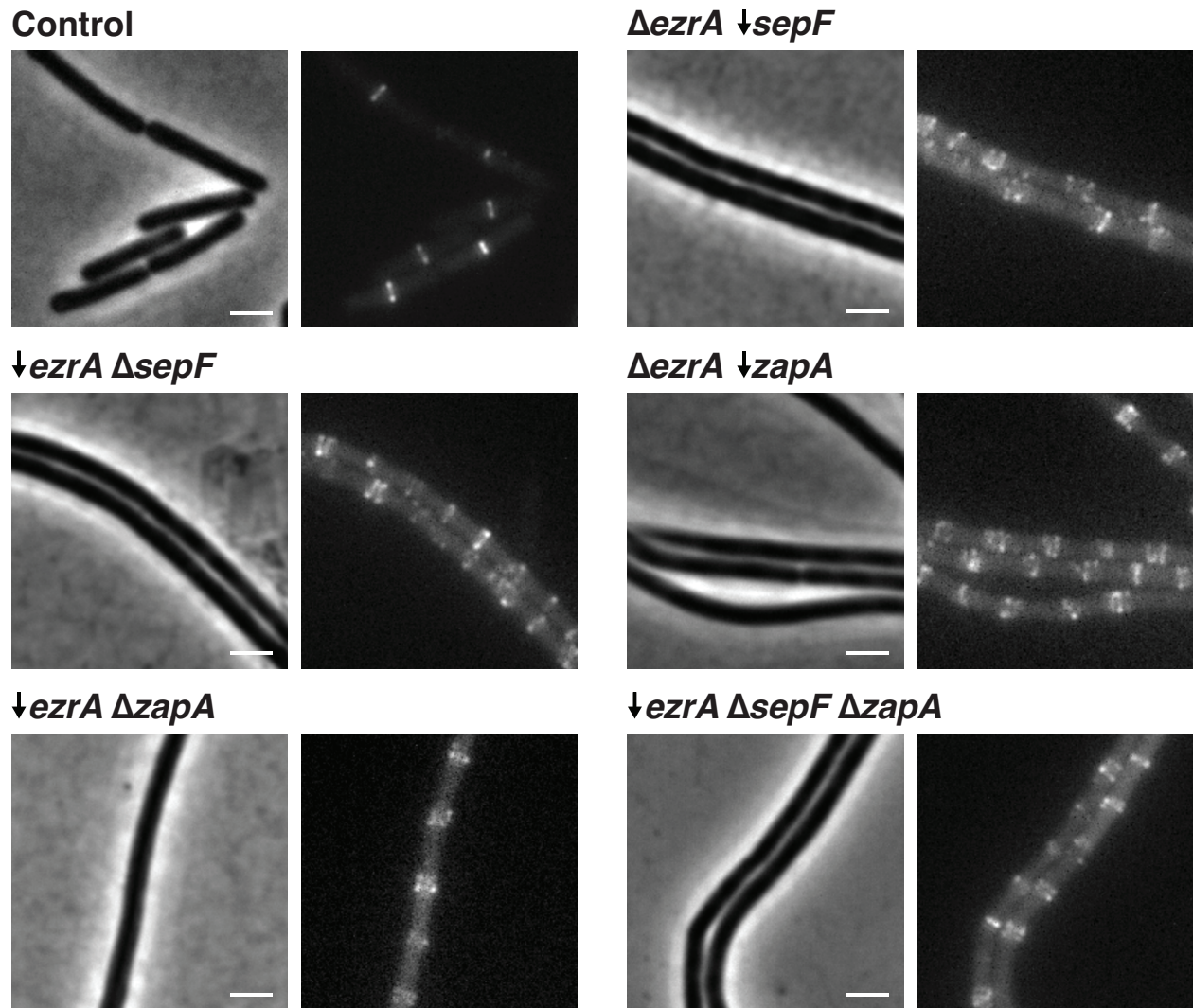


Figure 12—Synthetically lethal ZBP perturbations result in altered Z ring architecture

Phase contrast and epifluorescence image of Z ring in control cells and cells lacking synthetically lethal combinations of ZBPs. Depletions were performed by expressing each gene under an inducible promoter until the start of the experiment, then withdrawing the inducer for 7 hours. This was repeated for all permutations of synthetically lethal combinations of ZBPs; all these combinations result in elongated cells and disrupted Z ring architecture. Scale bars: 2 μm .

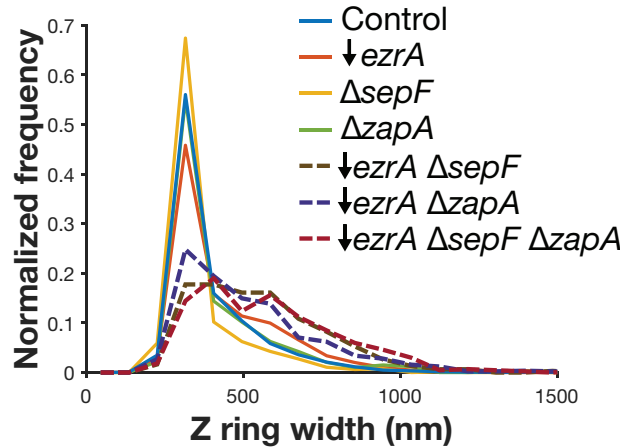
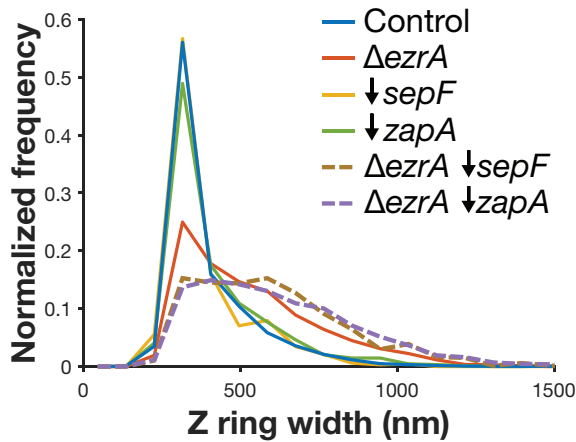


Figure 13—Z rings are wider in synthetically lethal ZBP perturbations

Widths of Z rings in each synthetic lethal combination of ZBPs, control cells, and constituent backgrounds. Z rings in cells missing synthetically lethal combinations of ZBPs are wider than control cells and cells missing individual ZBPs. Z rings were visualized using epifluorescence. Depletions were performed by expressing the gene under an inducible promoter until the start of the experiment, then withdrawing the inducer for 7 hours.

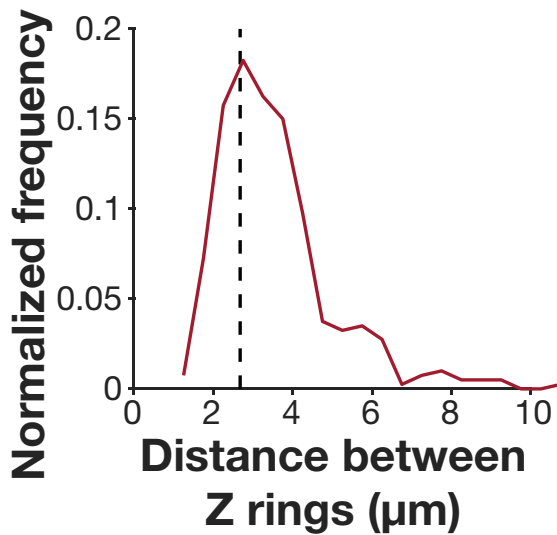


Figure 14—Perturbation of Z ring width does not perturb Z ring spacing along filaments

Distances between neighboring Z rings in Δ ZBPs cells. Δ ZBPs cells have *ezrA* depleted and *sepF* and *zapA* deleted. Dashed line: estimated spacing between Z rings in non-dividing *B. subtilis* cells, based on wildtype cell length (as described in the methods section).

These FtsZ bands were still regularly spaced apart from one another, indicating that FtsZ was still able to localize to the division site under these conditions (Figure 14). These loosely-organized filaments resemble the transient FtsZ structures that occur when FtsZ first arrives at the division site (Figure 15). Over time under normal conditions, the width occupied by these FtsZ bands decreases, ultimately condensing into a Z-ring (Figure 15).

This width also correlates with a known fiducial of maturation of the division site: recruitment of cell wall synthesis machinery (Figure 16).

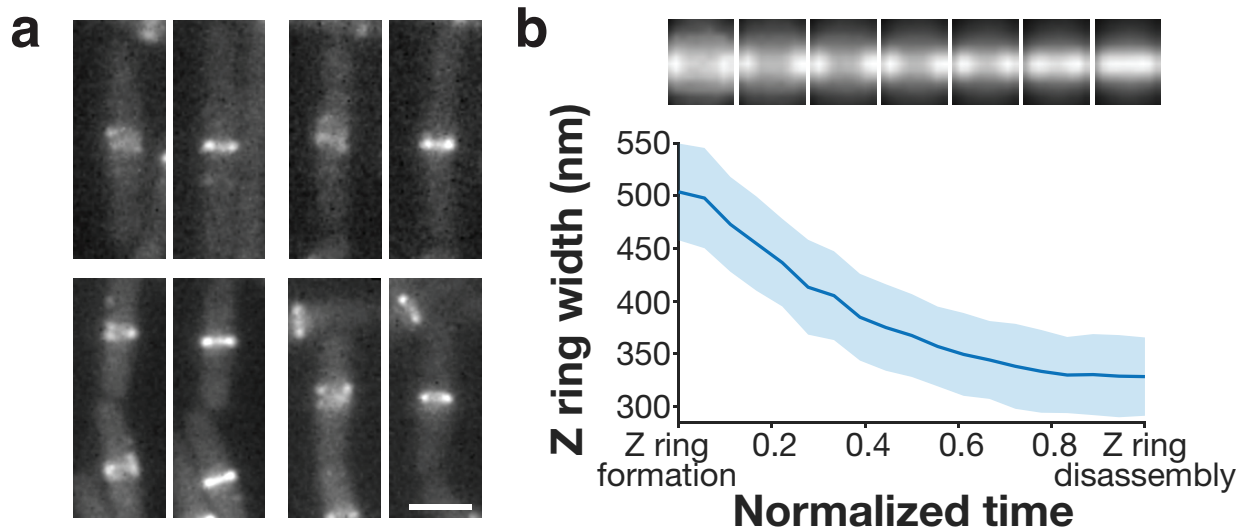


Figure 15—Z rings condense in healthy cells

(a) Z ring condensation in control cells. Each pair of images shows a newly formed Z ring that has not yet condensed (left), and the same Z ring after condensation (right). Representative images from 4 replicates. (b) *Top*: Average intensity projections of Z rings from normalized time points over the cell cycle. *Bottom*: Z ring width over the cell cycle, measured as the full width at half maximum of the average intensity projections. Time from Z ring formation to Z ring disassembly (defined as the first and last frames in which the Z ring could be detected) was normalized for each cell. Shading: bootstrapped standard error.

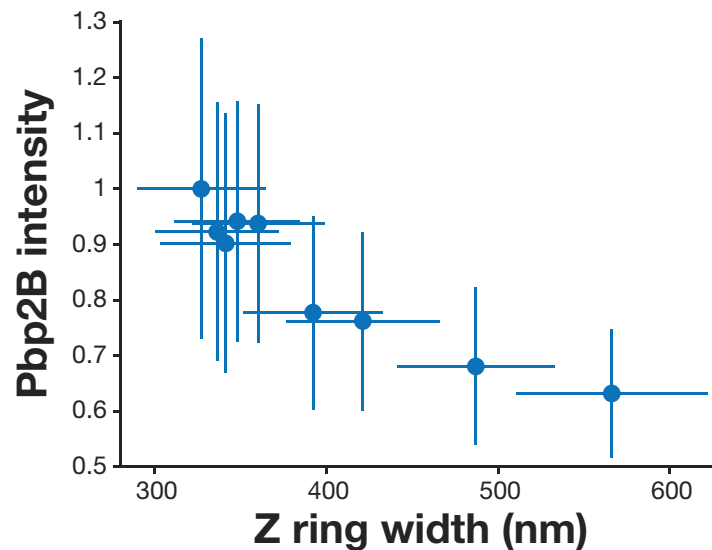


Figure 16—Z ring condensation correlates with Pbp2B recruitment in healthy cells

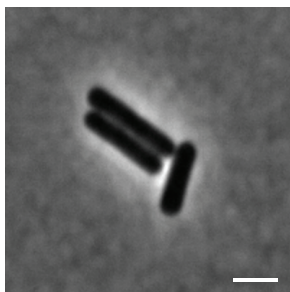
Z ring width versus Pbp2B recruitment in control cells. Pbp2B intensity at midcell is higher when Z rings are more condensed; this is expected given that Pbp2B recruitment and Z ring condensation both increase over time.

Simultaneously, FtsZ recruitment increases, further concentrating FtsZ into a smaller area. However, without ZBPs Z-ring condensation never occurs (Figure 12, Figure 13). These results agree with previous observations that ZapA and SepF promote FtsZ bundling, whereas EzrA has previously been described as an inhibitor of Z-ring formation and bundling. Here, we find that the ZBPs work collectively to promote Z-ring condensation. Thus, without ZBPs, FtsZ filaments treadmill normally and localize correctly, but cannot condense into Z-rings or divide the cell.

FtsZ bundling is responsible for Z-ring condensation

We next sought to clarify whether the Z-ring condensation is specifically due to lateral bundling of FtsZ filaments by ZBPs. If this were the case, we might expect to isolate mutations that promote lateral bundling of FtsZ filaments in cells lacking ZBPs. Thus, we conducted a suppressor screen in the Δ ZBPs strain (see methods for details). Whole-genome sequencing of the resulting suppressor candidates revealed a charge-inverting mutation (K86E) in helix H3 of FtsZ; both this helix and the homologous residue have been shown to affect lateral FtsZ filament interactions in *E. coli*^{121,122}. We hypothesized that this mutation might restore viability in the absence of ZBPs by enhancing filament interactions. Indeed, FtsZ(K86E) restored viability

FtsZ(K86E)



FtsZ(K86E) Δ ezrA Δ zapA

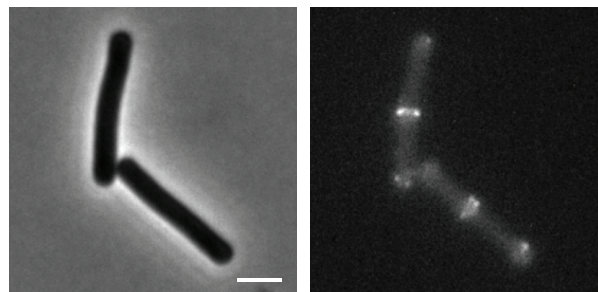


Figure 17—FtsZ(K86E) rescues Z ring morphology in synthetically lethal Δ ezrA Δ zapA

Phase contrast and epifluorescence image of Z ring in FtsZ(K86E) and FtsZ(K86E) Δ ezrA Δ zapA cells. Z rings in FtsZ(K86E) Δ ezrA Δ zapA are somewhat perturbed, but less so than typical cells missing synthetically lethal combinations of ZBPs. The extra Z rings seen here at the poles are also found in Δ ezrA cells⁶⁶. Scale bars: 2 μ m.

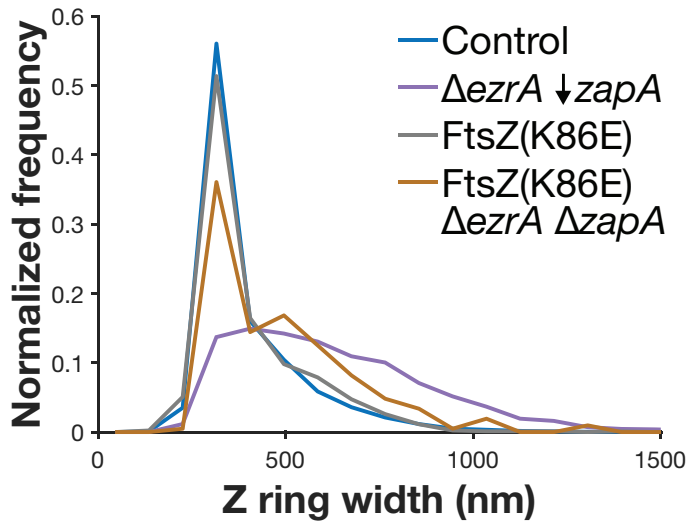


Figure 18—Quantification of FtsZ(K86E) rescue of Z ring width in $\Delta ezrA \Delta zapA$

FtsZ(K86E) $\Delta ezrA \Delta zapA$ cells have wider Z rings than control and FtsZ(K86E) cells, but Z ring width is reduced relative to the lethal depletion of ZapA in $\Delta ezrA$ cells.

and partially restored Z-ring

condensation in $\Delta ezrA \Delta zapA$ cells

(Figure 17, Figure 18, Supplemental

Table 3). Thus, Z-ring condensation

occurs due to bundling of FtsZ

filaments by ZBPs.

Interestingly, the FtsZ(K86E)

suppressor mutant can rescue the

$\Delta ezrA \Delta zapA$ cells but not other

synthetic lethal combinations.

Although the ZBPs work collectively to bundle FtsZ filaments, they may each affect bundling

differently. Beyond their role as bundlers, the ZBPs have been shown to have distinct

functions⁵⁵. Thus, the fact that FtsZ(K86E) can replace EzrA and ZapA but not SepF may reflect

that each ZBP has different effects on FtsZ superstructure.

Z-ring condensation increases cell wall synthesis, but this is not essential

Next, we investigated whether Δ ZBPs cells were unable to divide due to decreased septal cell wall synthesis, which is required for cell division. In Δ ZBPs cells, we investigated the localization and motion of the division-specific cell wall synthesis enzyme Pbp2B, as well as septal cell wall synthesis activity. Pbp2B recruitment to the Z-ring decreased by 50% in Δ ZBPs relative to control cells (Figure 19).

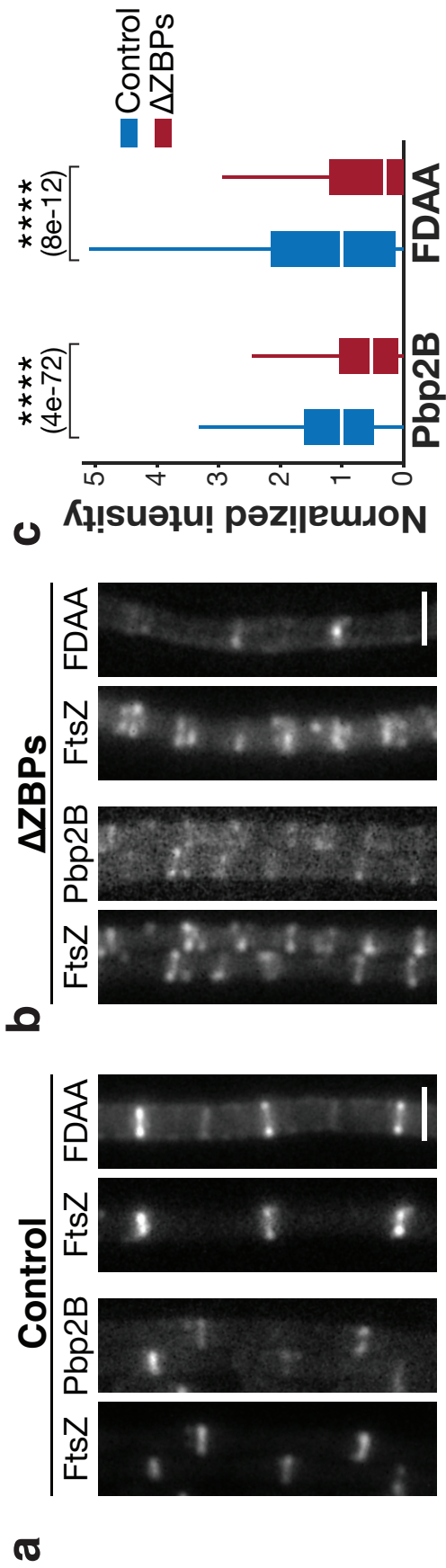


Figure 19—Cell wall synthesis protein localization and activity are reduced at non-condensed Z rings Colocalization of Pbp2B and FDAA labelling with FtsZ in in (a) control cells and (b) Δ ZBPs cells (*ezrA* depletion in a Δ *sepf* Δ *zapA* background). At least two replicates for each condition. (c) Amount of Pbp2B and FDAA labelling at the division site, measured by fluorescence intensity. N > 1000 for each condition. For each box plot, the white line indicates the median, the box extends to the 25th and 75th percentiles, and the whiskers indicate 1.5x interquartile range. P-values were obtained from a two-sided t-test; **** indicates p<0.0001, and p-values are included in parenthesis.

We found that in Δ ZBPs cells, Pbp2B continued to move directionally at midcell; because the directional motion of Pbp2B reflects its activity, this suggests that it remains active under these conditions (Figure 20, Figure 21). To assay the activity of cell wall synthesis enzymes more directly, we measured the incorporation of fluorescent D-amino acids (FDAAs) into the division site²⁶. FDDA incorporation was still present in Δ ZBPs but reduced 40% relative to the control (Figure 19). Thus, septal cell wall synthesis enzymes are still active in the absence of the ZBPs. Next, to

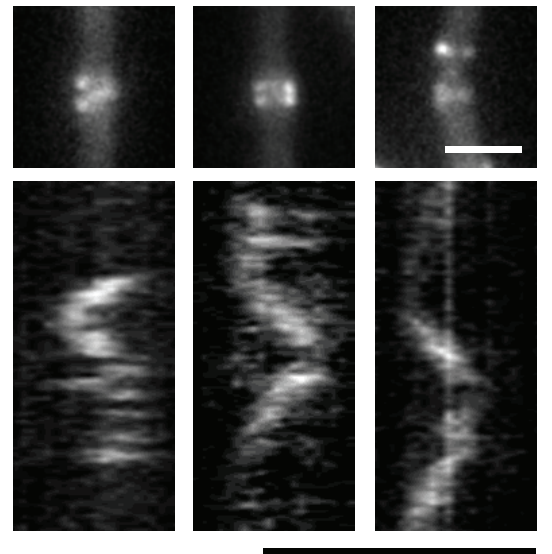


Figure 20—Pbp2B dynamics are observed at non-condensed Z rings

Pbp2B dynamics in Δ ZBPs. *Top*: Z rings imaged by epifluorescence. *Bottom*: Kymographs drawn at these Z rings of single-molecule Pbp2B motion. Scale bars: horizontal: 2 μ m, vertical: 1 min.

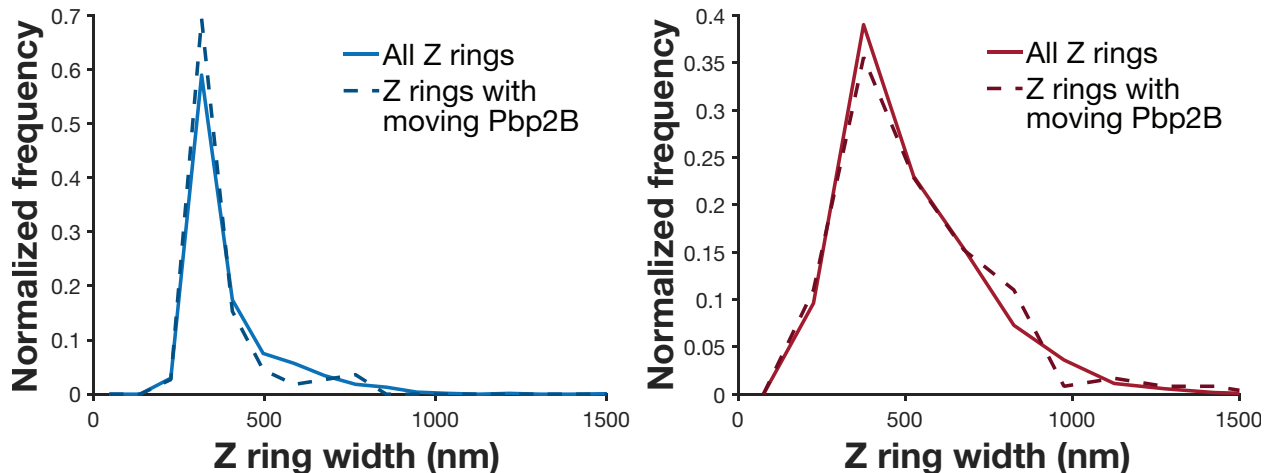


Figure 21—Pbp2B directional motion is seen at Z rings of all widths

Z ring width distributions of all Z rings (solid lines) and the Z rings at which Pbp2B directional motion was identified by particle tracking (dotted lines; tracking as described in the methods section). The difference in Z ring width profiles is evident between healthy cells (left) and Δ ZBPs cells (right). In both conditions, Pbp2B directional motion is found at Z rings representative of the entire population.

understand whether the decrease in Pbp2B recruitment was due to FtsZ's inability to condense in Δ ZBPs cells, we asked whether the FtsZ(K86E) suppressor mutant restored Pbp2B localization to midcell. Although this mutant allowed Δ ezrA Δ zapA cells to divide and partially rescued Z-ring condensation, it did not rescue Pbp2B recruitment (Figure 22). This indicates that the failure of Δ ZBPs cells to divide is not due to defects in Pbp2B recruitment. This also suggests that the ZBPs may play a role in recruiting the late proteins to the division site that is independent of their effects on FtsZ.

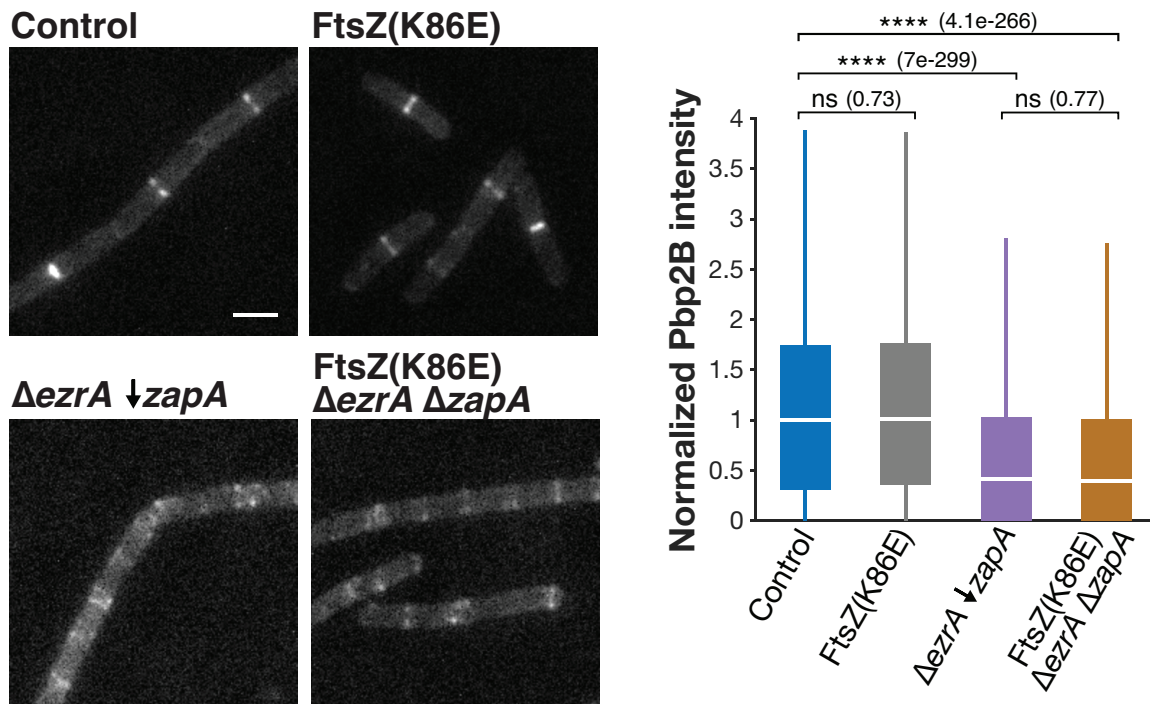


Figure 22—Pbp2B recruitment is not rescued by FtsZ(K86E)

Pbp2B intensity at midcell in FtsZ(K86E) mutant cells. *Left*: Representative images of Pbp2B in the indicated strains, visualized by epifluorescence imaging of cells expressing Pbp2B-mNeonGreen. *Right*: Pbp2B intensity at the division site in each strain. Although the FtsZ(K86E) restores viability in a Δ ezrA Δ zapA strain, it does so without rescuing Pbp2B recruitment to midcell.

FtsA knockouts are severely perturbed, unlike for other FtsZ binding proteins

Finally, we investigated the effects of FtsA on FtsZ filaments. FtsA is an actin homolog that serves as FtsZ's primary membrane tether, and *B. subtilis* Δ ftsA cells are less viable and have a strong division defect and altered Z-ring morphology^{58,62,63}. FtsA has been shown *in vitro*

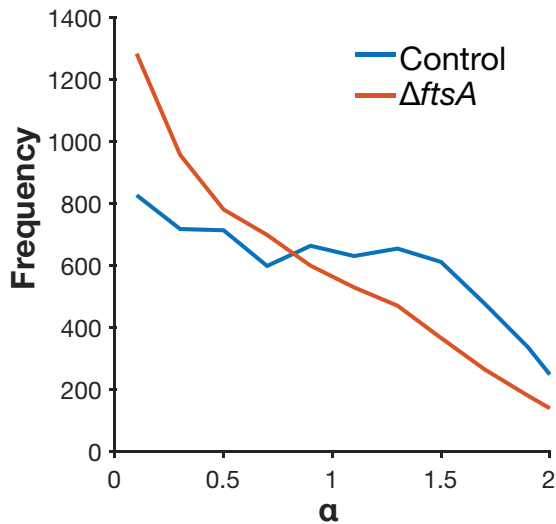


Figure 23—FtsZ motion is perturbed in \DeltaftsA cells
 α values for FtsZ motion in control and \DeltaftsA cells, obtained by tracking FtsZ filament motion and fitting each track to $MSD(\Delta t) = D \cdot \Delta t^\alpha$. $\alpha > 1$ indicates directional motion, so FtsZ filaments in \DeltaftsA cells exhibit less directional treadmilling compared to control cells.

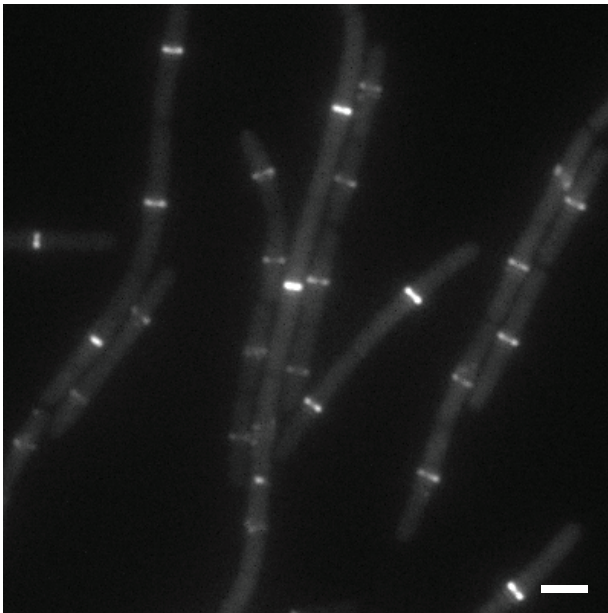
and *in vivo* to modulate FtsZ treadmilling^{26,49}.

Indeed, \DeltaftsA cells showed a decrease in the fraction of directionally-treadmilling FtsZ filaments (Figure 23, Supplementary Video 7).

Thus, unlike the ZBPs, FtsA modulates FtsZ filament treadmilling. It has also been suggested that FtsA might regulate FtsZ bundling¹²³. We

observe Z-ring morphology defects in the \DeltaftsA strain, but these defects are distinct from the condensation defect observed in the $\Delta ZBPs$ strain (Figure 24). Because \DeltaftsA cells have

Control



\DeltaftsA

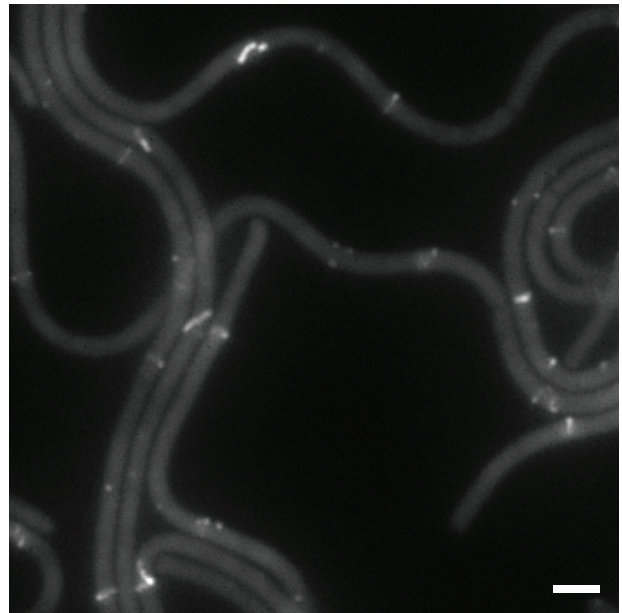


Figure 24—FtsZ localization is severely perturbed in \DeltaftsA cells

Epifluorescence images of Z rings in control cells and \DeltaftsA cells. FtsZ-mNeonGreen induced with 30 mM xylose for 2 hours) in control cells and \DeltaftsA cells. In \DeltaftsA cells, FtsZ is expressed with 10 μ M IPTG from the pHyperSpank promoter; higher or lower expression levels do not allow for cell survival. Scale bar: 2 μ m.

severely perturbed FtsZ filaments, it will be difficult to decouple these effects from any possible higher-order effects on their bundling state.

Discussion

Combined with past work, these experiments provide new insights into the mechanisms underlying bacterial cell division. The cell division process begins with short treadmilling FtsZ filaments that are restricted to midcell by negative regulators. Our data reveal that FtsZ filaments treadmill at their biochemical steady state; their dynamics are not modulated by other factors. However, FtsZ cannot form a functional Z-ring on its own: ZBPs are also required to bundle FtsZ filaments into a condensed Z-ring, transiently interacting with stationary FtsZ subunits without affecting filament dynamics. Z-ring condensation increases the recruitment of cell wall synthesis enzymes to the division site, which move around the division site as part of a directionally-moving complex. This condensation is ultimately necessary for cell division (Figure 25). FtsZ bundling proteins have been identified across the bacterial tree and even in archaea, suggesting that Z-ring condensation may be an important process across diverse organisms^{18,78,83,124–126}.

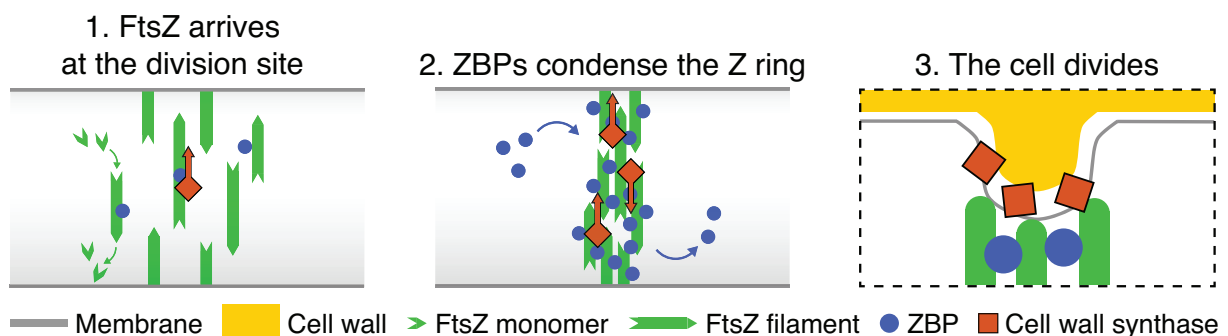


Figure 25—Condensation is necessary for cell division

Left: At the start of the cell division process, FtsZ filaments treadmill around the cell circumference at midcell. *Centre:* Stationary ZBPs transiently bind to FtsZ filaments to condense the Z ring. *Right:* ZBP-driven bundling of FtsZ filaments may also function during cytokinesis, where crowding may induce inward membrane deformations, both concentrating cell wall synthesis to the Z ring and orienting it to divide the cell in two.

These results also yield new insights into the role of Z-ring condensation in bacterial cytokinesis. Why is FtsZ filament bundling required for division, and what role does it play in the process? In contrast to previous models, FtsZ bundling does not modulate FtsZ treadmilling dynamics, but rather condenses the Z-ring^{121,127}. While condensation is not required for the activity of division-associated cell wall synthesis enzymes, it may be necessary to concentrate their activity in a small enough region to allow for productive septation. It is also possible that lateral filament association serves to inwardly deform the membrane. FtsZ has been seen to deform liposomes when filaments coalesce and crowding of membrane-associated proteins is sufficient to deform membranes^{24,37,128}. Such deformations may be easier if the periplasm is iso-osmotic with the cytoplasm, which would reduce the force required for membrane deformation^{129,130}. This membrane deformation could then direct circumferential septal wall synthesis inward to divide the cell^{26,131}.

Chapter III—Discussion

This systematic investigation of the divisome has 1) defined new functional groups of proteins *in vivo*, 2) revealed how these proteins help organize the underlying FtsZ filaments, and 3) demonstrated how these proteins are in turn collectively organized by FtsZ. As this work has focused on understanding the divisome as an entire complex, I will begin this discussion by focusing on each of its two subcomplexes: first stationary FtsZ and FtsZ binding proteins and then the directionally-moving subcomplex. I will then discuss what we do and do not understand about how these subcomplexes interact. Finally, I will address what studying these groups of proteins collectively reveals about the central organizing role of FtsZ—specifically, how architecture and dynamics represent separable modes of organization. All these results and discussions are best considered not only in the light of the pre-existing literature, but the considerable concurrent effort on all these topics by a dedicated community of researchers.

The stationary divisome

Cell wall synthesis enzymes can move processively along treadmilling FtsZ filaments. Ultimately, then, there is an interface in the divisome between stationary and moving components (the nature of this interface is discussed below). Since FtsA, EzrA, SepF, and ZapA are all stationary, this interface is not at a known FtsZ binding site. This contrasts with a homolog of FtsZ (TubZ: also prokaryotic and also treadmilling in cells) that has an associated tip-tracking mechanism. In this system, TubR binds the C-terminal tail of TubZ and, in complex with the DNA element *tubC*, can processively track the tails of treadmilling TubZ¹³². This paradigm resembles eukaryotic systems where microtubule binding proteins move directionally (albeit diffusively) along the filament^{132,133}. In contrast, known FtsZ binding proteins (with FtsA, EzrA,

and SepF binding the C-terminal tail of FtsZ, reminiscent of TubR-TubZ interaction) do not show motion along treadmilling FtsZ.

Perhaps obviously, when imaged in bulk (rather than as single molecules), these proteins will display the dynamics of the underlying FtsZ scaffold. This has been shown for *EzrA* in *S. aureus* and *S. pneumoniae*, with this intuition formalized in a “diffusion-and-capture” model^{22,54,134}. There is variation in details of these dynamics, as seen in the single-molecule residence times of the proteins (Figure 7, Supplemental Table 1). However, these residence times are either similar to or shorter than FtsZ residence times. There are no noticeably longer residence times despite the fact that non-FtsZ structures are observed at the *B. subtilis* division site using cryo-electron tomography and multiple FtsZ binding proteins can self-interact^{51,65,74,77,85,135}.

In the context of dynamics, then, it is perhaps best to think about the FtsZ binding proteins as an extension of the FtsZ filament. They do not introduce the directional motion along the filament but remain stably associated with stationary FtsZ subunits.

The dynamic divisome

FtsW-Pbp2B

This work is part of a larger effort that has shown that the two division-specific cell wall synthesis proteins—FtsW and Pbp2B in *B. subtilis*—work in tandem. The role of SEDS proteins (FtsW and its family) as cell wall synthesis proteins was only recently discovered^{91,136}. FtsW’s glycosyltransferase activity has since been verified *in vitro* and *in vivo* in *E. coli*^{90,92}. *In vitro* the activity of FtsW from a variety of species depends on the presence of that species’ Pbp2B homolog (though the Pbp2B can be catalytically inert)⁹⁰. Consistent with this, *in vivo* FtsW and

Pbp2B single-molecule imaging reveals coincident dynamics in *S. pneumoniae*, *E. coli*, and—in this study—*B. subtilis*^{54,92}.

The peptidoglycan cell wall is organized along two axes—chains extended by glycotransferase activity and crosslinked by transpeptidase activity. Now we know that these two activities are coordinated by SEDS-Pbp complexes *in vivo* and *in vitro*. While these SEDS-Pbp complexes separate the two activities between two enzymes, bacteria do encode bifunctional cell wall synthesis enzymes capable of both glycosyltransferase and transpeptidase activity. However, it has been shown in *E. coli* that these proteins are unnecessary in the context of the filament-protein based elongation and division systems¹³⁷. Perhaps comparisons between regulation of bifunctional and SEDS-Pbp complexes will reveal advantages for separating these activities between two proteins at both elongation and division sites. In *E. coli*, slowing down FtsZ results in more crosslinking of strands but fewer elongated strands (and the nature of the crosslinks is altered)²⁵. Perhaps separation of these two reactions into two proteins allows them to be tuned relative to each other.

The division Pbp2B-FtsW complex should also be compared to the equivalent complex in the elongation system. *B. subtilis* elongation involves a SEDS-Pbp complex moving along with the filament-forming actin-homolog MreB. However, in the elongation system, MreB subunits move along with the entire filament; motion depends on cell wall synthesis, not polymerization; and MreB filaments act as a rudder, not an engine^{138,139}. Future study may reveal how regulation of and interactions with SEDS-Pbp complexes vary with such well defined differences in the directional motion of these complexes. Alternatively, future studies may reveal that

these complexes offer robust cell wall synthesis mechanisms that allow them to be coupled to markedly different scaffolds with little adaptation.

One other contrast presents itself in these results: between the *E. coli* and *B. subtilis* divisomes. The homologous *E. coli* FtsW-FtsI complex moves processively at two different speeds. The faster 32nm/sec depends on FtsZ; a slower movement at about 8nm/sec depends on peptidoglycan synthesis and is thought to represent active FtsW-FtsI⁹². This slow-moving complex additionally includes FtsN, which has no *B. subtilis* homolog¹⁴⁰. Here we found that Pbp2B and FtsW do not show this bimodal velocity distribution. This discrepancy emphasizes the importance of studying cell biology throughout a range of diverse bacteria. *B. subtilis* septum closure is slowed when FtsZ treadmilling is slowed, but *E. coli* septum closure is not^{20,26}. The architecture of *B. subtilis* and *E. coli* cells walls are markedly different with *B. subtilis* adding material to the inside of a thick cell wall and *E. coli* tightly coordinating construction with recycling old material³³. Given that FtsW-FtsI occupy these “two tracks” in *E. coli* but not in *B. subtilis*, it would be informative to know whether the spatially separable rings of FtsZ and the cell wall synthesis proteins seen in *E. coli* are also found in *B. subtilis*^{141,142}. Further study of the FtsW-Pbp2B complex in bacteria with diverse physiology will certainly reveal further distinctions, perhaps revealing relationships between cellular morphology and the molecular details of division.

One promising avenue into this complex’s activity and regulation should be briefly noted: so-called “hyperactive” mutants have been identified in *E. coli* and *C. crescentus*; however, the nature of this increased FtsW-FtsI complex activity is not yet understood.^{91,143}

DivIB-DivIC-FtsL

The *E. coli* homologs of DivIB, DivIC, and FtsL—FtsQ, FtsB, and FtsL, respectively—are better studied than their *B. subtilis* counterparts. FtsB and FtsL interact with each other by a leucine zipper and with FtsQ at their periplasmic C-termini to localize to the division site^{144,145}. An *E. coli* FtsBLQ complex is well established and can form with 1:1:1 or 2:2:2 stoichiometry^{146,147}.

Considerably less is known about a putative Gram-positive DivIB-DivIC-FtsL complex. Various *in vitro*, bacterial two-hybrid, and yeast three-hybrid studies in *B. subtilis* and *S. pneumoniae* establish interaction between these proteins, Pbp2B, and FtsW^{114,148–151}. This study not only verifies these results *in vivo*, but shows that these interactions are long-lived: DivIB, DivIC, FtsL, Pbp2B, and FtsW remain stably associated as they move processively around the division site.

A concurrent, complementary set of results shows that *P. aeruginosa* FtsBLQ increases glycosyltransferase activity of the FtsW-FtsI complex *in vitro*¹⁵². Omitting FtsQ, a FtsBL complex shows similar glycosyltransferase stimulation, and two FtsL mutants defunct for this stimulation display dominant-negative phenotypes *in vivo*, suggesting physiological relevance¹⁵².

Both that *in vitro* study and this *in vivo* work would be bolstered by complementary work in the other's organism. This work's finding that *B. subtilis* DivIB, DivIC, and FtsL form a complex *in vivo* would be furthered by testing for similar stimulation of *B. subtilis* cell wall synthesis *in vitro*. In turn, the physiological relevance of the *in vitro* activity would be better understood with an understanding of how FtsB, FtsL, and FtsQ move in *E. coli*. It would be informative to see if these proteins are enriched with the slower-moving FtsI-FtsW-FtsN complex, which is thought to be actively synthesizing cell wall^{92,140}.

The idea that DivIB, DivIC, and FtsL are handles for regulating cell wall synthesis is attractive based on previous results. 1) These proteins' levels are readily changed and therefore their activities readily regulated. FtsL degrades rapidly—even more so in the absence of DivIB—and reducing FtsL degradation also reduces DivIC degradation^{94,153}. In this paradigm, the putative chaperone POTRA domain in DivIB may play this FtsL stabilizing role¹⁰³. This is consistent with FtsL overexpression rescuing $\Delta divIB$ at lethally high temperatures¹⁵³. However, the relationship between these proteins is not straightforward: even though DivIB protects FtsL from degradation, DivIC is degraded in a DivIB-dependent manner in the absence of FtsL^{148,153}. 2) As discussed in the introduction, FtsL levels integrate signals from beyond the divisome. FtsL is a known target of the metalloprotease RasP, and is protected from RasP degradation by dimerization with DivIC^{94–96}. Perhaps structural proteins are regulated in other pathways also. 3) There is evidence relating *in vivo* Pbp2B activity and these proteins in *B. subtilis*. Point mutations in Pbp2B's periplasmic region can rescue $\Delta divIB$ in lethal conditions¹⁴⁸. Additionally, cells with Pbp2B's enigmatic PASTA domain deleted resemble $\Delta divIB$ cells and this PASTA domain is required for interaction with DivIB⁸⁹. Taken together, these results strongly suggest that the stationary proteins provide regulatory handles on the directionally-moving divisome complex. Indeed, the cell length distributions of DivIB, DivIC, and FtsL fusions (Figure 3) show that these fusions can support not only wildtype length but even shorter cells, suggesting that these proteins are limiting for division.

In any case, if these recent FtsBLQ *in vitro* results hold for *B. subtilis*, then the divisome's dynamic subcomplex contains not only two orthogonal modes for cell wall synthesis, but also additional proteins regulating their activity. This complex not only conducts and regulates these

multiple chemical reactions, but also processively moves along with a treadmilling filament (the topic of more discussion below). Clearly, bacterial cytokinesis is not as simple as localizing enzymes in a ring. Not only are complex spatiotemporal patterns established by FtsZ filaments, but processes downstream of these filaments are multifaceted and sophisticated.

Coordination of stationary and dynamic divisome subcomplexes

These results make explicit a realization implied by early single molecule results of FtsZ and Pbp2B: the divisome “complex” is not a single long-lived assembly of proteins. Rather one part is a scaffold (FtsZ) with many binding partners and the other is a processively moving group of at least five proteins.

So how are the stationary and moving subcomplexes interacting? The dynamic subcomplex moves with treadmilling FtsZ filaments—even though any given molecular site in those filaments is stationary—presenting a new, uncharacterized molecular motor system. However, the nature and molecular details of the interaction between the processively moving complex and the underlying FtsZ filament are still not understood. Two models for this interaction present themselves: direct and indirect.

Direct interaction

As discussed in the introduction, there is no known interaction between FtsZ and the cell wall synthesis proteins. However, in the light of these results there is a more severe lack of knowledge in *B. subtilis*: there is no known protein-protein interaction between any stationary protein and any moving protein. While these results provide a drastic problem, they also assist any search for a direct-interaction solution by providing a well-defined group of stationary and mobile proteins (and, by extension, a more limited potential interface between them).

Unfortunately, much of the insight from the more-extensively studied *E. coli* is of little use as the best characterized direct interactions between the homologs of these groups is mediated by FtsN, which is absent in *B. subtilis*^{55,134,140,154,155}. Alternatively, it has been recently found that *E. coli* FtsQ's cytoplasmic region can colocalize with FtsA and FtsZ on membrane *in vivo*¹³⁴. However, this region of *B. subtilis* DivIB is dispensable in conditions where DivIB is essential⁹⁸. Perhaps most promising are multiple lines of complex genetics experiments in *E. coli* looking for mutations in divisome proteins that can bypass the loss of other divisome components^{143,155–159}. Looking broadly at these results, special attention might be paid to FtsA, FtsL, and FtsW; however, relevant residues are often not conserved in *B. subtilis* (especially in FtsL) making it hard to translate the research based on the genetic data alone¹⁵⁸. Additionally, none of these results are definitive proof of direct interaction. For example, the only evidence directly testing direct interaction between FtsA and FtsW comes from bacterial two-hybrids, therefore more stringent verification is warranted¹⁵⁹.

Despite a lack of evidence, the strongest argument for processive motion involving direct interaction is precedent from other systems. Principles from such systems have allowed the dynamics of the divisome to be modelled as a Brownian ratchet invoking only diffusion of the moving components and their binding to FtsZ¹⁶⁰. Hopefully, future models in this vein will consider that the directionally-moving complex interacts multivalently with the cell wall. In addition to FtsW and Pbp2B, which interact with peptidoglycan at their catalytic site, DivIB also binds PG *in vitro*¹⁰⁵.

Indirect Interaction

Given the lack of known direct interactions, a model by which stationary and mobile divisome proteins interact indirectly—particularly via membrane deformation—is alluring. The combination of polymerization and membrane-interaction found at the division site can underlie membrane deformation. Enriching amphipathic helices and crowding of proteins on membranes are known to induce membrane curvature^{128,161}. This effect has been demonstrated *in vitro* for multiple bacterial systems: *E. coli* MinD can deform lipids by assembling into larger structures, as can rings formed from *E. coli* FtsA and FtsZ^{39,162}. Recent cryo-electron tomography structures show multiple ordered protein structures at the *B. subtilis* division site, with an additional filament closer to the membrane than FtsZ, thought to be FtsA¹³⁵.

Notably, SepF and FtsA both have amphipathic helices that can bind membrane, and both self-interact^{51,74,77,85}. SepF is essential in bacteria without FtsA, such as Mycobacteria and Actinobacteria^{82,83}. In *B. subtilis*, which has both SepF and FtsA, the proteins are synthetically lethal, and while $\Delta ftsA$ is clearly severely impaired (Figure 24), its growth rate is recovered by SepF overexpression⁸¹. In the SepF-less *E. coli*, FtsA is essential, even though there is another membrane anchor for FtsZ, ZipA¹⁶³.

These results, taken together, are highly suggestive that SepF and FtsA play a key role in any membrane deformation that may occur at the division site. However, direct *in vivo* evidence is lacking. The most readily available starting point may be an *E. coli* FtsA in which the amphipathic helix was replaced with the transmembrane of a non-division protein¹⁶⁴. This construct is viable, but no aspect of its cell biology has been investigated—it would be

informative to know if such a radical change in the membrane interaction leads to any division or physiological defects.

Another next step is to perturb the indirect intermediary—the membrane—and look at the effects on division and its dynamics *in vivo*. The increasing complexity that is achieved in *in vitro* reconstitution systems will also offer tractable experimental handles on how various complexes of division proteins both induce and respond to membrane deformations^{134,165}.

If FtsZ and the FtsZ binding proteins do curve the membrane, how does this lead to the localization and directional motion of the downstream complex? The only substantial insight comes from a structure of the FtsBLQ complex—the Gram-negative homologs of DivIB, DivIC, and FtsL. The shape of this complex suggests that it would associate with a convex membrane, such as that found at the septum as it is constructed¹⁴⁷. However, as tempting as these results are, it must be noted that CLEM (correlative light-electron microscopy) results show that FtsZ is unable to constrict membrane in *E. coli* cells without cell wall synthesis⁴⁰. Additionally, it is difficult to imagine how such an indirect interaction could lead to the processive motion of proteins at the same velocity with treadmilling FtsZ filaments. If enriching membrane interactions and crowding proteins on the membrane is critical, why is processive motion still found when FtsZ does not form a condensed ring (Figure 20, Figure 21)?

Separability of modes of FtsZ organization

This result (that FtsZ supports processive motion of the cell wall synthesis machinery even when Z-ring morphology is considerably perturbed) reveals a powerful principle behind organization at the division site. FtsZ is organized in multiple independent modes. This idea was

perhaps best captured previously in studies of EzrA. EzrA's ability to inhibit the formation of extra Z-rings at cell poles is separable from its destabilization of the Z-ring at midcell using the QNR patch mutant⁷⁶. While in this case, the molecular basis of each type of organization is not easily described, the principle is evident: there are multiple facets of division that can be independently tweaked.

Here we again find two independent facets of division. They are literally orthogonal axes of organization: treadmilling along the length of the protofilament and bundling by lateral interaction across protofilaments. FtsZ has long been thought of as a signal integration point, whose organization is impacted by a breadth of regulating factors¹⁶⁶. Perhaps having multiple modes of organization allows for such integration as it provides distinct handles for regulation. These forms of oligomerization (filaments and bundles) provide independent parameters underlying this fundamental biological process. One parameter could be changed without drastically altering another facet of the system.

Curiously, there may be a relationship between these results and the earlier EzrA results. In addition to being involved in every synthetic lethal combination shown here (Figure 12), EzrA also regulates FtsZ subunit lifetime and protofilament length¹²⁰. As with previous EzrA phenotypes, these effects are separable¹²⁰. It will be straightforward and informative to learn which of these effects are disrupted in the QNR patch mutant.

The idea that FtsZ organization is compartmentalized is useful but obviously the reality is more complicated. For instance, regulation of these otherwise separate modes is combined in EzrA.

The essential nature of Z-ring condensation

Given that Z-ring condensation is separable from dynamics, what is the downstream effect of bundling? Why do the synthetic lethal conditions fail to divide? At this point, only speculation is possible. Cell wall synthesis must be evenly distributed around the *B. subtilis* division site for efficient division, perhaps it must also be concentrated laterally for a septum to emerge from the side wall. Progress may be achieved by studying systems in which similar phenotypes were previously observed: *E. coli* and *C. crescentus* $\Delta zapA$ cells have dispersed non-ring FtsZ clusters and *C. crescentus* cells with FtsZ's linker removed from the C terminus also forms into wider regions^{19,167,168}. A similar phenotype was also reported in $\Delta ftsA$ null *B. subtilis*, but that was not observed in this study (Figure 24)⁶³.

The relationship between Z-ring condensation and recruitment of downstream proteins is also unclear. Pbp2B localization and activity are reduced in the synthetic lethal conditions (Figure 19), but this reduction persists as Z-ring width is recovered and viability is restored with FtsZ(K86E) (Figure 22). Perhaps Pbp2B localization is reduced in one of the constitutive deletions (particularly $\Delta ezrA$ which is common to all synthetic lethal backgrounds) and this reduction is a cause, not a downstream effect, of the synthetic lethality.

This ability to recover viability without recovering Pbp2B localization is not the only complication in the relationship between Z-ring width and viability. Scrutiny of Z-ring width distributions (Figure 13) reveals that while viable $\Delta ezrA$ cells have more condensed FtsZ than synthetically lethal backgrounds, the distribution is clearly wider than wildtype, $\Delta zapA$, and $\Delta sepF$ cells. These viable $\Delta ezrA$ cells are slightly longer than wildtype cells in minimal media and more than twice as long in the richer conditions used in this study (Figure 4)⁶⁶. Apparently, Z-

ring condensation can be perturbed to an extent before the effect is lethal, and it is unclear what specific change delineates these two regimes.

All these results are consistent with, but do not require, a model in which both the amount and distribution of cell wall synthesis along the length of the cell are important for efficient cytokinesis. It will be worth testing if increasing the amount or activity of Pbp2B at the division site changes the extent to which Z-ring condensation can be perturbed before cells die.

Cytokinesis and bacterial cell biology

This work is part of a large, long-term concerted effort to understand how the filament-forming FtsZ and its associated coterie of division proteins reorganize one bacterium into two bacteria through cytokinesis. By bringing many proteins, each with their own rich literature, into systematic frameworks, we are beginning to paint a clearer picture of what the divisome is, how it is organized, and how this organization impacts physiology. At the core is a self-interacting protein, FtsZ, capable of multiple forms of spatiotemporal patterning. Filaments of FtsZ are adorned with multiple binding partners that collectively lead to structures beyond the protofilament scale. Meanwhile, complexes of multiple cell division proteins and their putative regulators move around and along with the moving protofilaments in these structures, building cell wall.

Hopefully this work is followed by studies that identify: how FtsZ dynamics are transduced across the membrane to processively moving complexes; if and how DivIB, DivIC, and FtsL regulate their associated cell synthesis enzymes; and how perturbation of FtsZ condensation prevents efficient cell division. Repeating these assays in a diverse range of prokaryotes will also be valuable. Variation among organisms helps identify the most deeply

conserved elements of prokaryotic division: unifying mechanisms and principles that underpin life across an enormous evolutionary space. Discovering variation among organisms is also intrinsically valuable. Prokaryotes proliferate in a spectacular array of shapes³¹. Division not only captures the themes common to this broad clade, but also the variation intrinsic to their successful adaptation and radiation.

Further into the future it will be thrilling to find out what this work missed, got wrong, and which clear future directions eluded us. Our understanding of prokaryotic cytokinesis is intrinsically linked to the methods and technology available to us. When SepF was first identified, its discoverers thought to observe the synthetic lethality of cells lacking SepF and EzrA, as has been repeated here⁷⁴. They looked at FtsZ and Pbp2B localization, seeing some abnormal Z-rings, but finding that this was a relatively rare phenotype⁷⁴. The discovery of FtsZ condensation in this study came from the ability to reliably image cells for hours at higher resolution and with more readily quantifiable data. (It also came from the willingness to reinvestigate something that had not been looked at in over a decade.) As live-cell imaging techniques improve, reconstitution systems become more complex, and structural studies can tackle larger assemblies of proteins our understanding of bacterial cytokinesis will advance both predictably and surprisingly. Surely, though, the notion that superficially-simple single-celled organisms consist of sophisticated molecular underpinnings will persist and develop as it has here.

Appendix A—Methods for Chapter II

Culture growth

Strains were stored as glycerol stocks at -80°C . At the start of each experiment, strains were streaked onto LB agar plates containing the appropriate antibiotic and incubated overnight at 37°C . For strains whose survival was dependent on the induction of a promoter, these plates were additionally top spread with xylose or IPTG at the appropriate concentration. For imaging, single colonies were inoculated into 1 mL casein hydrolysate (CH) media and grown on a roller at 37°C until they reached mid-exponential-phase growth (OD_{600} around 0.2). Cells were back diluted 1:10 and again grown until mid-exponential phase; this process was repeated until cells were ready for imaging. Alternately, cells were grown overnight in CH on a roller at 25°C . These cultures were grown in a 1:10 dilution series out to 1:10,000; the next day, the culture whose OD_{600} was nearest to 0.2 was back diluted 1:10 and grown in CH at 37°C as above.

Microscopy

Sample preparation

Cells were grown in 1 mL CH media at 37°C to OD_{600} around 0.2 as described above. Cultures were concentrated approximately 10-fold by centrifugation for 2 minutes at 7,000 RPM and resuspended in CH. Agarose pads were prepared using square plastic frames with inner dimensions 1.5 cm x 1.5 cm x 1 mm. Frames were placed on a cleaned glass pane, molten CH + 2% agarose was poured into the frames, and a second glass plane was placed on top to form a mold. Pads were allowed to solidify at room temperature, and excess agarose was cut away from the outside of the frame. To prepare slides for imaging, 2 μL of concentrated cells were pipetted

onto a base-washed coverslip, and an agarose pad was placed on top. For multi-hour acquisitions, glass-bottom dishes (MatTek) were used instead of coverslips; these were also base-washed before use, and a moist KimWipe was wound around the edge of the dish to retain humidity.

Phase contrast, epifluorescence, and TIRFM

Phase contrast, epifluorescence, and Total Internal Reflection Fluorescence Microscopy (TIRFM) images were collected on a Nikon Ti-E microscope using a Nikon CFI Plan Apochromat DM Lambda 100X Oil objective, 1.45 NA, phase ring Ph3. Cameras used were an ORCA-Flash4.0 V2 sCMOS (Hamamatsu) and an iXon Ultra 897 EMCCD (Andor). Fluorescence excitation was achieved using a MLC4008 laser launch (Agilent), with a 488 nm laser used for mNeonGreen imaging and a 561 nm laser used for JF549 imaging. For fluorescence emission, a C-NSTORM QUAD filter cube was used, along with an additional ET525/50m filter for green emission and ET600/50m filter for red emission (Chroma). The microscope was enclosed in a chamber heated to 37°C. Images were acquired using NIS-Elements version 5.02.01.

Confocal

Confocal images were collected on a Nikon TI microscope with Yokogawa CSU-10 spinning disk confocal unit using a Nikon 100X NA 1.45 TIRF objective and an ImagEM EM-CCD camera (Hamamatsu). A 494 nm excitation laser and a 609/57 nm bandpass emission filter were used for imaging of FM5-95. Images were acquired using MetaMorph version 7.8.1.0.

Induction, depletion, and HaloTag labelling

Specific conditions for each experiment are listed in Supplemental Table 4—Strains and . For FtsZ imaging, FtsZ-mNeonGreen or FtsZ-HaloTag were expressed from the IPTG-inducible pHyperSpank promoter. In all cases except the Δ *ftsA* strain, FtsA was co-expressed from the same

promoter, preserving the native operon structure. These constructs were merodiploid, meaning that the inducible FtsZ constructs were cloned into the chromosome at an ectopic site; the native untagged operon remained intact. Labelled FtsZ was induced by adding 20 μ M IPTG to the growth media for 1 hour before imaging. For single-molecule imaging, strains containing FtsZ-HaloTag were labelled by adding 20 pM JF549-HaloTag Ligand (JF549-HTL) to the growth media for 1 hour before imaging¹¹³. For total labelling, 5 nM JF549-HTL was used.

For the Δ *ftsA* strain, FtsZ was induced continuously from an ectopic locus under the pHyperSpank promoter induced with 10 μ M IPTG; IPTG concentrations above or below this did not permit cell growth. To image FtsZ, FtsZ-mNeonGreen was expressed at a different ectopic locus from the pXyl promoter and induced by adding 30 mM xylose to the growth media for 1 hour prior to imaging.

Single-molecule imaging of other divisome proteins was conducted as follows. FtsA, EzrA, and ZapA HaloTag constructs were expressed as a sole copy from their native promoters and labelled with 50 pM, 300 pM, and 600 pM JF549-HTL, respectively. SepF-HaloTag was expressed as a merodiploid under an IPTG-inducible promoter; no IPTG was added, as leaky expression from the promoter was sufficient for single-molecule imaging. SepF-HaloTag was labelled with 200 pM JF549-HTL. DivIB, DivIC, and FtsW HaloTag constructs were expressed as sole copies from xylose-inducible promoters. They were induced continuously with 1 mM, 5 mM, and 8 mM xylose, and labelled with 400 pM, 500 pM, and 300 pM JF549-HTL, respectively. FtsL-HaloTag and Pbp2B-HaloTag were expressed as a sole copy from an IPTG-inducible promoter, induced continuously with 30 μ M and 20 μ M IPTG, and labelled with 400 pM and 200 pM JF549-HTL, respectively. All JF549-HTL labelling was performed for 15 minutes before imaging; when JF549-HTL

concentrations were sufficiently high, cells were washed once in 1 mL CH media before imaging to remove excess dye.

For overexpression of ZBPs, xylose was added at the indicated concentration for 2 hours before imaging. For depletion of ZBPs, cells were grown initially in 1 mM xylose; xylose was then withdrawn, and cells were imaged at the point when they had filamented but were largely still alive, approximately 7 hours after xylose withdrawal. We judged whether cells were alive based on their appearance by phase contrast microscopy and whether they contained fluorescent signal. For imaging of Pbp2B dynamics in these mutants, cells were grown overnight in 100 μ M IPTG and 1 mM xylose; 7 hours before imaging, xylose was withdrawn and the concentration of IPTG was reduced to 20 μ M. Pbp2B-HaloTag was labelled with 100 pM JF549-HaloTag Ligand for 15 minutes before imaging.

Antibiotic treatment

To confirm cells were healthy and showing robust directional motion of DivIB, a time-lapse was taken of the pad prior to treatment. Then a new field of view was selected, 5 μ L of 10mg/mL Penicillin G was added on top of the CH + 2% agarose pad, and the sample was left to incubate for four minutes before imaging.

Cell length measurements

To determine whether the fluorescent fusions in this study impacted the functioning of the division machinery, we measured the cell length in each strain; cells with division defects show an increase in cell length. In *B. subtilis*, simple imaging of the cells by e.g., phase contrast microscopy, cannot be reliably used to measure cell length because of cell chaining, so a membrane stain was used. We grew cells for imaging as described above. Cell membranes were

labelled by staining with 1 µg/mL FM5-95 for 1 minute at room temperature, washed once with 1mL CH, and were immediately imaged at room temperature. Images were taken by spinning disk confocal microscopy at a 1 s exposure. Cell lengths were measured manually using ImageJ, with images anonymized and shuffled before analysis. Violin plots were generated in MATLAB using violin.m¹⁶⁹. N>149 for each sample.

Velocity measurements

To measure FtsZ treadmilling velocity, cells expressing FtsZ-mNeonGreen were imaged by TIRFM. Time lapses were taken using the sCMOS camera with 1 s exposures for 4 minutes total; after each time lapse, a phase-contrast image was taken to visualize cells. Velocity was measured by kymograph analysis²⁶. Kymographs were created from these time lapses of fluorescently labelled FtsZ filaments by manually drawing ROIs along the short axis of cells in ImageJ. Regions of these kymographs containing diagonal bands of fluorescence, representing directional treadmilling, were selected and their slopes were measured manually in ImageJ.

Velocity measurements of the single-molecule motions of DivIB, DivIC, FtsL, FtsW, and Pbp2B were taken similarly; cells were labelled for single-molecule imaging as described above and imaged by TIRFM. Each of these cells additionally expressed FtsZ-mNeonGreen to visualize the division site. Time lapses were taken using the sCMOS camera with 1-second exposures for 2-4 minutes total; before and after each time lapse, a phase-contrast image was taken to visualize cells, and a green epifluorescence image was taken to visualize the division site. Kymograph analysis of velocities was performed as summarized above; in this case, molecules that colocalized with the division site were specifically selected for analysis. A summary of these results is provided in Supplemental Table 2—Velocities of directionally-moving proteins.

To characterize the stationary behavior of EzrA, SepF, and ZapA, cells were labelled for single-molecule imaging and imaged by TIRFM as above. These cells also expressed FtsZ-mNeonGreen to visualize the division site. The microscopy protocol was identical to that in the previous paragraph; molecules that colocalized with the division site were selected for analysis.

Cell segmentation

Phase-contrast images of cells were segmented using DeepCell, a deep learning-based cell segmentation platform¹⁷⁰. A different custom net was trained for each combination of objective and camera used. Training sets were manually generated and varied in size but were generally around 20 images each. For cells in synthetic lethal conditions, masks were refined manually to omit dead cells.

Single-molecule lifetime measurements

Automated

To measure the single-molecule lifetimes of FtsZ and the ZBPs, HaloTag fusions were grown and labelled for single-molecule imaging as described above. TIRFM time lapses were taken using the emCCD camera, with 500 ms exposures for 4 minutes total; after each time lapse, a phase-contrast image was taken to visualize cells. To analyze the data, first, the phase images of cells were segmented using DeepCell to generate cell masks. Next, TrackMate was used to identify single particles in the image and preliminarily link them together¹⁷¹. Spots were detected with a 1.5-pixel radius and an intensity threshold that was manually selected for each data set. Spots were then linked roughly into tracks, with a 3-pixel linking distance and a maximum gap of 10 frames; in this way, only localizations with at least one other spot detected nearby were

considered for further analysis, which decreased computational load in the next stage. These data were exported into MATLAB for further analysis.

The track list from TrackMate was then filtered and converted to intensity traces. First, the spot positions in each track were averaged to generate a mean position of each spot. Next, spots that were not inside cells were excluded using the cell masks generated by DeepCell. Spots within 3 pixels of one another were then combined, and a new average position was calculated, weighted based on the length of each track. Then, for each spot, an intensity trace was generated: intensity was averaged in a 5 x 5 pixel window around the mean spot position, and the local background was averaged in a 2-pixel frame around the window and subtracted to generate a background-subtracted trace. Finally, intensity traces were filtered; only traces with a maximum background-subtracted intensity above 500 counts were included for further analysis.

To measure each single molecule lifetime, these intensity traces were fit to a Hidden Markov Model (HMM) using the MATLAB package vbFRET¹⁷². To rule out spots which contained no single-molecule fluorescence events, and to exclude cases where multiple single molecules overlap, models were fit with 1, 2, 3, and 4 states. Bayesian model selection was used to select the best-fitting model, and only traces in which the 2-state model fit best were included. Traces for which the difference between state 1 (no fluorescence) and state 2 (single-molecule fluorescence) was less than 60 counts were also discarded. The duration of each state 2 event was measured; dwell times less than 2 seconds (4 frames) were discarded, as were events that overlapped with the start or end of the trace since they cannot be measured accurately. Traces containing more than 2 events were also excluded. The resulting single-molecule lifetimes were

fit to a single exponential distribution and the mean lifetime was computed. We measured the contribution of photobleaching to our lifetimes by repeating the experiment at 1 second imaging intervals rather than 500 ms intervals without changing the exposure time; the measured lifetime did not change, indicating that the photobleaching contribution was negligible. To compare lifetimes, p-values were calculated using a Wilcoxon rank-sum test. Results are summarized in Supplemental Table 1—Lifetimes of stationary proteins.

Manual

To confirm that the automated single-molecule lifetime measurements described above were accurate, single-molecule lifetimes were also measured by hand. FtsZ-HaloTag was imaged as described in the Single-molecule lifetime measurements section above, although the sCMOS camera was used instead of the emCCD camera for ease of visualization. Kymographs were drawn manually in ImageJ. These kymographs were then examined for single-molecule events, and the duration of these events was measured manually in ImageJ.

Z-ring identification, spacing, width, and average projections

To visualize the Z-ring, cells expressing FtsZ-mNeonGreen under an IPTG-inducible promoter were grown for imaging as usual. Cells were imaged using the sCMOS camera; at each position, one phase-contrast image to visualize cells and 1 green epifluorescence image to visualize Z-rings were taken. To identify Z-rings in the image, cells were segmented using DeepCell to generate binary masks. The pill mesh function in Morphometrics was then used to generate midlines down the long axis of each cell¹⁷³. Using custom MATLAB code, the fluorescence intensity of FtsZ was averaged along each cell midline by taking the average along each mesh spline, these intensity traces were smoothed, and Z-rings were identified by peak detection.

To measure the spacing between Z-rings, the distances between neighboring peaks were measured. The predicted spacing between Z-rings was calculated as follows. Z-rings assemble around 25% of the way through the cell cycle, and because Δ ZBPs cells do not divide, these division sites remain indefinitely available for division protein localization¹⁰⁷. Thus, the expected Z-ring spacing is equal to the cell length for cells at or below the 25th percentile for length and is $\frac{1}{2}$ the cell length for cells above the 25th percentile. To calculate this, we used the cell length distribution shown for WT cells in Figure 3.

To plot the Z-ring width distributions, the full width at half maximum of each Z-ring peak was calculated. To measure Z-ring width, a 1 μ m region around each peak was sub-selected from each intensity trace, and these traces were averaged to create an average intensity trace. The Z-ring width was measured by calculating the full width at half maximum of the Z-ring peak in these intensity traces. Results are summarized in Supplemental Table 3—Z-ring widths. To display average projections of Z-rings, regions of each corresponding cell were sub-selected around each peak, using the meshes to align and straighten cells and normalize cell width; these images were averaged to create an average projection.

Z-ring features across the cell cycle

To quantify the appearance of the Z-ring over the cell cycle, FtsZ-mNeonGreen cells were grown as above. Cells were then imaged in phase and epifluorescence as above, repeated every minute for 2 hours. Time lapses were registered in ImageJ, and phase images were segmented using DeepCell. Morphometrics was used to generate midlines down each cell, as well as to track cells over time. Fluorescent images and cell meshes were then imported into MATLAB for further analysis.

First, cell tracks from Morphometrics were filtered for quality control. Cell tracks with a duration less than 20 frames (20 minutes) were discarded. Additionally, the total cell length for each frame in the track was then fit to a line, and tracks for which the R^2 of this fit was less than 0.99 were also discarded.

Bleach correction was applied by measuring the average intensity I_{avg} in each cell over time in all cells which had appreciable photobleaching, defined as cells whose final intensity was at least 40 counts lower than their initial intensity. For each cell, we fit this to $I_{avg}(t) = I_o * e^{-kt} + I_{bg}$ where I_o is the initial intensity, k is the photobleaching coefficient, I_{bg} is the background intensity, and t is time. We plotted the distributions of I_{bg} and k for all our fits, used gaussian fitting to extract the peak value for each, and assigned these as our final I_{bg} and k values. We then computed the corrected intensities for each cell in each frame $I_{corr} = (I_m - I_{bg}) / e^{-kt}$ where I_m is the measured intensity.

Next, Z-rings in the cell in each frame were identified as described above. These Z-rings were then linked together between frames by particle tracking to create Z-ring tracks: Z-rings were linked if they were within 5 pixels (325 nm) and 5 frames (5 minutes) of one another. Only Z-ring tracks between 20 and 40 minutes in duration were considered for further analysis. Time was normalized for each track, and average Z-ring intensity traces and projections were computed at each time point as described above. Z-ring peak width, peak height, and total intensity were computed by measuring the full width at half maximum, height above baseline, and peak area of each average Z-ring intensity trace. $N = 760$ Z-rings.

Pbp2B localization

To quantify the localization of Pbp2B at the division site, cells were grown containing FtsZ-HaloTag under an IPTG-inducible promoter and Pbp2B-mNeonGreen under its native promoter. The ZBP depletion strain was depleted for 7 hours before imaging as usual. FtsZ-HaloTag was induced with 20 μ M IPTG and labelled with 5 nM JF549 for 1 hour before imaging. Cells were imaged at 20 positions using the sCMOS camera; at each position, in order, 1 phase contrast image, 1 red epifluorescence image, and 1 green epifluorescence image were taken. Images were background-subtracted in ImageJ with rolling ball radius 50. To analyze, Z-rings were identified in each cell as described above. These same peak regions were selected from the corresponding Pbp2B image, to visualize Pbp2B intensity at the Z-ring. Finally, the area under these peak regions was calculated to estimate the amount of Pbp2B at midcell in each strain. N>1000 division sites analyzed in each condition. Box plots were generated using the boxplot function in MATLAB.

Cell wall synthesis labelling

For live-cell fluorescent D-amino acid (FDAA) labelling of cell wall synthesis, cells were grown for imaging as normal; the ZBP depletion strain was depleted for 7 hours before imaging as usual. All FDAA labelling experiments were performed in a Δ *dacA* background. To visualize the division site, these cells also expressed FtsZ-HaloTag, which was induced with 20 μ M IPTG and labelled with 5 nM JF549 for 1 hour before imaging. Cells were pelleted at 8000 RPM for 30 seconds and resuspended in 10 μ L CH + 1 mM fluorescent D-lysine (FDL). Cells were incubated for 3 minutes to allow labelling to occur, after which 1 mL CH was added to the tube to halt FDL labelling. Cells were pelleted at 8000 RPM for 30 seconds, resuspended in 100 μ L CH, and immediately placed under an agarose pad for imaging.

The average time between the end of FDL labelling and the start of imaging was 3 minutes and 20 seconds. Image acquisition was automated to increase speed and took an additional 1 minute. Cells were imaged at 10 positions using the sCMOS camera; at each position, in order, 1 phase contrast image, 1 red epifluorescence image, and 1 green epifluorescence image were taken. There is in total a ~4-minute delay between FDAA labelling and imaging, and in some cases the positions of Z-rings may have changed during this time. For instance, if a Z-ring constricted and disassembled during this delay, we would observe FDAA labelling without a Z-ring, and vice versa for a newly assembled Z-ring. However, we expect these events to be relatively rare because the cell cycle duration is roughly 30 minutes under these conditions.

Images were background-subtracted in ImageJ with a rolling ball radius of 50. To analyze colocalization, Z-rings were identified in each cell as described above. These same regions were selected from the corresponding FDAA image. To correct for differences in labelling efficiency between cells, the FDAA signal at midcell was normalized to signal in the nearby sidewall. Finally, the area under these peak regions was calculated to estimate the amount of FtsZ and FDAA at midcell in each strain. $N > 1000$ division sites analyzed in each condition. Box plots were generated using the boxplot function in MATLAB.

***ΔftsA* analysis**

To characterize FtsZ dynamics in the *ΔftsA* strain, FtsZ dynamics were imaged in each strain as described above. FtsZ filaments were tracked using the FIJI plugin TrackMate with the following parameters: spots with a diameter of 210 nm were identified using the Laplacian of Gaussians (LoG) detector; these spots were tracked over a 140 nm search radius using the Sparse LAP Tracker with no frame gaps. The resulting tracks were filtered to exclude tracks whose

duration was less than 10 or greater than 25 frames (10 and 25 seconds, respectively) using a custom MATLAB script, as described previously²⁶. Mean squared displacement (MSD) vs time interval (Δt) was computed for each track and fit to $MSD(\Delta t) = D \cdot \Delta t^\alpha$ (D : diffusion coefficient) to obtain the α coefficient. $N > 6000$ tracks analyzed in each condition.

Pbp2B dynamics

To visualize Pbp2B dynamics at the division site, cells expressed both Pbp2B-HaloTag from an inducible promoter to visualize single-molecule Pbp2B dynamics and FtsZ-mNeonGreen from an ectopic site under its native promoter to visualize the Z-ring. Cells were plated overnight on LB plates top spread with 100 μ M IPTG; 1 mM xylose was also added to the plate for the synthetic lethal depletion strain. The following day, single colonies were inoculated into 1 mL CH + 1 mM xylose + 100 μ M IPTG cultures and grown overnight at room temperature with shaking. The next morning, cells were washed once in 1 mL CH media and then grown for 7 hours in CH media + 20 μ M IPTG without xylose. This both began the depletion process for the synthetic lethal strain and decreased Pbp2B expression to a level suitable for single-molecule analysis. 15 minutes before imaging, cells were labelled with 100 pM JF549-HaloTag Ligand. Cells were imaged by TIRFM: time lapses were taken using the sCMOS camera with 1-second exposures for 4 minutes total; before and after each time lapse, a phase-contrast image was taken to visualize cells, and a green epifluorescence image was taken to visualize the division site. Kymographs were created manually as described above. Z-ring images were assigned to these kymographs by extracting a 61 x 61 pixel region from the FtsZ epifluorescence image taken before TIRFM, centered on the midpoint of the kymograph.

To characterize Z-rings at which Pbp2B moved directionally, directionally-moving Pbp2B particles were identified by particle tracking. Particles were tracked using the FIJI plugin TrackMate with the following parameters: spots with a diameter of 400 nm were identified using the Laplacian of Gaussians (LoG) detector; these spots were tracked over a 100 nm search radius using the Sparse LAP Tracker with no frame gaps. The resulting tracks were further filtered to obtain a selection of tracks with clear directional motion using a custom MATLAB script, as described previously²⁶. Tracks between 10 and 25 seconds and with end-to-end displacement above 225 nm were included for further analysis; further quality control was achieved by selecting tracks well fit ($r^2 > 0.95$) linearly to a log-log plot of mean squared displacement (MSD) vs time interval (Δt). Any remaining diffusing particles were omitted by ensuring a nonzero velocity from the fit $MSD(\Delta t) = 4 * D * \Delta t + (v * \Delta t)^2$ (v : velocity; D : diffusion coefficient). Tracks were assigned to cells using phase images segmented as described above. Z-rings were identified in these cells (described above) and tracks were assigned to the nearest Z-ring up to a maximum distance of 1 μm .

Suppressor screen

To isolate potential mutations that could suppress the synthetic lethality of the ZBPs, cells of strain bGS308 ($\Delta sepF$, $\Delta zapA$, xylose-inducible *ezrA*) were plated overnight on LB plates without xylose. Colonies grew overnight, as expected since EzrA depletion is slow and cells that are inhibited for division can grow for some time before death. The following day, colonies were inoculated into 3 mL LB cultures in triplicate and grown for 8 hours at 37°C with shaking. During the 8 hours of growth, the OD first increased, then decreased as cell death occurred, and then began to increase again. After 8 hours, 200 μL of each culture was plated on LB plates and grown

overnight. The following day, 5 colonies from each plate were restreaked for single colonies. Each colony was also patched onto LB plates top-spread with 25 mM xylose: because *EzrA* overexpression is lethal, candidates with an intact xylose-inducible promoter were expected to die on high xylose plates. Of the 15 candidate colonies, 4 did not grow after restreaking, and 3 had become insensitive to high xylose; the remaining 8 were submitted for whole-genome sequencing.

All 8 candidates had mutations in the xylose-inducible promoter; 4 candidates also had additional mutations. Of these, strain bGS390 (containing the *FtsZ(K86E)* mutation) was selected for further analysis. To verify that this mutation was capable of suppressing ZBP synthetic lethality, the *FtsZ(K86E)* mutation was introduced into a WT background. Individual Δ *ezrA*, Δ *sepF*, and Δ *zapA* mutations were introduced into this background and combined by crossing. As expected, the Δ *sepF* Δ *zapA* double mutant was viable, since these proteins are not synthetically lethal even in the WT background. Additionally, the normally synthetically lethal Δ *ezrA* Δ *zapA* mutants could be combined in the *FtsZ(K86E)* background, verifying that this mutation is a bona fide suppressor; the presence of the *FtsZ(K86E)* mutation was confirmed in this strain by Sanger sequencing. As a control, a Δ *ezrA* Δ *zapA* cross was attempted in parallel in the WT background; as expected, although colonies appeared on the transformation plate after overnight incubation, these colonies could not be further grown in liquid culture and became transparent after an additional day of incubation, verifying that these mutations are indeed synthetically lethal.

To rule out the possibility of additional suppressors arising during cloning, a *FtsZ(K86E)* Δ *zapA* xylose-inducible *ezrA* strain was constructed. This strain was maintained in 1 mM xylose during the cloning process, conditions under which cells containing WT *FtsZ* are viable; this same

process was used to generate the synthetic lethal depletion mutants. After cloning, xylose was withdrawn; unlike WT FtsZ-containing cells, which die after xylose is withdrawn, FtsZ(K86E) mutant cells remained viable after xylose was withdrawn.

Interestingly, neither the $\Delta ezrA \Delta sepF$ nor the $\Delta ezrA \Delta sepF \Delta zapA$ mutants could be constructed in the FtsZ(K86E) background. We suspect that the ability of this mutant to survive in the $\downarrow ezrA \Delta sepF \Delta zapA$ condition during the initial suppressor screen was due to some leaky expression from the xylose promoter, which may have been enhanced by the mutations in the promoter that arose during the screen.

Strain construction

All strains were constructed in *B. subtilis* strain PY79; strains used in this study are listed in Supplemental Table 5—Strain descriptions. Constructs were assembled by PCR amplification and Gibson cloning. These Gibson products were transformed directly into competent *B. subtilis*, where they were integrated into the chromosome by homologous recombination with homology regions that were engineered at each end of the construct. Each construct was initially transformed into the WT background except for the $\Delta ftsAZ$ construct, which was transformed into a strain containing an inducible FtsAZ operon at an ectopic locus. Transformants were selected by growth on LB plates containing the appropriate antibiotic. The resulting strains were verified by PCR and, when appropriate, by sequencing. Constructs used in this study are listed in Supplemental Table 6—Construct descriptions.

To combine constructs in the same strain, parent strains containing the constructs to be combined were crossed by transforming genomic DNA from one strain into the other. When two strains to be combined contained the same antibiotic marker, the marker was removed from one

of the parent strains. All antibiotic resistance cassettes used were engineered with loxP sites flanking the cassette, and so these cassettes could be removed by transforming cells with a plasmid that expresses Cre recombinase (plasmid pDR244, a gift from David Rudner). This plasmid also has a temperature-sensitive origin of replication, so after incubating cells at 30°C for 24 hours to remove the antibiotic cassette, cells were shifted to 45°C and incubated overnight to remove the plasmid. The removal of the cassette was verified by lack of growth on antibiotic selective plates.

Many of the strains used to investigate synthetic lethal conditions, namely bGS204, bGS206, bGS290, bGS293, bGS297, bGS298, bGS306, bGS308, bGS316, and bGS331, were additionally verified by whole genome sequencing to confirm that no suppressor mutations had arisen during cloning.

Statistical analysis

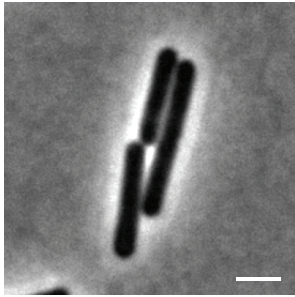
Single-molecule lifetime distributions were compared using a two-sided Wilcoxon rank sum test, with $p < 0.05$ considered significant. Results are presented in Supplemental Table 1—Lifetimes of stationary proteins. FDAA and Pbp2B intensities were compared using a two-sided t-test, with $p < 0.05$ considered significant. Results are presented in Figure 19 and Figure 22

Code

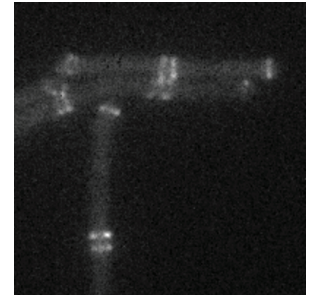
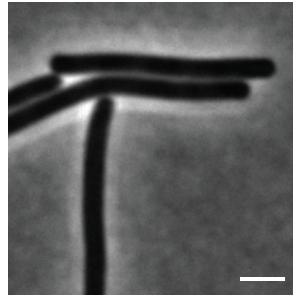
Custom MATLAB code is available at: <https://bitbucket.org/garnerlab/squyres-2020>

Appendix B—Supplemental figures for Chapter II

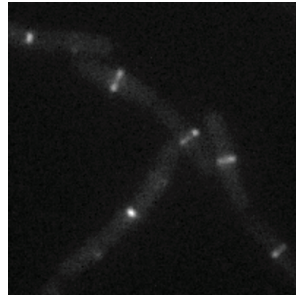
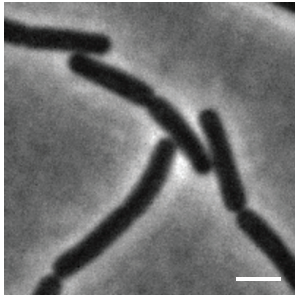
Control



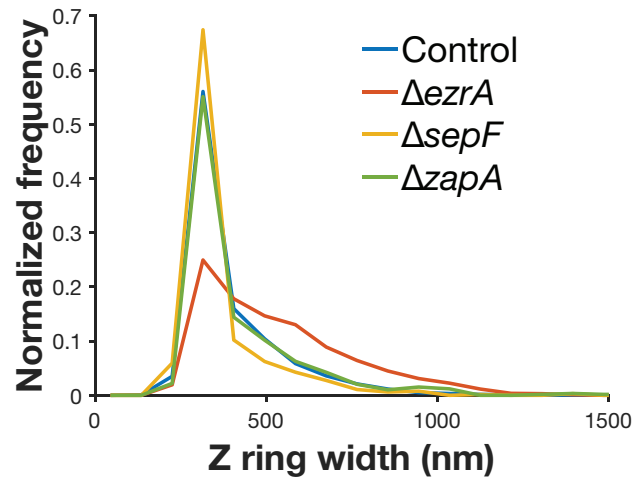
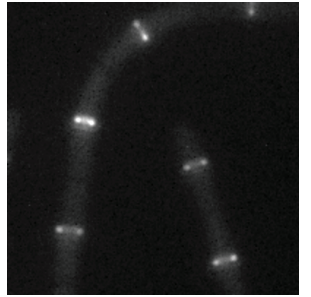
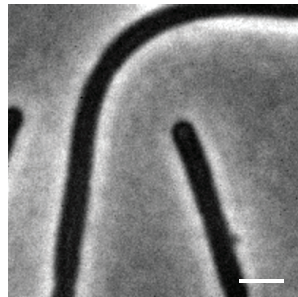
$\Delta ezrA$



$\Delta sepF$

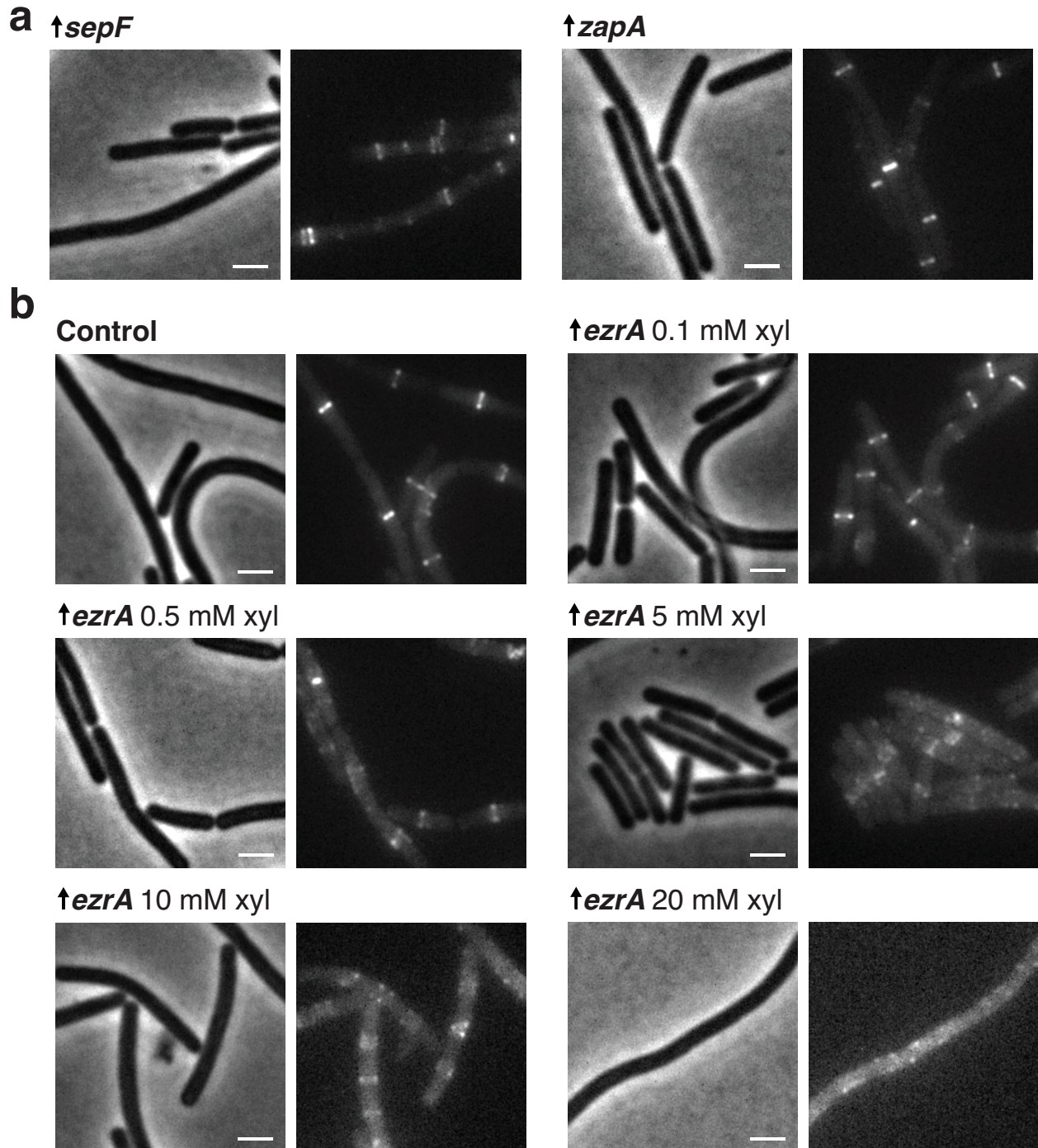


$\Delta zapA$



Supplemental Figure 1—Z ring architecture in individual ZBP knockouts

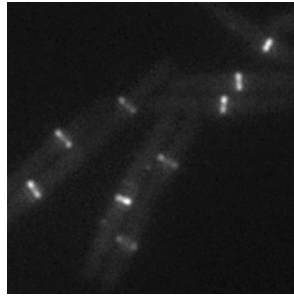
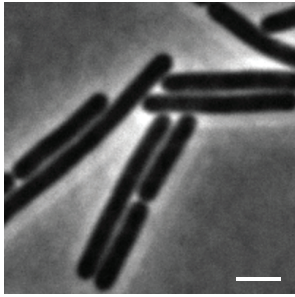
Top: Phase contrast and epifluorescence image in control cells, compared to cells with individual ZBPs deletions. $\Delta ezrA$ cells have less condensed Z rings, along with the expected Z rings near their poles⁶⁶. $\Delta sepF$ and $\Delta zapA$ cells have normal Z rings. *Bottom:* The distribution of Z ring widths in each strain. Representative images from at least two replicates of each condition. Scale bars: 2 μm



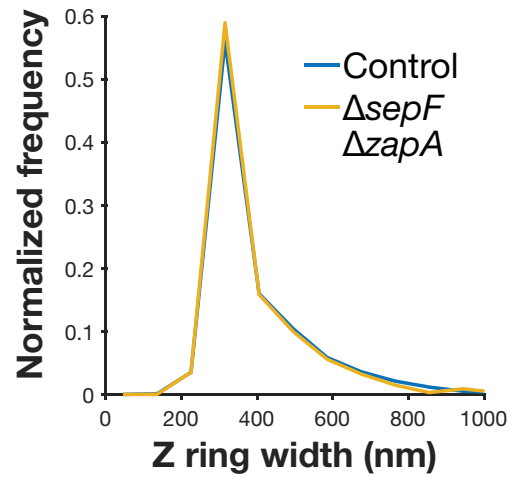
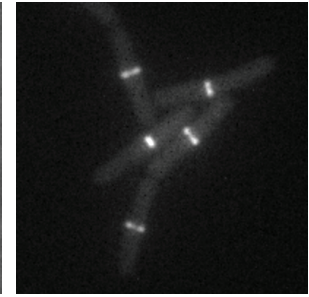
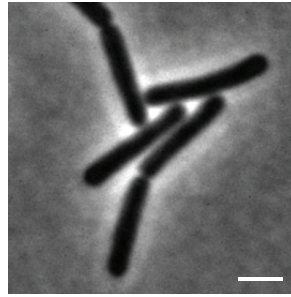
Supplemental Figure 2—Z-ring architecture with ZBP overexpression

(a) Phase contrast and epifluorescence image of Z-ring in cells overexpressing SepF and ZapA. These cells have normal Z-ring morphology except for some polar Z-rings in SepF-overexpressing cells. Second copies of *sepF* and *zapA* were expressed from a xylose-inducible promoter with 30 mM xylose for 2 hours. Representative images from at least two replicates of each condition. Scale bars: 2 μ m. **(b)** Phase contrast and epifluorescence image of Z-rings in control cells and cells with EzrA overexpressed. EzrA-overexpressing cells have perturbed Z-ring morphology, as expected, a phenotype exacerbated with increasing induction⁶⁹ A second copy of *ezrA* was expressed from a xylose-inducible promoter by adding xylose at the indicated mM concentration. Representative images from at least two replicates of each condition. Scale bars: 2 μ m.

Control



$\Delta sepF \Delta zapA$



Supplemental Figure 3—Z-ring architecture in $\Delta sepF \Delta zapA$ cells

Top: Phase contrast and epifluorescence image of Z-ring in control cells and cells with both *sepF* and *zapA* knocked out: $\Delta sepF \Delta zapA$ is the only combination of ZBP deletions that is not synthetically lethal, and their Z-ring morphology is normal. Representative images from at least two replicates of each condition. *Bottom:* $\Delta sepF \Delta zapA$ cells have similar Z-ring widths to control cells. Scale bars: 2 μ m.

Appendix C—Supplemental tables for Chapter II

Supplemental Table 1—Lifetimes of stationary proteins

Lifetime given as mean followed by 95% confidence intervals from a single exponential fit. P-value computed from Wilcoxon rank-sum test vs control. ns $p \geq 0.05$, *** $p < 0.001$, **** $p < 0.0001$. For strains and conditions, see Figure 7 and associated information in Supplemental Table 4.

Protein	Strain	Lifetime (s)	N	p-value
FtsZ	bAB309, bGS104	8.1 (7.6, 8.7)	1897	
FtsA	bAB213	4.5 (3.9, 5.5)	222	****
EzrA	bMH03	4.7 (4.1, 5.4)	1160	****
SepF	bMH332	8 (6, 12)	642	***
ZapA	bMH559	6.7 (5.4, 8.7)	647	ns

Supplemental Table 2—Velocities of directionally-moving proteins

Velocity given as mean \pm standard deviation. For strains and conditions, see Figure 9 and associated information in Supplemental Table 4.

Protein	Strain	Velocity (nm/s)	N
DivIB	bAB366	26.2 \pm 4.8	270
DivIC	bAB367	26.7 \pm 5.1	285
FtsL	bGS165	25.4 \pm 4.7	261
FtsW	bAB368	24.1 \pm 7.5	120
Pbp2B	bGS31	25.6 \pm 6.8	98

Supplemental Table 3—Z-ring widths

Z-ring width given as full width at half maximum of the average Z-ring intensity peak \pm bootstrapped standard error. \downarrow indicates a depletion. For strains and conditions, see Figure 13, Figure 18, Supplemental Figure 3, and associated information in Supplemental Table 4.

Condition	Strain	Z-ring width (nm)	N
Control	bAB219	330 \pm 40	2427
\downarrow ezrA	bGS588	390 \pm 40	1685
Δ ezrA	bGS256	490 \pm 50	1651
\downarrow sepF	bGS590	320 \pm 40	667
Δ sepF	bGS254	300 \pm 40	657
\downarrow zapA	bGS586	330 \pm 40	885
Δ zapA	bGS250	320 \pm 40	590
Δ sepF Δ zapA	bGS368	310 \pm 40	341
Δ ezrA \downarrow sepF	bGS290	590 \pm 60	668
\downarrow ezrA Δ sepF	bGS298	510 \pm 50	304
Δ ezrA \downarrow zapA	bGS293	610 \pm 60	1555
\downarrow ezrA Δ zapA	bGS297	470 \pm 50	822
\downarrow ezrA Δ sepF Δ zapA (Δ ZBPs)	bGS308	550 \pm 50	436
FtsZ(K86E)	bGS432	340 \pm 40	888
FtsZ(K86E) Δ ezrA Δ zapA	bGS463	450 \pm 50	208

Appendix D—Strains used in Chapter II

Strains and conditions listed by figure

Supplemental Table 4—Strains and conditions listed by figure

Figure 2		
Referenced as	Strain	Condition
Native SepF-HaloTag	bMH21	12nMJF549-HaloLigand for 15 min
Second site SepF-HaloTag	bMH332	No IPTG 12nMJF549-HaloLigand for 15 min
Figure 3		
Referenced as	Strain	Condition
WT	PY79	
EzrA-HT	bMH03	
SepF-HT	bMH332	No IPTG
ZapA-HT	bMH559	
HT-DivIB	bAB352	1mM xylose
HT-DivIC	bAB347	10mM xylose
HT-FtsL	bMH47	50μM IPTG
HT-FtsW	bAB350	10mM xylose
HT-Pbp2B	bGS28	50μM IPTG
Figure 4		
Referenced as	Strain	Condition
WT	PY79	
$\Delta ezrA$	bMH45	
$\Delta sepF$	bSW234	
$\Delta zapA$	RL2638	
$\Delta divIB$	bMH92	
Figure 5		
Referenced as	Strain	Condition
$\Delta zapA$	RL2638	
$\Delta zapA$ EzrA-HT	bMH221	
$\Delta ezrA$	bMH45	
$\Delta ezrA$ SepF-HT	bMH542	
$\Delta ezrA$ ZapA-HT	bMH565	
Figure 6		
Referenced as	Strain	Condition

EzrA	bMH42	300pMJF549-HaloLigand for 15 min
SepF	bMH372	200pMJF549-HaloLigand for 15 min
ZapA	bMH560	600pMJF549-HaloLigand for 15 min
Figure 7		
Referenced as	Strain	Condition
FtsZ	bAB309 and bGS104	20µM IPTG for 1 hr 20pM JF549-HaloLigand for 1 hr
FtsA	bAB213	50pM JF549-HaloLigand for 15 min
EzrA	bMH03	300pM JF549-HaloLigand for 15 min
SepF	bMH332	No IPTG 200pM JF549-HaloLigand for 15 min
ZapA	bMH559	600pM JF549-HaloLigand for 15 min
Figure 8		
Referenced as	Strain	Condition
DivIB	bAB366	1mM xylose 400pM JF549-HaloLigand for 15 min
DivIC	bAB367	5mM xylose 500pM JF549-HaloLigand for 15 min
FtsL	bGS165	30µM IPTG 40pM JF549-HaloLigand for 15 min
FtsW	bAB368	8mM xylose 300pM JF549-HaloLigand for 15 min
Pbp2B	bGS31	20µM xylose 200pM JF549-HaloLigand for 15 min
Figure 9		
Referenced as	Strain	Condition
DivIB	bAB366	1mM xylose 400pM JF549-HaloLigand for 15 min
DivIC	bAB367	5mM xylose

		500pM JF549-HaloLigand for 15 min
FtsL	bGS165	30μM IPTG 40pM JF549-HaloLigand for 15 min
FtsW	bAB368	8mM xylose 300pM JF549-HaloLigand for 15 min
Pbp2B	bGS31	20μM xylose 200pM JF549-HaloLigand for 15 min
Referenced as	Figure 10 Strain	Condition
DivIB	bAB366	1mM xylose 400pM JF549-HaloLigand for 15 min
DivIB + PenG	bAB366	1mM xylose 400pM JF549-HaloLigand for 15 min 5μL of 10mg/mL PenG on top of pad, waited 4 min before imaging
Referenced as	Figure 11—Velocity Strain	Condition
Control	bAB219	20μM IPTG for 1 hr
$\Delta ezrA \downarrow sepF$	bGS290	Depleted from 1mM xylose for 7 hr 20μM IPTG for 1 hr
$\downarrow ezrA \Delta sepF$	bGS298	Depleted from 1mM xylose for 7 hr 20μM IPTG for 1 hr
$\Delta ezrA \downarrow zapA$	bGS293	Depleted from 1mM xylose for 7 hr 20μM IPTG for 1 hr
$\downarrow ezrA \Delta zapA$	bGS297	Depleted from 1mM xylose for 7 hr 20μM IPTG for 1 hr
$\downarrow ezrA \Delta sepF \Delta zapA$	bGS308	Depleted from 1mM xylose for 7 hr 20μM IPTG for 1 hr
Referenced as	Figure 11—Lifetime Strain	Condition
Control	bAB309 and bGS104	20μM IPTG for 1 hr

		20pM JF549-HaloLigand for 1hr
<i>ΔezrA ↓sepF</i>	bGS204	Depleted from 1mM xylose for 7 hr 20μM IPTG for 1 hr 20pM JF549-HaloLigand for 1hr
<i>↓ezrA ΔsepF</i>	bGS316	Depleted from 1mM xylose for 7 hr 20μM IPTG for 1 hr 20pM JF549-HaloLigand for 1hr
<i>ΔezrA ↓zapA</i>	bGS206	Depleted from 1mM xylose for 7 hr 20μM IPTG for 1 hr 20pM JF549-HaloLigand for 1hr
<i>↓ezrA ΔzapA</i>	bGS306	Depleted from 1mM xylose for 7 hr 20μM IPTG for 1 hr 20pM JF549-HaloLigand for 1hr
<i>↓ezrA ΔsepF ΔzapA</i>	bGS331	Depleted from 1mM xylose for 7 hr 20μM IPTG for 1 hr 20pM JF549-HaloLigand for 1hr
	Figure 12	
Referenced as	Strain	Condition
Control	bAB219	20μM IPTG for 1 hr
<i>ΔezrA ↓sepF</i>	bGS290	Depleted from 1mM xylose for 7 hr 20μM IPTG for 1 hr
<i>↓ezrA ΔsepF</i>	bGS298	Depleted from 1mM xylose for 7 hr 20μM IPTG for 1 hr
<i>ΔezrA ↓zapA</i>	bGS293	Depleted from 1mM xylose for 7 hr 20μM IPTG for 1 hr
<i>↓ezrA ΔzapA</i>	bGS297	Depleted from 1mM xylose for 7 hr 20μM IPTG for 1 hr

$\downarrow ezrA \Delta sepF \Delta zapA$	bGS308	Depleted from 1mM xylose for 7 hr 20 μ M IPTG for 1 hr
Figure 13		
Referenced as	Strain	Condition
Control	bAB219	20 μ M IPTG for 1 hr
$\Delta ezrA$	bGS256	20 μ M IPTG for 1 hr
$\downarrow sepF$	bGS590	Depleted from 1mM xylose for 7 hr 20 μ M IPTG for 1 hr
$\downarrow zapA$	bGS586	Depleted from 1mM xylose for 7 hr 20 μ M IPTG for 1 hr
$\Delta ezrA \downarrow sepF$	bGS290	Depleted from 1mM xylose for 7 hr 20 μ M IPTG for 1 hr
$\Delta ezrA \downarrow zapA$	bGS293	Depleted from 1mM xylose for 7 hr 20 μ M IPTG for 1 hr
$\downarrow ezrA$	bGS588	Depleted from 1mM xylose for 7 hr 20 μ M IPTG for 1 hr
$\Delta sepF$	bGS254	20 μ M IPTG for 1 hr
$\Delta zapA$	bGS250	20 μ M IPTG for 1 hr
$\downarrow ezrA \Delta sepF$	bGS298	Depleted from 1mM xylose for 7 hr 20 μ M IPTG for 1 hr
$\downarrow ezrA \Delta zapA$	bGS297	Depleted from 1mM xylose for 7 hr 20 μ M IPTG for 1 hr
$\downarrow ezrA \Delta sepF \Delta zapA$	bGS308	Depleted from 1mM xylose for 7 hr 20 μ M IPTG for 1 hr
Figure 14		
Referenced as	Strain	Condition
$\Delta ZBPs$	bGS308	Depleted from 1mM xylose for 7 hr 20 μ M IPTG for 1 hr
Figure 15		
Referenced as	Strain	Condition
	bAB219	20 μ M IPTG for 1 hr
Figure 16		
Referenced as	Strain	Condition

	bGS104	20μM IPTG for 1 hr 5nM JF549-HaloLigand for 1 hr
Figure 17		
Referenced as	Strain	Condition
FtsZ(K86E)	bGS432	20μM IPTG for 1hr
FtsZ(K86E) <i>ΔezrAΔzapA</i>	bGS463	20μM IPTG for 1hr
Figure 18		
Referenced as	Strain	Condition
Control	bAB219	20μM IPTG for 1hr
FtsZ(K86E)	bGS432	20μM IPTG for 1hr
FtsZ(K86E) <i>ΔezrAΔzapA</i>	bGS463	20μM IPTG for 1hr
<i>ΔezrA ↓zapA</i>	bGS293	Depleted from 1mM xylose for 7 hr 20μM IPTG for 1 hr
Figure 19		
Referenced as	Strain	Condition
Control—Pbp2B	bGS104	20μM IPTG for 1 hr 5nM JF549-HaloLigand for 1 hr
Control—FDAA	bMH510	20μM IPTG for 1 hr 5nM JF549-HaloLigand for 1 hr 1mM FDL for 3 minutes
ΔZBPs—Pbp2B	bMH445	Depleted from 1mM xylose for 7 hr 20μM IPTG for 1 hr 5nM JF549-HaloLigand for 1 hr
ΔZBPs—FDAA	bMH508	Depleted from 1mM xylose for 7 hr 20μM IPTG for 1 hr 5nM JF549-HaloLigand for 1 hr 1mM FDL for 3 minutes
Figure 20		
Referenced as	Strain	Condition
	bMH443	Depleted from 1mM xylose for 7 hr Depletion from 100μM IPTG to 20μM IPTG for 7 hr

		100pM JF549-HaloLigand for 15 min
Referenced as	Figure 21 Strain	Condition
Control	bMH512	Depletion from 100μM IPTG to 20μM IPTG for 7 hr 100pM JF549-HaloLigand for 15 min
ΔZBPs	bMH443	Depleted from 1mM xylose for 7 hr Depletion from 100μM IPTG to 20μM IPTG for 7 hr 100pM JF549-HaloLigand for 15 min
Referenced as	Figure 22 Strain	Condition
Control	bGS104	20μM IPTG for 1 hr 5nM JF549-HaloLigand for 1 hr
FtsZ(K86E)	bGS618	20μM IPTG for 1 hr 5nM JF549-HaloLigand for 1 hr
FtsZ(K86E) ΔezrAΔzapA	bGS628	20μM IPTG for 1 hr 5nM JF549-HaloLigand for 1 hr
ΔezrA ↓zapA	bGS644	Depleted from 1mM xylose for 7 hr 20μM IPTG for 1 hr 5nM JF549-HaloLigand for 1 hr
Referenced as	Figure 23 Strain	Condition
Control	bGS630	30mM xylose for 1hr
ΔftsA	bGS639	10μM IPTG 30mM xylose for 1hr
Referenced as	Figure 24 Strain	Condition
Control	bGS630	30mM xylose for 1hr
ΔftsA	bGS639	10μM IPTG 30mM xylose for 1hr
Referenced as	Supplemental Figure 1 Strain	Condition
Control	bAB219	20μM IPTG for 1 hr

<i>ΔezrA</i>	bGS256	20μM IPTG for 1 hr
<i>ΔsepF</i>	bGS254	20μM IPTG for 1 hr
<i>ΔzapA</i>	bGS250	20μM IPTG for 1 hr
Supplemental Figure 2		
Referenced as	Strain	Condition
↑sepF	bGS260	30mM xylose for 2 hr 20μM IPTG for 1 hr
↑zapA	bGS259	30mM xylose for 2 hr 20μM IPTG for 1 hr
Control	bAB219	50μM IPTG for 1 hr
↑ezrA	bGS263	various concentrations of xylose for 2hr 50μM IPTG for 1 hr
Supplemental Figure 3		
Referenced as	Strain	Condition
Control	bAB219	20μM IPTG for 1 hr
<i>ΔsepF ΔzapA</i>	bGS368	20μM IPTG for 1 hr

Strain descriptions

Supplemental Table 5—Strain descriptions

Unless otherwise noted, strains are original to the version of this work previously published as¹²⁰

Strain	Description	Citation
bAB213	<i>ftsAZ::erm-ftsA-HaloTag(sw)-ftsZ-cat multicopy</i>	26,174
bAB219	<i>amyE::erm-Phyperspank-ftsA-mNeonGreen-15aa-ftsZ</i>	26
bAB309	<i>amyE::erm-Phyperspank-ftsA-HaloTag-15aa-ftsZ</i>	
bAB347	<i>divIC::erm-Pxyl-HaloTag-15aa-divIC</i>	
bAB350	<i>ftsW::erm-Pxyl-HaloTag-15aa-ftsW</i>	
bAB352	<i>divIB::erm-Pxyl-HaloTag-15aa-divIB</i>	
bAB366	<i>ftsZ::mNeonGreen-15aa-ftsZ multicopy, divIB::erm-Pxyl-HaloTag-15aa-divIB</i>	
bAB367	<i>ftsZ::mNeonGreen-15aa-ftsZ multicopy, divIC::erm-Pxyl-HaloTag-15aa-divIC</i>	
bAB368	<i>ftsZ::mNeonGreen-15aa-ftsZ multicopy, ftsW::erm-Pxyl-HaloTag-15aa-ftsW</i>	
bGS28	<i>pbp2b::erm-pHyperSpank-HaloTag-15aa-pbp2b</i>	26
bGS31	<i>ftsZ::erm-mNeonGreen-15aa-ftsZ-cat multicopy, pbp2b::erm-pHyperSpank-HaloTag-15aa-pbp2b</i>	26
bGS104	<i>amyE::erm-Phyperspank-ftsA-HaloTag-15aa-ftsZ, pbp2B::mNeonGreen-15aa-pbp2B</i>	
bGS165	<i>ftsZ::mNeonGreen-15aa-ftsZ multicopy, ftsL::erm-Phyperspank-HaloTag-15aa-ftsL</i>	

bGS204	<i>amyE::erm-Phyperspank-ftsA-HaloTag-15aa-ftsZ, ezrA::scar, sepF::cat-pXyl-sepF</i>
bGS206	<i>amyE::erm-Phyperspank-ftsA-HaloTag-15aa-ftsZ, ezrA::scar, zapA::cat-pXyl-zapA</i>
bGS250	<i>amyE::erm-Phyperspank-ftsA-mNeonGreen-15aa-ftsZ, zapA-yshBD::tet</i>
bGS254	<i>amyE::erm-Phyperspank-ftsA-mNeonGreen-15aa-ftsZ, sepF::tet</i>
bGS256	<i>amyE::erm-Phyperspank-ftsA-mNeonGreen-15aa-ftsZ, ezrA::cat</i>
bGS259	<i>amyE::erm-Phyperspank-ftsA-mNeonGreen-15aa-ftsZ, ycgO::cat-pXyl-zapA</i>
bGS260	<i>amyE::erm-Phyperspank-ftsA-mNeonGreen-15aa-ftsZ, ycgO::cat-pXyl-sepF</i>
bGS263	<i>amyE::erm-Phyperspank-ftsA-mNeonGreen-15aa-ftsZ, ycgO::cat-pXyl-ezrA</i>
bGS290	<i>amyE::erm-Phyperspank-ftsA-mNeonGreen-15aa-ftsZ, ezrA::scar, sepF::cat-pXyl-sepF</i>
bGS293	<i>amyE::erm-Phyperspank-ftsA-mNeonGreen-15aa-ftsZ, ezrA::scar, zapA::cat-pXyl-zapA</i>
bGS297	<i>amyE::erm-Phyperspank-ftsA-mNeonGreen-15aa-ftsZ, zapA-yshBD::tet, ezrA::cat-pXyl-ezrA</i>
bGS298	<i>amyE::erm-Phyperspank-ftsA-mNeonGreen-15aa-ftsZ, sepF::tet, ezrA::cat-pXyl-ezrA</i>

bGS306	<i>amyE::erm-Phyperspank-ftsA-HaloTag-15aa-ftsZ, zapA-yshBD::tet, ezrA::cat-pXyl-ezrA</i>
bGS308	<i>amyE::erm-Phyperspank-ftsA-mNeonGreen-15aa-ftsZ, sepF::scar, zapA-yshBD::tet, ezrA::cat-pXyl-ezrA</i>
bGS316	<i>amyE::erm-Phyperspank-ftsA-HaloTag-15aa-ftsZ, sepF::scar, ezrA::cat-pXyl-ezrA</i>
bGS331	<i>amyE::erm-Phyperspank-ftsA-HaloTag-15aa-ftsZ, zapA-yshBD::tet, sepF::scar, ezrA::cat-pXyl-ezrA</i>
bGS368	<i>amyE::erm-Phyperspank-ftsA-HaloTag-15aa-ftsZ, zapA-yshBD::tet, sepF::scar</i>
bGS432	<i>ftsZ::ftsZ(K86E), amyE::erm-Phyperspank-FtsA-mNeonGreen-15aa-FtsZ(K86E)</i>
bGS463	<i>ftsZ::ftsZ(K86E), amyE::erm-Phyperspank-FtsA-mNeonGreen-15aa-FtsZ(K86E), ezrA::cat, zapA-yshBD::tet</i>
bGS586	<i>amyE::erm-Phyperspank-ftsA-mNeonGreen-15aa-ftsZ, zapA::cat-pXyl-zapA</i>
bGS588	<i>amyE::erm-Phyperspank-ftsA-mNeonGreen-15aa-ftsZ, ezrA::cat-pXyl-ezrA</i>
bGS590	<i>amyE::erm-Phyperspank-ftsA-mNeonGreen-15aa-ftsZ, sepF::cat-pXyl-sepF</i>

bGS618	<i>ftsZ::ftsZ(K86E), pbp2B::mNeonGreen-15aa- pbp2B, amyE::erm-Phyperspank- ftsA-HaloTag-15aa- ftsZ(K86E)</i>	
bGS628	<i>ftsZ::ftsZ(K86E), pbp2B::mNeonGreen-15aa- pbp2B, amyE::erm-Phyperspank- ftsA-HaloTag-15aa- ftsZ(K86E), zapA-yshBD::tet, ezrA::cat</i>	
bGS630	<i>ycgO::cat-pXyl-mNeonGreen- 15aa-ftsZ</i>	
bGS639	<i>ftsAZ::spec, amyE::pHyperspank-ftsZ, ycgO::cat-pXyl-mNeonGreen- 15aa-ftsZ</i>	
bGS644	<i>pbp2B::mNeonGreen-15aa- pbp2B, amyE::Phyperspank-ftsA- HaloTag-15aa-ftsZ, zapA::pXyl-zapA, ezrA::cat</i>	
bMH03	<i>ezrA::ezrA-30aa-HaloTag-cat</i>	
bMH21	<i>SepF::SepF-30aa-Halo-scar</i>	Original to this thesis
bMH42	<i>ftsZ::mNeonGreen-15aa-ftsZ multicopy, ezrA::ezrA-30aa-HaloTag-cat</i>	
bMH45	<i>ezrA::cat</i>	
bMH47	<i>ftsL::erm-Phyperspank- HaloTag-15aa-ftsL</i>	
bMH92	<i>divIB::cat</i>	
bMH221	<i>zapA-yshBD::tet, ezrA::ezrA-30aa-HaloTag-cat</i>	
bMH332	<i>amyE::erm-Phyperspank- sepF-30aa-HaloTag</i>	
bMH372	<i>ftsZ::mNeonGreen-15aa-ftsZ multicopy, amyE::erm-Phyperspank- sepF-30aa-HaloTag</i>	

bMH443	<i>pbp2B::erm-Phyperspank-HaloTag-15aa-pbp2B, amyE::kan-Paz-ftsA-mNeonGreen-15aa-ftsZ, sepF::scar, zapA-yshBD::tet, ezrA::cat-pXyl-ezrA</i>	
bMH445	<i>pbp2B::mNeonGreen-15aa-pbp2B, amyE::erm-Phyperspank-ftsA-HaloTag-15aa-ftsZ, sepF::scar, zapA-yshBD::tet, ezrA::cat-pXyl-ezrA</i>	
bMH508	<i>amyE::erm-Phyperspank-ftsA-HaloTag-15aa-ftsZ, sepF::scar, zapA-yshB::tet, ezrA::cat-pXyl-ezrA, dacA::kan</i>	
bMH510	<i>amyE::erm-Phyperspank-ftsA-HaloTag-15aa-ftsZ, dacA::kan</i>	
bMH512	<i>pbp2B::erm-Phyperspank-HaloTag-15aa-pbp2B, amyE::kan-Paz-ftsA-mNeonGreen-15aa-ftsZ</i>	
bMH542	<i>ezrA::cat, amyE::erm-Phyperspank-sepF-30aa-HaloTag</i>	
bMH559	<i>zapA::zapA-30aa-HaloTag-cat</i>	
bMH560	<i>ftsZ::mNeonGreen-15aa-ftsZ multicopy, zapA::zapA-30aa-HaloTag-cat</i>	
bMH565	<i>ezrA::scar, zapA::zapA-30aa-HaloTag-cat</i>	
bSW234	<i>sepF::tet</i>	
PY79	<i>wildtype</i>	175
RL2638	<i>zapA-yshBD::tet</i>	64

Construct descriptions

Supplemental Table 6—Construct descriptions

Lower case in primer sequences indicates overhang with adjoining fragment

Constructs original to the version of this work previously published as ¹²⁰	
Fragment	Primer: Sequence (5' to 3')
<i>amyE::erm-Phyerspank-ftsA-HaloTag-15aa-ftsZ</i>	
<i>amyE(up)-erm-Phyerspank-ftsA</i>	oMD191: TTTGGATGGATTCAGCCCGATTG oAB13: ccagtaccgatttctgcatGCTAAATCCTCCTAATCTGCCGAATG
<i>HaloTag-15aa</i>	oJE32: ATGGCAGAAATCGGTACTGG oAB14: tggcctgagcccggctccctggccagatccctcgagGCCGCTGATTTCTAAGGTAGAAAG
<i>15aa-ftsZ-amyE(down)</i>	oAB140: ggaccgggctcaggccaaggaagcggcATGTTGGAGTTCGAAACAAACATAGACG oMD197: TCACATACTCGTTTTCAAACGGATC
<i>amyE::kan-Paz-ftsA-mNeonGreen-15aa-ftsZ</i>	
<i>amyE(up)-kan</i>	oMD191: TTTGGATGGATTCAGCCCGATTG oSW42: TTCTGCTCCCTCGC
<i>pAZ-ftsA(partial)</i>	oAB76: gaacggtactgagcgaggagcagaaGTATTTGTTTCCGGTTTCT oAB38: GCGAAGCTCTTCTGA
Transformed directly into bAB219	
<i>ycgO::cat-pXyl-mNeonGreen-15aa-ftsZ</i>	
<i>ycgO(up)-cat-pXyl</i>	oMD247: ATCGAACTGGCAAAGGCAAAC oMD226: GGTAGTTCCTCCTTAATCGATCCATTCAAATACAGATGCATTTTATTC
<i>mNeonGreen-15aa-ftsZ</i>	oGS35: tcgattaaggaggaactaccATGGTTTCGAAAGGAGAGGAGGATAATATG oGS40: gggacagccccttctcctccttctgatctTTAGCCGCGTTTATTACGGTTTC
<i>ycgO(down)</i>	oMD257: AGATCGAAAGGAGGAGGAAGG oMD252: CAAGTTTTGAGCAGCTCAGTG
<i>ftsAZ::spec</i>	
<i>ftsA(up)</i>	oAB23: GCGGGTGAAATAGATTGAAAATAAAGC oAB72: atgctatacgaacggtagttgaccagtgtccctgTCTATGGCACCTCCTCACAT
<i>spec</i>	oSW40: CAGGGAGCACTGGTC oSW42: TTCTGCTCCCTCGC

<i>ftsZ(down)</i>	oAB73: acattatacgaacgggtactgagcggaggagcagaaTGTAAGGACAAAATCGTTT oAB30: CCATCCTCATATGTCTGACC
Transformed into a strain containing a second copy of <i>ftsAZ</i> under inducible control	
<i>ftsZ::ftsZ(K86E)-kan</i>	
<i>ftsZ(up)-ftsZ(K86E)</i>	oWM20: ATGAACAACAATGAACTTTACGTC oWM66: caggagcactggtaactaccgttcgtatTTAGCCGCGTTTATTACGGT
<i>kan</i>	oSW40: CAGGGAGCACTGGTC oSW42: TTCTGCTCCCTCGC
<i>ftsZ(down)</i>	oAB73: acattatacgaacgggtactgagcggaggagcagaaTGTAAGGACAAAATCGTTT oAB30: CCATCCTCATATGTCTGACC
<i>amyE::erm-Phyperspank-FtsA-mNeonGreen-15aa-FtsZ(K86E)</i>	
<i>amyE(up)-erm-Phyperspank</i>	oMD191: TTTGGATGGATTCAGCCCGATTG oMD232: GGTAGTTCCTCCTTAAAGCTTAATTGTTATCCGCTCACAAT
<i>ftsA-mNeonGreen-15aa</i>	oAB78: agcggataacaattaagctttaaggaggaactaccATGAACAACAATGAACTTTACGTC oZB34: tggcctgagcccggctccctggccagatccctcgagCTTATAGAGTTCATCCATACCCATC
<i>15aa-FtsZ(K86E)</i>	oAB140: ggaccgggctcaggccaaggaagcggcATGTTGGAGTTCGAAACAAACATAGACG oAB94: ctttcggttaagtcccgtctagccttgcccTTAGCCGCGTTTATTACGGTTTC
<i>amyE(down)</i>	oMD196: GGGCAAGGCTAGACGGG oMD197: TCACATACTCGTTTCCAAACGGATC
<i>amyE::erm-Phyperspank-FtsA-HaloTag-15aa-FtsZ(K86E)</i>	
<i>amyE(up)-erm-Phyperspank</i>	oMD191: TTTGGATGGATTCAGCCCGATTG oMD232: GGTAGTTCCTCCTTAAAGCTTAATTGTTATCCGCTCACAAT
<i>ftsA-HaloTag-15aa</i>	oAB78: agcggataacaattaagctttaaggaggaactaccATGAACAACAATGAACTTTACGTC oAB14: tggcctgagcccggctccctggccagatccctcgagGCCGCTGATTTCTAAGGTAGAAAG
<i>15aa-FtsZ(K86E)</i>	oAB140: ggaccgggctcaggccaaggaagcggcATGTTGGAGTTCGAAACAAACATAGACG oAB94: ctttcggttaagtcccgtctagccttgcccTTAGCCGCGTTTATTACGGTTTC
<i>amyE(down)</i>	oMD196: GGGCAAGGCTAGACGGG oMD197: TCACATACTCGTTTCCAAACGGATC
<i>sepF::tet</i>	

<i>sepF(up)</i>	oMH43: TATTGGCCCGTCTATCAG oMH98: gcgagggagcagaaCTCATTGCTGTACACCCC
<i>tet</i>	oSW40: CAGGGAGCACTGGTC oSW42: TTCTGCTCCCTCGC
<i>sepF(down)</i>	oMH20: tgaccagtgtccctgAGCGAGATGATCCTTTATCAAG oMH21: CTATGTATGAAGGATCTTCAACCA
<i>ezrA::cat</i>	
<i>ezrA(up)</i>	oMH53: GACATCTCCCGCTTGATG oAB99: cgaacggtactgagcgagggagcagaaAATGAGCCCCCTTGCTGT
<i>cat</i>	oJM28: TTCTGCTCCCTCGCTCAG oJM29: CAGGGAGCACTGGTCAAC
<i>ezrA(down)</i>	oMH05: tgaccagtgtccctgATAATCACGACCATGAAAAAGAG oMH06: GTTGTGGATCGAGTCGGA
<i>ycgO::cat-pXyl-ezrA</i>	
<i>ycgO(up)</i>	oMD247: ATCGAACTGGCAAAGGCAAAC oMD248: tacgaacggtagttgaccagtgtccctgTCCCGCCATATAAATACAAATCGAAATAATC
<i>cat-pXyl</i>	oSW40: CAGGGAGCACTGGTC oMD226: GGTAGTTCCTCCTTAATCGATCCATTCAAATACAGATGCATTTTATTTTC
<i>ezrA</i>	oMH14: atcgattaaggaggaactaccATGGAGTTTGTTCATTGGATTATTA oGS37: acagccccttctctctcttcgatctCTAAGCGGATATGTCAGCTT
<i>ycgO(down)</i>	oMD257: AGATCGAAAGGAGGAGGAAGG oMD252: CAAGGTTTTGAGCAGCTCAGTG
<i>ycgO::cat-pXyl-sepF</i>	
<i>ycgO(up)</i>	oMD247: ATCGAACTGGCAAAGGCAAAC oMD248: tacgaacggtagttgaccagtgtccctgTCCCGCCATATAAATACAAATCGAAATAATC
<i>cat-pXyl</i>	oSW40: CAGGGAGCACTGGTC oMD226: GGTAGTTCCTCCTTAATCGATCCATTCAAATACAGATGCATTTTATTTTC
<i>sepF</i>	oGS38: atggatcgattaaggaggaactaccATGAAAAATAAACTGAAAACTTTTTCTCAATGG oGS39: gggacagccccttctctctcttcgatctTTAGCCGCGTTTATTACGGTTTC
<i>ycgO(down)</i>	oMD257: AGATCGAAAGGAGGAGGAAGG oMD252: CAAGGTTTTGAGCAGCTCAGTG

<i>ycgO::cat-pXyl-zapA</i>	
<i>ycgO(up)</i>	oMD247: ATCGAACTGGCAAAGGCAAAC oMD248: tacgaacggtagttgaccagtgtccctgTCCCGCCATATAAATACAAATCGAAATAATC
<i>cat</i>	oSW40: CAGGGAGCACTGGTC oSW42: TTCTGCTCCCTCGC
<i>pXyl-zapA</i>	oSW38: cattatacgaacggtactgagcgagggagcagaaGAATTCGAGCTTGCATG oGS36: acagccccttctctccttttgatctTCAATCCTTTTCTTTAAGCTGACGC
<i>ycgO(down)</i>	oMD257: AGATCGAAAGGAGGAGGAAGG oMD252: CAAGGTTTTGAGCAGCTCAGTG
<i>ezrA::cat-pXyl-ezrA</i>	
<i>ezrA(up)</i>	oMH35: GAATATGTCCGTCTCGCT oMH54: tgaccagtgtccctgAATGAGCCCCCTTGCTG
<i>cat-pXyl</i>	oSW40: CAGGGAGCACTGGTC oMD226: GGTAGTTCCTCCTTAATCGATCCATTCAAATACAGATGCATTTTATTTTC
<i>ezrA(partial)</i>	oMH14: atcgattaaggaggaactaccATGGAGTTTGTCATTGGATTATTA oMH56: CTTAGTACGGATTGACCGG
<i>sepF::cat-pXyl-sepF</i>	
<i>sepF(up)</i>	oAB109: GCCCGTGAGTATCACACG oAB110: gctatacgaacggtagttgaccagtgtccctgACTCATTGCTGTACACCCCC
<i>cat-pXyl</i>	oSW40: CAGGGAGCACTGGTC oMD226: GGTAGTTCCTCCTTAATCGATCCATTCAAATACAGATGCATTTTATTTTC
<i>sepF-sepF(down)</i>	oGS38: atggatcgattaaggaggaactaccATGAAAAATAAACTGAAAACTTTTTCTCAATGG oAB112: GCCAAAACCTCTGATAGACAGC
<i>zapA::cat-pXyl-zapA</i>	
<i>zapA(up)</i>	oMH22: AATGGCTTCAGGCTTTACTC oMH58: tgaccagtgtccctgCGTTTCTCCTCCATTCCG
<i>cat-pXyl</i>	oSW40: CAGGGAGCACTGGTC oMD226: GGTAGTTCCTCCTTAATCGATCCATTCAAATACAGATGCATTTTATTTTC
<i>zapA-zapA(down)</i>	oAB152: gtatttgaatggatcgattaaggaggaactaccTTGTCTGACGGCAAAAAACA oMH31: AGAGATTCTGCATCGTGT
<i>ezrA::ezrA-30aa-HaloTag-cat</i>	

<i>ezaA(partial)</i>	oMH01: GATTGCAAAGCTCAAGGATG oMH02: AGCGGATATGTCAGCTTTGA
<i>30aa-HaloTag</i>	oMH03: caaagctgacatatccgctCTTGAGGGTAGCGGACAAG oMH04: agcgagggagcagaaTTAGCCGCTGATTTCTAAGGTAG
<i>cat</i>	oJM28: TTCTGCTCCCTCGCTCAG oJM29: CAGGGAGCACTGGTCAAC
<i>ezaA(down)</i>	oMH05: tgaccagtgtccctgATAATCACGACCATGAAAAAGAG oMH06: GTTGTGGATCGAGTCGGA
<i>amyE::erm-Phyperspank-sepF-30aa-HaloTag</i>	
<i>amyE(up)-erm-pHyperSpank</i>	oMD191: TTTGGATGGATTCAGCCCGATTG oSW28: GGTAGTTCCTCCTTAAAGC
<i>SepF-15aa-HaloTag</i>	oMH45: ttaagcttaaggaggaactaccATGAGTATGAAAAATAAACTGAAAACTT oAB257: cggtaagtcccgtctagccttgcccTTAGCCGCTGATTTCTAAGG
<i>amyE(down)</i>	oMD196: GGGCAAGGCTAGACGGG oMD197: TCACATACTCGTTTCCAAACGGATC
<i>zapA::zapA-30aa-HaloTag-cat</i>	
<i>zapA(up)</i>	oMH22: AATGGCTTCAGGCTTTACTC oMH24: gtccgctaccctcaagATCCTTTTCTTTAAGCTGACGC
<i>30aa-HaloTag-cat</i>	oMH25: CTTGAGGGTAGCGGACAA oSW40: CAGGGAGCACTGGTC
<i>zapA-zapA(down)</i>	oMH29: tgaccagtgtccctgacaactATGCTAGATATCATCATC oMH31: AGAGATTCTGCATCGTGT
<i>divIB::cat</i>	
<i>divIB(up)</i>	oAB235: GCCTGAGTATTTAAAGGCCATTG oAB236: gtagtgaccagtgtccctgTGCTGTTCACCTCATTCAA
<i>cat</i>	oJM28: TTCTGCTCCCTCGCTCAG oJM29: CAGGGAGCACTGGTCAAC
<i>divIB(down)</i>	oMH100: tgagcgagggagcagAATTGAGGGGCAAATCAGC oAB238: CGCAAGCGATAAATAGTTTGAG
<i>divIB::erm-Pxyl-HaloTag-15aa-divIB</i>	

<i>divIB(up)</i>	oAB235: GCCTGAGTATTTAAAGGCCATTG oAB236: gtagttgaccagtgtccctgGCCTGTTACCTCATTCAA
<i>erm-Pxyl-HaloTag-15aa</i>	oJM29: CAGGGAGCACTGGTCAAC oAB14: tggcctgagcccgggtccctggccagatccctcgagGCCGCTGATTTCTAAGGTAGAAAAG
<i>15aa-divIB-divIB(down)</i>	oAB237: ctggccagggaccgggctcaggccaaggaagcggcATGAACCCGGGTCAAGAC oAB238: CGCAAGCGATAAATAGTTTGAG
<i>divIC::erm-Pxyl-HaloTag-15aa-divIC</i>	
<i>divIC(up)</i>	oAB239: CGGCGTACACTAGCGAA oAB240: gtagttgaccagtgtccctgACCAGACGGTCCTCCTTTC
<i>erm-Pxyl-HaloTag-15aa</i>	oJM29: CAGGGAGCACTGGTCAAC oAB14: tggcctgagcccgggtccctggccagatccctcgagGCCGCTGATTTCTAAGGTAGAAAAG
<i>15aa-divIC-divIC(down)</i>	oAB241: ctggccagggaccgggctcaggccaaggaagcggcTTGAATTTTTCCAGGGAACG oAB242: CAGTGAATGCAAATGATGAGTC
<i>ftsL::erm-Phyerspank-HaloTag-15aa-ftsL</i>	
<i>ftsL(up)</i>	oMH49: CTTCTTCGTGAAACCGTAGA oMH50: tgaccagtgtccctgaGGCTGATGACCTCCTTTTA
<i>erm-Phyerspank-HaloTag-15aa</i>	oSW40: CAGGGAGCACTGGTC oAB14: tggcctgagcccgggtccctggccagatccctcgagGCCGCTGATTTCTAAGGTAGAAAAG
<i>15aa-ftsL</i>	oMH61: agggaccgggctcaggccaaggaagcggcATGAGCAATTTAGCTTACCAACC oMH52: CGCTCCTTCAAATACTTATCCA
<i>ftsW::erm-Pxyl-HaloTag-15aa-ftsW</i>	
<i>ftsW(up)</i>	oME1: GAGAGACTTGATTATTTGCTTTCTTTTATC oAB234: gtagttgaccagtgtccctgAACATCCTCTTCCCTGCTTC
<i>erm-Pxyl-HaloTag-15aa</i>	oJM29: CAGGGAGCACTGGTCAAC oAB14: tggcctgagcccgggtccctggccagatccctcgagGCCGCTGATTTCTAAGGTAGAAAAG
<i>15aa-ftsW</i>	oME6: ctcagggatctggccagggaccgggctcaggccaaggaagcggcATGTTAAAAAATGCTAA AATCTTATGATTACTCAC

oME7: GTACACACTTGTTTTTACAGATAAACAGoME6:
ctcgagggatctggccagggaccgggctcaggccaaggaagcggcATGTTAAAAAATGCTAA
AATCTTATGATTACTCAC
oME7: GTACACACTTGTTTTTACAGATAAACAG

Construct original to this thesis	
Fragment	Primer: Sequence (5' to 3')
<i>SepF::SepF-30aa-HaloTag-cat</i>	
<i>sepF(up)</i>	oMH16: GCATCACCTGCCTCG oMH17: tgtccgctaccctcaagCCACCTCTGATGTTTCGTCT
<i>30aa-HaloTag</i>	oMH18: CTTGAGGGTAGCGGACAA oMH19: agcgaggagcagaaCCTTAGCCGCTGATTTCTAAGGTAG
<i>cat</i>	oJM28: TTCTGCTCCCTCGCTCAG oJM29: CAGGGAGCACTGGTCAAC
<i>sepF(down)</i>	oMH20: tgaccagtgtccctgAGCGAGATGATCCTTTATCAAG oMH21: CTATGTATGAAGGATCTTCAACCA
Constructs from other studies	
Construct	Reference
<i>amyE::erm-Phyerspank-ftsA-mNeonGreen-15aa-ftsZ</i>	26
<i>ftsZ::mNeonGreen-15aa-ftsZ multicopy</i>	26,174
<i>ftsAZ::erm-ftsA-HaloTag(sw)-ftsZ-cat multicopy</i>	26,174
<i>pbp2B::mNeonGreen-15aa-pbp2B</i>	26
<i>pbp2b::erm-pHyperSpank-HaloTag-15aa-pbp2b</i>	26
<i>zapA-yshBD::tet</i>	64
<i>dacA::kan</i>	139

References

1. Vaughan, S., Wickstead, B., Gull, K. & Addinall, S. G. Molecular evolution of FtsZ protein sequences encoded within the genomes of archaea, bacteria, and eukaryota. *Journal of molecular evolution* 58, 19–29 (2004).
2. Rivas-Marin, E. *et al.* Non-essentiality of canonical cell division genes in the planctomycete *Planctopirus limnophila*. *Sci Rep-uk* 10, 66 (2020).
3. Wagstaff, J. & Löwe, J. Prokaryotic cytoskeletons: protein filaments organizing small cells. *Nat Rev Microbiol* 16, 187–201 (2018).
4. Vitha, S., McAndrew, R. S. & Osteryoung, K. W. FtsZ ring formation at the chloroplast division site in plants. *The Journal of cell biology* 153, 111–120 (2001).
5. Kiefel, B. R., Gilson, P. R. & Beech, P. L. Diverse eukaryotes have retained mitochondrial homologues of the bacterial division protein FtsZ. 155, 105–115 (2004).
6. Busiek, K. K. & Margolin, W. Bacterial Actin and Tubulin Homologs in Cell Growth and Division. *Curr Biol* 25, R243–R254 (2015).
7. Leaver, M., Domínguez-Cuevas, P., Coxhead, J. M., Daniel, R. A. & Errington, J. Life without a wall or division machine in *Bacillus subtilis*. 457, 849–853 (2009).
8. Erickson, H. P. & Osawa, M. Cell division without FtsZ--a variety of redundant mechanisms. *Molecular microbiology* 78, 267–270 (2010).
9. Ouellette, S. P., Lee, J. & Cox, J. V. Division without Binary Fission: Cell Division in the FtsZ-Less *Chlamydia*. *J Bacteriol* 202, (2020).
10. Nogales, E., Downing, K. H., Amos, L. A. & Löwe, J. Tubulin and FtsZ form a distinct family of GTPases. *Nature structural biology* 5, 451–458 (1998).
11. Bi, E. & Lutkenhaus, J. Isolation and characterization of *ftsZ* alleles that affect septal morphology. 174, 5414–5423 (1992).
12. Wang, X., Wang, X. & Lutkenhaus, J. The FtsZ protein of *Bacillus subtilis* is localized at the division site and has GTPase activity that is dependent upon FtsZ concentration. *Molecular microbiology* 9, 435–442 (1993).
13. Erickson, H. P., Anderson, D. E. & Osawa, M. FtsZ in Bacterial Cytokinesis: Cytoskeleton and Force Generator All in One†. *Microbiology and Molecular Biology Reviews* 74, 504–528 (2010).

14. Buske, P. J. & Levin, P. A. A flexible C-terminal linker is required for proper FtsZ assembly in vitro and cytokinetic ring formation in vivo. *Molecular microbiology* 89, 249–263 (2013).
15. Osawa, M. & Erickson, H. P. FtsZ from divergent foreign bacteria can function for cell division in Escherichia coli. *Journal of bacteriology* 188, 7132–7140 (2006).
16. Buske, P. J. & Levin, P. A. Extreme C terminus of bacterial cytoskeletal protein FtsZ plays fundamental role in assembly independent of modulatory proteins. *The Journal of biological chemistry* 287, 10945–10957 (2012).
17. Rodrigues, C. D. A. & Harry, E. J. The Min System and Nucleoid Occlusion Are Not Required for Identifying the Division Site in Bacillus subtilis but Ensure Its Efficient Utilization. *PLoS Genetics* 8, e1002561 (2012).
18. Huang, K.-H., Durand-Heredia, J. & Janakiraman, A. FtsZ ring stability: of bundles, tubules, crosslinks, and curves. *Journal of bacteriology* 195, 1859–1868 (2013).
19. Buss, J. *et al.* In vivo organization of the FtsZ-ring by ZapA and ZapB revealed by quantitative super-resolution microscopy. *Molecular microbiology* 89, 1099–1120 (2013).
20. Coltharp, C., Buss, J., Plumer, T. M. & Xiao, J. Defining the rate-limiting processes of bacterial cytokinesis. *Proceedings of the National Academy of Sciences of the United States of America* 113, E1044-53 (2016).
21. Holden, S. J. *et al.* High throughput 3D super-resolution microscopy reveals Caulobacter crescentus in vivo Z-ring organization. *Proceedings of the National Academy of Sciences of the United States of America* 111, 4566–4571 (2014).
22. Strauss, M. P. *et al.* 3D-SIM super resolution microscopy reveals a bead-like arrangement for FtsZ and the division machinery: implications for triggering cytokinesis. *PLoS Biol* 10, e1001389 (2012).
23. Fu, G. *et al.* In vivo structure of the E. coli FtsZ-ring revealed by photoactivated localization microscopy (PALM). *PLoS one* 5, e12682 (2010).
24. Szwedziak, P., Wang, Q., Bharat, T. A. M., Tsim, M. & Löwe, J. Architecture of the ring formed by the tubulin homologue FtsZ in bacterial cell division. *eLife* 3, e04601 (2014).
25. Yang, X. *et al.* GTPase activity-coupled treadmilling of the bacterial tubulin FtsZ organizes septal cell wall synthesis. *Science* 355, 744–747 (2017).
26. Bisson-Filho, A. W. *et al.* Treadmilling by FtsZ filaments drives peptidoglycan synthesis and bacterial cell division. *Science* 355, 739–743 (2017).

27. Leisch, N. *et al.* Growth in width and FtsZ ring longitudinal positioning in a gammaproteobacterial symbiont. *Current biology : CB* 22, R831-2 (2012).
28. Leisch, N. *et al.* Asynchronous division by non-ring FtsZ in the gammaproteobacterial symbiont of *Robbea hypermnestra*. *Nature microbiology* 2, 16182 (2016).
29. Rueda, S., Vicente, M. & Mingorance, J. Concentration and assembly of the division ring proteins FtsZ, FtsA, and ZipA during the *Escherichia coli* cell cycle. *Journal of bacteriology* 185, 3344–3351 (2003).
30. Weart, R. B. & Levin, P. A. Growth rate-dependent regulation of medial FtsZ ring formation. *Journal of bacteriology* 185, 2826–2834 (2003).
31. Kysela, D. T., Randich, A. M., Caccamo, P. D. & Brun, Y. V. Diversity Takes Shape: Understanding the Mechanistic and Adaptive Basis of Bacterial Morphology. *Plos Biol* 14, e1002565 (2016).
32. Pasquina-Lemonche, L. *et al.* The architecture of the Gram-positive bacterial cell wall. *Nature* 582, 294–297 (2020).
33. Koch, A. L. Growth and Form of the Bacterial Cell Wall. *American Scientist* 78, 327–341 (1990).
34. Hayhurst, E. J., Kailas, L., Hobbs, J. K. & Foster, S. J. Cell wall peptidoglycan architecture in *Bacillus subtilis*. *Proceedings of the National Academy of Sciences of the United States of America* 105, 14603–14608 (2008).
35. Xiao, J. & Goley, E. D. Redefining the roles of the FtsZ-ring in bacterial cytokinesis. 34, 90–96 (2016).
36. Erickson, H. P. Modeling the physics of FtsZ assembly and force generation. *Proceedings of the National Academy of Sciences of the United States of America* 106, 9238–9243 (2009).
37. Osawa, M., Anderson, D. E. & Erickson, H. P. Reconstitution of Contractile FtsZ Rings in Liposomes. *Science* 320, 792–794 (2008).
38. Osawa, M. & Erickson, H. P. Inside-out Z rings--constriction with and without GTP hydrolysis. *Molecular microbiology* 81, 571–579 (2011).
39. Osawa, M. & Erickson, H. P. Liposome division by a simple bacterial division machinery. *Proceedings of the National Academy of Sciences of the United States of America* 110, 11000–11004 (2013).

40. Daley, D. O., Skoglund, U. & Söderström, B. FtsZ does not initiate membrane constriction at the onset of division. *Scientific reports* 6, 33138 (2016).
41. Whitley, K. D. *et al.* FtsZ treadmilling is essential for Z-ring condensation and septal constriction initiation in *Bacillus subtilis* cell division. *Nat Commun* 12, 2448 (2021).
42. Silber, N., Mayer, C., Opitz, C. L. M. de & Sass, P. Progression of the late-stage divisome is unaffected by the depletion of the cytoplasmic FtsZ pool. *Commun Biology* 4, 270 (2021).
43. Monteiro, J. M. *et al.* Peptidoglycan synthesis drives an FtsZ-treadmilling-independent step of cytokinesis. *Nature* 554, 528–532 (2018).
44. Erickson, H. P. How Teichoic Acids Could Support a Periplasm in Gram-Positive Bacteria, and Let Cell Division Cheat Turgor Pressure. *Front Microbiol* 12, 664704 (2021).
45. Daniel, R. A., Harry, E. J. & Errington, J. Role of penicillin-binding protein PBP 2B in assembly and functioning of the division machinery of *Bacillus subtilis*. *Molecular microbiology* 35, 299–311 (2000).
46. Gahlmann, A. & Moerner, W. E. Exploring bacterial cell biology with single-molecule tracking and super-resolution imaging. *Nat Rev Microbiol* 12, 9–22 (2014).
47. Stricker, J., Maddox, P., Salmon, E. D. & Erickson, H. P. Rapid assembly dynamics of the *Escherichia coli* FtsZ-ring demonstrated by fluorescence recovery after photobleaching. *Proceedings of the National Academy of Sciences* 99, 3171–3175 (2002).
48. Anderson, D. E., Gueiros-Filho, F. J. & Erickson, H. P. Assembly Dynamics of FtsZ Rings in *Bacillus subtilis* and *Escherichia coli* and Effects of FtsZ-Regulating Proteins. *Journal of Bacteriology* 186, 5775–5781 (2004).
49. Loose, M. & Mitchison, T. J. The bacterial cell division proteins FtsA and FtsZ self-organize into dynamic cytoskeletal patterns. *Nature Cell Biology* 16, 38–46 (2014).
50. Niu, L. & Yu, J. Investigating intracellular dynamics of FtsZ cytoskeleton with photoactivation single-molecule tracking. *Biophysical journal* 95, 2009–2016 (2008).
51. Barrows, J. M. & Goley, E. D. FtsZ dynamics in bacterial division: What, how, and why? *Curr Opin Cell Biol* 68, 163–172 (2021).
52. Wagstaff, J. M. *et al.* A Polymerization-Associated Structural Switch in FtsZ That Enables Treadmilling of Model Filaments. *mBio* 8, e00254-17 (2017).
53. Corbin, L. C. & Erickson, H. P. A Unified Model for Treadmilling and Nucleation of Single-Stranded FtsZ Protofilaments. *Biophys J* 119, 792–805 (2020).

54. Perez, A. J. *et al.* Movement dynamics of divisome proteins and PBP2x:FtsW in cells of *Streptococcus pneumoniae*. *Proc National Acad Sci* 116, 201816018 (2019).
55. Adams, D. W. & Errington, J. Bacterial cell division: assembly, maintenance and disassembly of the Z ring. *Nature Reviews Microbiology* 7, 642–653 (2009).
56. Haeusser, D. P. & Margolin, W. Splitsville: structural and functional insights into the dynamic bacterial Z ring. *Journal of Cell Biology* 14, 305–319 (2016).
57. Ent, F. van den & Löwe, J. Crystal structure of the cell division protein FtsA from *Thermotoga maritima*. *The EMBO journal* 19, 5300–5307 (2000).
58. Pichoff, S. & Lutkenhaus, J. Tethering the Z ring to the membrane through a conserved membrane targeting sequence in FtsA. *Molecular microbiology* 55, 1722–1734 (2005).
59. Dai, K. & Lutkenhaus, J. The proper ratio of FtsZ to FtsA is required for cell division to occur in *Escherichia coli*. *Journal of bacteriology* 174, 6145–6151 (1992).
60. Feucht, A., Lucet, I., Yudkin, M. D. & Errington, J. Cytological and biochemical characterization of the FtsA cell division protein of *Bacillus subtilis*. *Mol Microbiol* 40, 115–125 (2001).
61. Herricks, J. R., Nguyen, D. & Margolin, W. A thermosensitive defect in the ATP binding pocket of FtsA can be suppressed by allosteric changes in the dimer interface. *Molecular microbiology* 94, 713–727 (2014).
62. Beall, B. & Lutkenhaus, J. Impaired cell division and sporulation of a *Bacillus subtilis* strain with the *ftsA* gene deleted. *Journal of bacteriology* 174, 2398–2403 (1992).
63. Jensen, S. O., Thompson, L. S. & Harry, E. J. Cell division in *Bacillus subtilis*: FtsZ and FtsA association is Z-ring independent, and FtsA is required for efficient midcell Z-Ring assembly. *Journal of bacteriology* 187, 6536–6544 (2005).
64. Gueiros-Filho, F. J. & Losick, R. A widely conserved bacterial cell division protein that promotes assembly of the tubulin-like protein FtsZ. *Genes & Development* 16, 2544–2556 (2002).
65. Low, H. H., Moncrieffe, M. C. & Löwe, J. The Crystal Structure of ZapA and its Modulation of FtsZ Polymerisation. *Journal of Molecular Biology* 341, 839–852 (2004).
66. Levin, P. A., Kurtser, I. G. & Grossman, A. D. Identification and characterization of a negative regulator of FtsZ ring formation in *Bacillus subtilis*. *Proc National Acad Sci* 96, 9642–9647 (1999).

67. Land, A. D., Luo, Q. & Levin, P. A. Functional Domain Analysis of the Cell Division Inhibitor EzrA. *PLoS ONE* 9, e102616 (2014).
68. Levin, P. A., Schwartz, R. L. & Grossman, A. D. Polymer Stability Plays an Important Role in the Positional Regulation of FtsZ. *Journal of Bacteriology* 183, 5449–5452 (2001).
69. Haeusser, D. P., Schwartz, R. L., Smith, A. M., Oates, M. E. & Levin, P. A. EzrA prevents aberrant cell division by modulating assembly of the cytoskeletal protein FtsZ. *Molecular Microbiology* 52, 801–814 (2004).
70. Singh, J. K., Makde, R. D., Kumar, V. & Panda, D. A Membrane Protein, EzrA, Regulates Assembly Dynamics of FtsZ by Interacting with the C-Terminal Tail of FtsZ⁺. vol. 46 (American Chemical Society, 2007).
71. Chung, K.-M., Hsu, H.-H., Yeh, H.-Y. & Chang, B.-Y. Mechanism of Regulation of Prokaryotic Tubulin-like GTPase FtsZ by Membrane Protein EzrA. *Journal of Biological Chemistry* 282, 14891–14897 (2007).
72. Cleverley, R. M. *et al.* Structure and function of a spectrin-like regulator of bacterial cytokinesis. *Nature Communications* 5, 5421 (2014).
73. Steele, V. R., Bottomley, A. L., Garcia-Lara, J., Kasturiarachchi, J. & Foster, S. J. Multiple essential roles for EzrA in cell division of *Staphylococcus aureus*. *Molecular microbiology* 80, 542–555 (2011).
74. Hamoen, L. W., Meile, J., Jong, W. D., Noirot, P. & Errington, J. SepF, a novel FtsZ-interacting protein required for a late step in cell division. *Molecular Microbiology* 59, 989–999 (2006).
75. Chung, K.-M., Hsu, H.-H., Govindan, S. & Chang, B.-Y. Transcription regulation of *ezrA* and its effect on cell division of *Bacillus subtilis*. *Journal of bacteriology* 186, 5926–5932 (2004).
76. Haeusser, D. P., Garza, A. C., Buscher, A. Z. & Levin, P. A. The Division Inhibitor EzrA Contains a Seven-Residue Patch Required for Maintaining the Dynamic Nature of the Medial FtsZ Ring ∇ . *Journal of Bacteriology* 189, 9001–9010 (2007).
77. Duman, R. *et al.* Structural and genetic analyses reveal the protein SepF as a new membrane anchor for the Z ring. *Proceedings of the National Academy of Sciences of the United States of America* 110, E4601-10 (2013).
78. Pende, N. *et al.* SepF is the FtsZ anchor in archaea, with features of an ancestral cell division system. *Nat Commun* 12, 3214 (2021).
79. Nußbaum, P., Gerstner, M., Dingethal, M., Erb, C. & Albers, S.-V. The archaeal protein SepF is essential for cell division in *Haloferax volcanii*. *Nat Commun* 12, 3469 (2021).

80. Singh, J. K., Makde, R. D., Kumar, V. & Panda, D. SepF Increases the Assembly and Bundling of FtsZ Polymers and Stabilizes FtsZ Protofilaments by Binding along Its Length. *Journal of Biological Chemistry* 283, 31116–31124 (2008).
81. Ishikawa, S., Kawai, Y., Hiramatsu, K., Kuwano, M. & Ogasawara, N. A new FtsZ-interacting protein, YlmF, complements the activity of FtsA during progression of cell division in *Bacillus subtilis*. *Molecular Microbiology* 60, 1364–1380 (2006).
82. Gupta, S. *et al.* Essential protein SepF of mycobacteria interacts with FtsZ and MurG to regulate cell growth and division. *Microbiology (Reading, England)* 161, 1627–1638 (2015).
83. Sogues, A. *et al.* Essential dynamic interdependence of FtsZ and SepF for Z-ring and septum formation in *Corynebacterium glutamicum*. *Nat Commun* 11, 1641 (2020).
84. Król, E. *et al.* *Bacillus subtilis* SepF binds to the C-terminus of FtsZ. *PLoS one* 7, e43293 (2012).
85. Gündoğdu, M. E. *et al.* Large ring polymers align FtsZ polymers for normal septum formation. *The EMBO Journal* 30, 617–626 (2011).
86. Wenzel, M. *et al.* Control of septum thickness by the curvature of SepF polymers. *Proc National Acad Sci* 118, e2002635118 (2021).
87. Errington, J., Daniel, R. A. & Scheffers, D.-J. Cytokinesis in bacteria. *Microbiology and molecular biology reviews : MMBR* 67, 52-65-table of contents (2003).
88. Yanouri, A., Daniel, R. A., Errington, J. & Buchanan, C. E. Cloning and sequencing of the cell division gene *pbpB*, which encodes penicillin-binding protein 2B in *Bacillus subtilis*. *J Bacteriol* 175, 7604–7616 (1993).
89. Angeles, D. M., Macia-Valero, A., Bohorquez, L. C. & Scheffers, D.-J. The PASTA domains of *Bacillus subtilis* PBP2B strengthen the interaction of PBP2B with DivIB. *Microbiology+* 166, 826–836 (2020).
90. Taguchi, A. *et al.* FtsW is a peptidoglycan polymerase that is functional only in complex with its cognate penicillin-binding protein. *Nature Microbiology* 4, 587–594 (2019).
91. Daitch, A. K. & Goley, E. D. Uncovering Unappreciated Activities and Niche Functions of Bacterial Cell Wall Enzymes. *Curr Biol* 30, R1170–R1175 (2020).
92. Yang, X. *et al.* A two-track model for the spatiotemporal coordination of bacterial septal cell wall synthesis revealed by single-molecule imaging of FtsW. *Nat Microbiol* 1–10 (2021) doi:10.1038/s41564-020-00853-0.

93. Daniel, R. A., Harry, E. J., Katis, V. L., Wake, R. G. & Errington, J. Characterization of the essential cell division gene *ftsL*(*ylID*) of *Bacillus subtilis* and its role in the assembly of the division apparatus. *Molecular microbiology* 29, 593–604 (1998).
94. Bramkamp, M., Weston, L., Daniel, R. A. & Errington, J. Regulated intramembrane proteolysis of FtsL protein and the control of cell division in *Bacillus subtilis*. *Molecular microbiology* 62, 580–591 (2006).
95. Sievers, J. & Errington, J. The *Bacillus subtilis* cell division protein FtsL localizes to sites of septation and interacts with DivIC. *Molecular microbiology* 36, 846–855 (2000).
96. Wadenpohl, I. & Bramkamp, M. DivIC stabilizes FtsL against RasP cleavage. *Journal of bacteriology* 192, 5260–5263 (2010).
97. Levin, P. A. & Losick, R. Characterization of a cell division gene from *Bacillus subtilis* that is required for vegetative and sporulation septum formation. *J Bacteriol* 176, 1451–1459 (1994).
98. Katis, V. L. & Wake, R. G. Membrane-bound division proteins DivIB and DivIC of *Bacillus subtilis* function solely through their external domains in both vegetative and sporulation division. 181, 2710–2718 (1999).
99. Buddelmeijer, N., Judson, N., Boyd, D., Mekalanos, J. J. & Beckwith, J. YgbQ, a cell division protein in *Escherichia coli* and *Vibrio cholerae*, localizes in codependent fashion with FtsL to the division site. 99, 6316–6321 (2002).
100. Beall, B. & Lutkenhaus, J. Nucleotide sequence and insertional inactivation of a *Bacillus subtilis* gene that affects cell division, sporulation, and temperature sensitivity. 171, 6821–6834 (1989).
101. Rowland, S. L., Katis, V. L., Partridge, S. R. & Wake, R. G. DivIB, FtsZ and cell division in *Bacillus subtilis*. *Mol Microbiol* 23, 295–302 (1997).
102. Thompson, L. S., Beech, P. L., Real, G., Henriques, A. O. & Harry, E. J. Requirement for the cell division protein DivIB in polar cell division and engulfment during sporulation in *Bacillus subtilis*. 188, 7677–7685 (2006).
103. Robson, S. A. & King, G. F. Domain architecture and structure of the bacterial cell division protein DivIB. 103, 6700–6705 (2006).
104. Wadsworth, K. D., Rowland, S. L., Harry, E. J. & King, G. F. The divisomal protein DivIB contains multiple epitopes that mediate its recruitment to incipient division sites. *Molecular microbiology* 67, 1143–1155 (2008).

105. Bottomley, A. L. *et al.* Staphylococcus aureus DivIB is a peptidoglycan-binding protein that is required for a morphological checkpoint in cell division. *Molecular microbiology* 94, 1041–1064 (2014).
106. Aarsman, M. E. G. *et al.* Maturation of the Escherichia coli divisome occurs in two steps. *Molecular microbiology* 55, 1631–1645 (2005).
107. Gamba, P., Veening, J.-W., Saunders, N. J., Hamoen, L. W. & Daniel, R. A. Two-step assembly dynamics of the Bacillus subtilis divisome. *Journal of bacteriology* 191, 4186–4194 (2009).
108. Gamba, P., Hamoen, L. W. & Daniel, R. A. Cooperative Recruitment of FtsW to the Division Site of Bacillus subtilis. *Frontiers in microbiology* 7, 1808 (2016).
109. Katis, V. L., Wake, R. G. & Harry, E. J. Septal localization of the membrane-bound division proteins of Bacillus subtilis DivIB and DivIC is codependent only at high temperatures and requires FtsZ. 182, 3607–3611 (2000).
110. Goehring, N. W. & Beckwith, J. Diverse paths to midcell: assembly of the bacterial cell division machinery. 15, R514-26 (2005).
111. Meier, E. L. & Goley, E. D. Form and function of the bacterial cytokinetic ring. *Current Opinion in Cell Biology* 26, 19–27 (2014).
112. Gao, Y., Wenzel, M., Jonker, M. J. & Hamoen, L. W. Free SepF interferes with recruitment of late cell division proteins. *Scientific Reports* 7, 16928 (2017).
113. Grimm, J. B. *et al.* A general method to improve fluorophores for live-cell and single-molecule microscopy. *Nature Methods* 12, 244–50–3 p following 250 (2015).
114. Noirclerc-Savoye, M. *et al.* In vitro reconstitution of a trimeric complex of DivIB, DivIC and FtsL, and their transient co-localization at the division site in Streptococcus pneumoniae. *Molecular Microbiology* 55, 413–424 (2005).
115. Small, E. *et al.* FtsZ Polymer-bundling by the Escherichia coli ZapA Orthologue, YgfE, Involves a Conformational Change in Bound GTP. *J Mol Biol* 369, 210–221 (2007).
116. Dajkovic, A., Pichoff, S., Lutkenhaus, J. & Wirtz, D. Cross-linking FtsZ polymers into coherent Z rings. *Mol Microbiol* 78, 651–668 (2010).
117. Pacheco-Gómez, R. *et al.* Tetramerization of ZapA is required for FtsZ bundling. *Biochemical Journal* 449, 795–802 (2013).

118. Caldas, P. *et al.* Cooperative ordering of treadmilling filaments in cytoskeletal networks of FtsZ and its crosslinker ZapA. *Nat Commun* 10, 5744 (2019).
119. Monahan, L. G., Robinson, A. & Harry, E. J. Lateral FtsZ association and the assembly of the cytokinetic Z ring in bacteria. *Molecular Microbiology* 74, 1004–1017 (2009).
120. Squyres, G. R. *et al.* Single-molecule imaging reveals that Z-ring condensation is essential for cell division in *Bacillus subtilis*. *Nat Microbiol* 6, 553–562 (2021).
121. Guan, F. *et al.* Lateral interactions between protofilaments of the bacterial tubulin homolog FtsZ are essential for cell division. *Elife* 7, e35578 (2018).
122. Shin, J. Y., Vollmer, W., Lagos, R. & Monasterio, O. Glutamate 83 and arginine 85 of helix H3 bend are key residues for FtsZ polymerization, GTPase activity and cellular viability of *Escherichia coli*: lateral mutations affect FtsZ polymerization and *E. coli* viability. *Bmc Microbiol* 13, 26 (2013).
123. Krupka, M. & Margolin, W. Unite to divide: Oligomerization of tubulin and actin homologs regulates initiation of bacterial cell division. *F1000research* 7, 235 (2018).
124. Bhattacharya, D., Kumar, A. & Panda, D. WhmD promotes the assembly of *Mycobacterium smegmatis* FtsZ: A possible role of WhmD in bacterial cell division. *Int J Biol Macromol* 95, 582–591 (2017).
125. Eswara, P. J. *et al.* An essential *Staphylococcus aureus* cell division protein directly regulates FtsZ dynamics. *Elife* 7, e38856 (2018).
126. Rahman, M. *ur et al.* Assembly properties of bacterial tubulin homolog FtsZ regulated by the positive regulator protein ZipA and ZapA from *Pseudomonas aeruginosa*. *Sci Rep-uk* 10, 21369 (2020).
127. Mateos-Gil, P., Tarazona, P. & Vélez, M. Bacterial cell division: modeling FtsZ assembly and force generation from single filament experimental data. *Fems Microbiol Rev* 43, 73–87 (2018).
128. Guigas, G. & Weiss, M. Effects of protein crowding on membrane systems. *Biochimica Et Biophysica Acta Bba - Biomembr* 1858, 2441–2450 (2016).
129. Cayley, D. S., Guttman, H. J. & Record, M. T. Biophysical Characterization of Changes in Amounts and Activity of *Escherichia coli* Cell and Compartment Water and Turgor Pressure in Response to Osmotic Stress. *Biophys J* 78, 1748–1764 (2000).
130. Erickson, H. P. How bacterial cell division might cheat turgor pressure – a unified mechanism of septal division in Gram-positive and Gram-negative bacteria. *BioEssays* 39, 1700045 (2017).

131. Nguyen, L. T. *et al.* Simulations suggest a constrictive force is required for Gram-negative bacterial cell division. *Nat Commun* 10, 1259 (2019).
132. Fink, G. & Löwe, J. Reconstitution of a prokaryotic minus end-tracking system using TubRC centromeric complexes and tubulin-like protein TubZ filaments. *112*, E1845-50 (2015).
133. Powers, A. F. *et al.* The Ndc80 Kinetochore Complex Forms Load-Bearing Attachments to Dynamic Microtubule Tips via Biased Diffusion. *Cell* 136, 865–875 (2009).
134. Baranova, N. *et al.* Diffusion and capture permits dynamic coupling between treadmilling FtsZ filaments and cell division proteins. *Nat Microbiol* 5, 407–417 (2020).
135. Khanna, K., Garrido, J. L., Sugie, J., Pogliano, K. & Villa, E. Asymmetric localization of the cell division machinery during *Bacillus subtilis* sporulation. *Elife* 10, e62204 (2021).
136. Meeske, A. J. *et al.* SEDS proteins are a widespread family of bacterial cell wall polymerases. *537*, 634–638 (2016).
137. Cho, H. *et al.* Bacterial cell wall biogenesis is mediated by SEDS and PBP polymerase families functioning semi-autonomously. *Nature microbiology* 1, 16172 (2016).
138. Garner, E. C. *et al.* Coupled, Circumferential Motions of the Cell Wall Synthesis Machinery and MreB Filaments in *B. subtilis*. *Science (New York, N.Y.)* 333, 222–225 (2011).
139. Hussain, S. *et al.* MreB filaments align along greatest principal membrane curvature to orient cell wall synthesis. *eLife* 7, 1239 (2018).
140. Lyu, Z. *et al.* FtsN activates septal cell wall synthesis by forming a processive complex with the septum-specific peptidoglycan synthase in *E. coli*. *Biorxiv* 2021.08.23.457437 (2021) doi:10.1101/2021.08.23.457437.
141. Söderström, B. & Daley, D. O. The bacterial divisome: more than a ring? *Curr Genet* 63, 161–164 (2017).
142. Söderström, B., Chan, H., Shilling, P. J., Skoglund, U. & Daley, D. O. Spatial separation of FtsZ and FtsN during cell division. *Molecular Microbiology* 107, (2017).
143. Li, Y. *et al.* Genetic analysis of the septal peptidoglycan synthase FtsWI complex supports a conserved activation mechanism for SEDS-bPBP complexes. *Plos Genet* 17, e1009366 (2021).
144. Buddelmeijer, N. & Beckwith, J. A complex of the *Escherichia coli* cell division proteins FtsL, FtsB and FtsQ forms independently of its localization to the septal region. *Molecular microbiology* 52, 1315–1327 (2004).

145. Gonzalez, M. D. & Beckwith, J. Divisome under construction: distinct domains of the small membrane protein FtsB are necessary for interaction with multiple cell division proteins. *Journal of bacteriology* 191, 2815–2825 (2009).
146. Glas, M. *et al.* The Soluble Periplasmic Domains of Escherichia coli Cell Division Proteins FtsQ/FtsB/FtsL Form a Trimeric Complex with Submicromolar Affinity. *Journal of bacteriology* 290, 21498–21509 (2015).
147. Choi, Y. *et al.* Structural Insights into the FtsQ/FtsB/FtsL Complex, a Key Component of the Divisome. *Sci Rep-uk* 8, 18061 (2018).
148. Daniel, R. A., Noirot-Gros, M.-F., Noirot, P. & Errington, J. Multiple interactions between the transmembrane division proteins of Bacillus subtilis and the role of FtsL instability in divisome assembly. *Journal of bacteriology* 188, 7396–7404 (2006).
149. Robichon, C., King, G. F., Goehring, N. W. & Beckwith, J. Artificial septal targeting of Bacillus subtilis cell division proteins in Escherichia coli: an interspecies approach to the study of protein-protein interactions in multiprotein complexes. *Journal of bacteriology* 190, 6048–6059 (2008).
150. Masson, S. *et al.* Central domain of DivIB caps the C-terminal regions of the FtsL/DivIC coiled-coil rod. *The Journal of biological chemistry* 284, 27687–27700 (2009).
151. Noirclerc-Savoye, M. *et al.* Reconstitution of membrane protein complexes involved in pneumococcal septal cell wall assembly. *Journal of bacteriology* 8, e75522 (2013).
152. Marmont, L. S. & Bernhardt, T. G. A conserved subcomplex within the bacterial cytokinetic ring activates cell wall synthesis by the FtsW-FtsI synthase. *Proc National Acad Sci* 117, 23879–23885 (2020).
153. Daniel, R. A. & Errington, J. Intrinsic instability of the essential cell division protein FtsL of Bacillus subtilis and a role for DivIB protein in FtsL turnover. *Molecular microbiology* 36, 278–289 (2000).
154. Corbin, B. D., Geissler, B., Sadasivam, M. & Margolin, W. Z-Ring-Independent Interaction between a Subdomain of FtsA and Late Septation Proteins as Revealed by a Polar Recruitment Assay. *Journal of bacteriology* 186, 7736–7744 (2004).
155. Tsang, M.-J. & Bernhardt, T. G. A role for the FtsQLB complex in cytokinetic ring activation revealed by an ftsL allele that accelerates division. *Molecular microbiology* 95, 925–944 (2015).
156. Bernard, C. S., Sadasivam, M., Shiomi, D. & Margolin, W. An altered FtsA can compensate for the loss of essential cell division protein FtsN in Escherichia coli. *Molecular microbiology* 64, 1289–1305 (2007).

157. Liu, B., Persons, L., Lee, L. & Boer, P. A. J. de. Roles for both FtsA and the FtsBLQ subcomplex in FtsN-stimulated cell constriction in *Escherichia coli*. *Molecular microbiology* 95, 945–970 (2015).
158. Park, K.-T., Du, S. & Lutkenhaus, J. Essential Role for FtsL in Activation of Septal Peptidoglycan Synthesis. *Mbio* 11, (2020).
159. Park, K.-T., Pichoff, S., Du, S. & Lutkenhaus, J. FtsA acts through FtsW to promote cell wall synthesis during cell division in *Escherichia coli*. *Proc National Acad Sci* 118, e2107210118 (2021).
160. McCausland, J. W. *et al.* Treadmilling FtsZ polymers drive the directional movement of sPG-synthesis enzymes via a Brownian ratchet mechanism. *Nat Commun* 12, 609 (2021).
161. Simunovic, M., Evergren, E., Callan-Jones, A. & Bassereau, P. Curving Cells Inside and Out: Roles of BAR Domain Proteins in Membrane Shaping and Its Cellular Implications. *Annu Rev Cell Dev Bi* 35, 1–19 (2019).
162. Hu, Z., Gogol, E. P. & Lutkenhaus, J. Dynamic assembly of MinD on phospholipid vesicles regulated by ATP and MinE. *Proceedings of the National Academy of Sciences* 99, 6761–6766 (2002).
163. Pichoff, S. & Lutkenhaus, J. Unique and overlapping roles for ZipA and FtsA in septal ring assembly in *Escherichia coli*. *Embo J* 21, 685–693 (2002).
164. Shiomi, D. & Margolin, W. Compensation for the loss of the conserved membrane targeting sequence of FtsA provides new insights into its function. *Molecular microbiology* 67, 558–569 (2008).
165. Ramm, B. & Schwille, P. In vitro reconstitution of the bacterial cytoskeleton: expected and unexpected new insights. *Microb Biotechnol* 12, 74–76 (2019).
166. Romberg, L. & Levin, P. A. Assembly dynamics of the bacterial cell division protein FTSZ: poised at the edge of stability. *Annual Review of Microbiology* 57, 125–154 (2003).
167. Woldemeskel, S. A., McQuillen, R., Hessel, A. M., Xiao, J. & Goley, E. D. A conserved coiled-coil protein pair focuses the cytokinetic Z-ring in *Caulobacter crescentus*. *Mol Microbiol* 105, 721–740 (2017).
168. Barrows, J. M., Sundararajan, K., Bhargava, A. & Goley, E. D. FtsA Regulates Z-Ring Morphology and Cell Wall Metabolism in an FtsZ C-Terminal Linker-Dependent Manner in *Caulobacter crescentus*. *J Bacteriol* 202, (2020).

169. Hoffman, H. Violin plot. *Mathworks* <https://www.mathworks.com/matlabcentral/fileexchange/45134-violin-plot> (2015).
170. Valen, D. A. V. *et al.* Deep Learning Automates the Quantitative Analysis of Individual Cells in Live-Cell Imaging Experiments. *Plos Comput Biol* 12, e1005177 (2016).
171. Tinevez, J.-Y. *et al.* TrackMate: An open and extensible platform for single-particle tracking. *Methods (San Diego, Calif.)* 115, 80–90 (2017).
172. Bronson, J. E., Fei, J., Hofman, J. M., Gonzalez, R. L. & Wiggins, C. H. Learning Rates and States from Biophysical Time Series: A Bayesian Approach to Model Selection and Single-Molecule FRET Data. *Biophys J* 97, 3196–3205 (2009).
173. Ursell, T. *et al.* Rapid, precise quantification of bacterial cellular dimensions across a genomic-scale knockout library. *Bmc Biol* 15, 17 (2017).
174. Erratum for the Report: “Treadmilling by FtsZ filaments drives peptidoglycan synthesis and bacterial cell division” by A. W. Bisson-Filho, Y.-P. Hsu, G. R. Squyres, E. Kuru, F. Wu, C. Jukes, Y. Sun, C. Dekker, S. Holden, M. S. VanNieuwenhze, Y. V. Brun, E. C. Garner. *Science* 367, (2020).
175. Youngman, P. J., Perkins, J. B. & Losick, R. Genetic transposition and insertional mutagenesis in *Bacillus subtilis* with *Streptococcus faecalis* transposon Tn917. *Proc National Acad Sci* 80, 2305–2309 (1983).